University of Belgrade, Serbia

Georg-August University of Goettingen, Germany

MASTER THESIS

ERASMUS MUNDUS MASTERS COURSE - ASTROMUNDUS

The UV and Optical Spectral Properties of a Sample of Broad Line AGNs

Author:
PAYASWINI SAIKIA

Supervisors:
PROF LUKA POPOVIĆ, UNIVERSITY OF BELGRADE
PROF WOLFRAM KOLLATSCHNY, UNIVERSITY OF GOETTINGEN

Belgrade/Goettingen, July 2012

Acknowledgement

This Master Thesis is done through the joint Erasmus Mundus Masters Course in Astronomy and Astrophysics - 'Astromundus'. I would like to thank all the professors, officials and students who made this course a success. The work is a part of investigation on the projects : "Probing the structure and physics of the BLR using AGN variability" (supported by the Alexander von Hurboldt Foundation) and "Astrophysical Spectroscopy of Extragalactic Objects" (supported by the Ministry of Education and Science of Serbia).

I would like to thank my parents Mr Tarun Chandra Saikia and Mrs Minakshi Saikia and my two younger sisters Anasuya and Lupita for their encouragements. Undoubtedly it would not have been possible to achieve this stage of my academic life without their constant support.

This dissertation would not have been possible without the guidance and help of several individuals who in one way or another contributed and extended their valuable assistance in the preparation and completion of this study. First and foremost, my gratitude to Prof Luka Popović for his patience and unfailing support as my Thesis adviser. Prof Wolfram Kollatschny, the co-adviser of the thesis, for his expertise and steadfast encouragement. Dr Jelena Kovačević for her unselfish and moral support throughout this study, despite the distance. Dr Dragana Ilić for the insights she has shared. My sincere regards to Dr. Sonia Giovanna Temporin for being the first person to introduce me to the beauty of Extragalactic Astrophysics.

I would also like to thank all my friends - both in India and here in Europe for the healthy boost-up chats, their untiring efforts to motivate me whenever I needed it and the much needed relaxing outings time-to-time.

Contents

List of Figures

Chapter 1

Introduction

1.1 Motivation

Active Galactic Nuclei (AGNs) are undoubtedly some of the most interesting objects in the Universe. Their spectra have the strong broad and narrow emission lines, which originate from different emission regions. Analysis of the emission line profiles, their asymmetries, widths and flux ratios, as well as investigation of the correlations between different spectral properties, enable better understanding of the AGN nature. Namely, correlations between different spectral properties reflect the geometry, structure, kinematics and physics of emission regions.

Though many interesting correlations have been observed (Baldwin, 1977; Gaskell, 1985; Boroson & Green, 1992; Dong et al., 2009; Kovačević et al., 2010 etc.), there remains a number of open questions like location of the Fe II emission region and Fe II excitation mechanisms, physical reason behind increase of emission line's EW with a decrease in the continuum luminosity - Baldwin effect (Baldwin, 1977), influence of the inclination angle and Eddington ratio on the correlations between different line parameters like EW Fe II vs EW[O III]/EW Hβ and other 'EV 1' set of correlations from the paper Boroson & Green (1992).

In this work, the spectral properties between emission lines in the optical and UV wavelength ranges are compared, using a sample of AGNs. In optical part we analyse the Fe II lines, which are very interesting since there are many unresolved problems connected to their origin.

Also, we investigate Balmer lines (Hβ, Hγ and Hδ) as well as the forbidden [O III] $\lambda\lambda$ 4959,5007 lines. In the UV part of spectra we analyze the UV iron lines, as well as the Mg II line. We are focused in comparing properties between optical and UV iron lines, in order to investigate if they have the same place of origin, and to find the physical differences between their emission regions. Also, we investigate the influence of starbursts on AGN spectra.

1.2 Organization of the Thesis

The general overview of the AGN nature is outlined in Chapter 2. It will be followed in Chapter 3 by an introduction to spectroscopy, AGN spectra, spectral properties of the emission lines and their correlations. The sample for this investigation is obtained from the Sloan Digital Sky Survey (SDSS) database, Data Release 7. For the sample selection, SQL search was used to choose the spectra with the specifications required for this investigation. Details about the sample selection can be found in the 4th Chapter.

The obtained spectra were then corrected for the reddening and redshift using the DIPSO software. The continuum emission is subtracted and emission lines from optical and UV part are fitted using Gaussian functions. The emission lines are decomposed to Gaussians with each Gaussian representing the emission from one emission region. The numerous Fe II lines are fitted with the iron template given in paper Kovačević et al., 2010 and Shapovalova et al., 2012. Chapter 4 will contain details on the procedures used for reducing the spectra and fitting of emission lines.

Different parameters of line properties are obtained, as the width, shift, intensity, flux, equivalent width (EW); and they are compared between different lines in the UV and optical part, in order to search for some trends and correlations. The results of these investigations and the analysis of the obtained line parameters are given in Chapter 5. The discussion and conclusions of the work are presented respectively in 6th and 7th chapters.

Chapter 2

Active Galactic Nuclei

Galaxies are gravitationally bound collection of numerous stars and stellar remnants with dust, gas and probably dark matter residing in between the stars. Now-a-days it is widely accepted that most of massive galaxies have a supermassive black hole hidden in their cores (Magorrian et al., 1998; Kormendy and Gebhardt, 2001). In some galaxies, central supermassive black holes feed themselves at very high speed by accreting gas and other matter nearby. The process of accretion is very energetic and produce a high luminosity in the most of wavelengths of the electromagnetic spectrum. The nucleus of such galaxies is so bright that the central region is much more luminous (several order of magnitude) than rest of the host galaxy. These galaxies with a violently accreting massive black hole in its core are so called Active Galactic Nuclei or AGNs (Osterbrock, 1989; Shield et al., 1999; Tadhunter, 2008).

Active galactic nuclei are the most luminous objects in the Universe radiating steadily and powerfully over a vast range of wavelengths. They basically are the galaxies with highly energetic phenomena in the nuclei region whose origin cannot be attributed directly to stars. Theoretical predictions and recent observations suggest that source of radiation is a massive black hole residing in the central region of the galaxy which produces energy by accretion of gas. Central regions of AGNs are expected to be almost similar and are explained by so called Unified Model of AGNs. According to the Unification Model, the variation in AGN properties is just a result of their orientation with respect to the line of sight.

Unlike normal galaxies which emit mainly in the optical spectral range, AGNs emit powerfully over the wide wavelength range of the electromagnetic spectrum from the X-rays to the radio wavelengths. They very often show variability, that depending on wavelengths can be on different time scales, ranging from minutes to years.

AGNs are very luminous and hence can be observed at cosmological distances. Thus they can be used as probes of the intervening matter on cosmic scales. These objects are important for the studies of early Universe and cosmology in general. The study of AGNs is closely related to the subject of Galactic Evolution in general. Moreover they provide extreme environments for exotic physics, as e.g. extremely high gravitational field, supermassive black holes, enormous magnetic fields and highly powerful jets, etc.

2.1 Historical Sketch

In the year 1908, H. S. Lewitt found a relation between the luminosity and pulsation of Cepheids. E. P. Hubble used this relation to find the distance to M31 and showed that it is actually outside our galaxy. Thus, Extragalactic Astrophysics was born. In the same year, E. A. Fath took a spectrum of NGC 1068 (Fath, 1908). Though the spectrum was similar to that of a planetary nebulae but the emission lines were resolved and they had very large widths. So, astronomers knew as early as the beginning of 20th century that there are emission line nuclei in a few galaxies. C. Seyfert (Seyfert, 1943) observed 6 galaxies with a compact nucleus and found their optical spectra to be dominated by high excitation nuclear emission lines with thousands of km/s in widths. But even this systematic study by Seyfert was not enough to launch AGNs as a specific class of objects.

The breakthrough in the study of AGNs came with advances in the radio astronomy. K. Jansky in 1932 started the era of the radio astronomy. G. Reber followed him and made many advancements. The advances in the radio astronomy in the 1950s led to the discovery of quasars. Quasars were at first considered to be strange, exotic stars whose mystery was solved by M. Schmidt in 1963 by realising that these strange objects have a normal

seyfert-like spectra, only highly redshifted (Schmidt, 1963). But with the discovery of quasars commenced another confusion - this high redshift implied a distance of many Mpc. Even at such high distance, these objects have very large luminosity - implying the presence of a source of enormous high energy. To add to the confusion - their variability timescale is very small, which suggests the size of emission region to be very small.

With this confusion began speculations about the nature of these powerful energy sources. In 1958 Victor Hambardzumyan suggested exploding centers of galaxies, while Fred Hoyle in 1961 tried to explain this extreme luminosity as a consequence of chain reaction of supernovae at the center. In 1963 Hoyle and Fowler suggested a supermassive centrally placed star as a source of the gravitational and thermal energy for quasars (Hoyle & Fowler, 1963). The most accepted explanation is that the energy source is accretion onto a supermassive black hole and was first proposed by Salpeter and Zeldovich in 1964 (Salpeter, 1964; Zeldovich, 1964). Later, in 1969, Lyden-Bell put forward the possibility of having collapsed bodies like black holes as the galactic nuclei (Lynden-Bell, 1969). There was no looking back after this point. Since then AGNs have been a vigorous part of astronomy - investigations to know these luminous objects more clearly and precisely have been going on even now-a-days.

2.2 Properties of AGNs

The AGN family includes many different kinds of them having diverse properties. Unfortunately, not all of AGNs possess every property and hence there can not be one single defining list of properties for all AGNs. Nevertheless there are several observational signatures of AGNs which are common for the AGN family :

1. Very compact angular size of the central nuclear emission.
2. High luminosity - The luminosity of a typical AGN is of the order of $10^{12} L_{\odot}$. Such extreme energies can not be produced by stars alone - even the most massive stars emit in the order of around $10^{5} L_{\odot}$.
3. Broad-band continuum emission from the core - SED in AGNs stretches from the radio to gamma rays (see Figure 2.1).

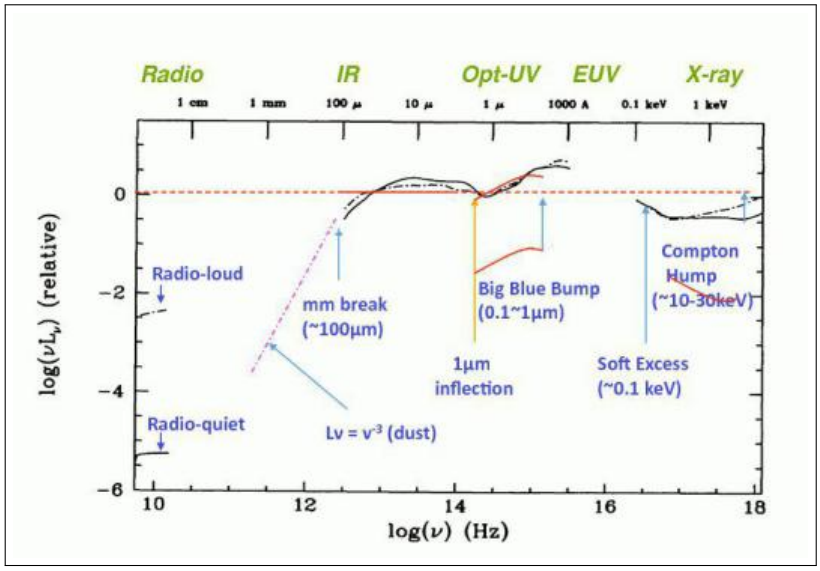

Figure 2.1: Schematic representation of the AGN broadband continuum spectral energy distribution (Elvis et al., 1994).

4. Emission Lines - very prominent with equivalent widths often in the range of ~ 100 Å, both narrow and broad lines are seen.

5. Variability of the continuum and spectral line emission - a strong variability is very strongly correlated with the strong polarization, compact radio structure and strong high-energy γ-ray emission. Moreover the variability is unpredictable and non-periodic - it can range from days to years depending on wavelengths.

6. Strong Radio Emission - many of the known AGNs are strong radio emitters.

2.3 Classification of AGNs

Classification commences the journey of investigation before having a stable and clear understanding of any object.

AGNs are a very heterogeneous group. They have many important and diverse signatures and hence there can be a number of different classification schemes. Classification helps in grouping together AGNs that share certain combinations of specific properties. It also makes easy for one to

identify interesting patterns whose interpretation might lead to many important realisations regarding the origin, structure and physics of these objects. Starting from the variability timescale, optical/radio morphology, luminosity, spectral shape to the presence of the broad/narrow emission lines in their spectra - it is possible to divide the AGNs in different groups. This diversity on classification method makes it flexible to accommodate different AGNs in various groups by taking into account their numerous properties. But this diversity of observational characteristics may also lead us to confusion. There are so many different classifying methods that more than one classification can be applied to each AGN. Moreover, often these classifying schemes just reflect historical differences in how objects were discovered or initially distinguished with a very little insight on the real physical differences in their structure or evolutionary stages.

Few glances of such diverse classification schemes can be found below -

1. **Classification using Optical Spectra** -

   (a) By analysing the optical spectra of AGNs, they are classified as Seyfert 1 (Sy1) and Seyfert 2 (Sy2). Seyferts are normal spiral galaxies with an unusually bright nucleus, boosting of powerful high-excitation emission lines in their spectra. A Seyfert 1 galaxy has both the broad permitted lines and narrow forbidden lines while Seyfert 2 spectra contain only the narrow (permitted and forbidden) lines.

   Based on spectroscopic details, Osterbrock (1981) has introduced some more subclasses of Seyfert galaxies : 1.5, 1.8 and 1.9. In Seyfert 1.9, the broad lines are detectable only for the $H\alpha$ line, while for 1.8, a weak broad Hβ line can be detected also, and for Seyfert 1.5 nuclei, the strengths of broad and narrow Hβ components are comparable.

   (b) There is another very interesting type of Seyferts called as the Narrow Line Seyfert 1 (NLS1) galaxies which have attracted attention for their pecularities and ambiguous characteristics. They were first introduced as a class of AGNs by Osterbrock & Pogge, 1985. This class of AGNs have all properties of type 1 Seyfert

galaxies (broad emission-line optical spectra) but additionally narrower Balmer lines than in Seyfert 1, much stronger Fe II emission (Osterbrock, 1989; Veron-Cetty et al., 2001); a weak [O III] emission (Boller et al., 1996) and extreme X-ray properties - a steep X-ray excess, a steep hard X-ray continuum, and a rapid large-amplitude X-ray variability (Leighly, 1999a; Leighly, 1999b; Leighly, 2000; Panessa et al., 2011).

Moreover, the permitted lines are only slightly broader than the forbidden ones. They have high accretion rates close to the Eddington rate, low black hole masses, perhaps young ages and enhanced radio quiteness (Komossa, 2008). What makes NLS1 more exciting is the fact that this class of AGNs seems to have challenged the Unified Model (Tarchi et al., 2011). Osterbrock & Pogge (1985) have pointed out that the equivalent widths of Balmer emission lines in NLS1s are smaller than typical values for normal Seyfert 1s, suggesting that they are not just normal Seyfert 1s seen at a particular viewing angle.

2. **Classification using Radio Spectra** -
AGNs can be divided according to their Radio Power as Radio-Loud and Radio-Quiet objects. Almost 10 percent of the AGNs are radio-loud while all others fall in the category of radio-quiet objects (Della Ceca et al., 1990). There are different classificatio schemes for these Radio-Loud Objects -

   - Radio Loud AGNs or Radio Galaxies have emission line spectra similar to the Seyferts but they are extremely bright in the radio wavelength range. These radio galaxies can be classified as Broad Line Radio Galaxies (BLRGs) which are just the radio-loud version of Seyfert 1s and Narrow Line Radio Galaxies (NLRGs) which are like Seyfert 2s with no broad emission lines in spectra, but having a strong radio emission.
   - The Radio Loud AGNs can also be divided into two subgroups on the basis of their radio structures - their extension and other observational radio properties. This classification was first suggested by Fanaroff and Riley (Fanaroff & Riley, 1974) and are

hence termed after them as FR I and FR II. FR Is have edge-darkened extended radio structures while the extended radio structures of FR II are edge-brightened. Moreover, FR IIs are intrinsically brighter than FR I radio sources.

- Another classification scheme regarding Radio Loud AGNs help us distinguish these objects in terms of the slope of their radio spectrum - Steep Spectrum Radio Loud Quasars (SSRLQ) and Flat Spectrum Radio Loud Quasars (FSRLQ).

3. Few AGNs show extremely rapid variability in all the frequencies. They have a smooth featurless continuum with a strong and variable radio emission. They are called Blazars and are divided into BL Lac objects having weak lines relative to continuum (Strittmatter et al., 1972) and OVVs or Optically Violent Variables (Penston & Cannon, 1970).

The most convenient and effective way to classify AGNs is based on their spectral characteristics. All AGNs can be classified into four broad types as shown in Figure 2.2.

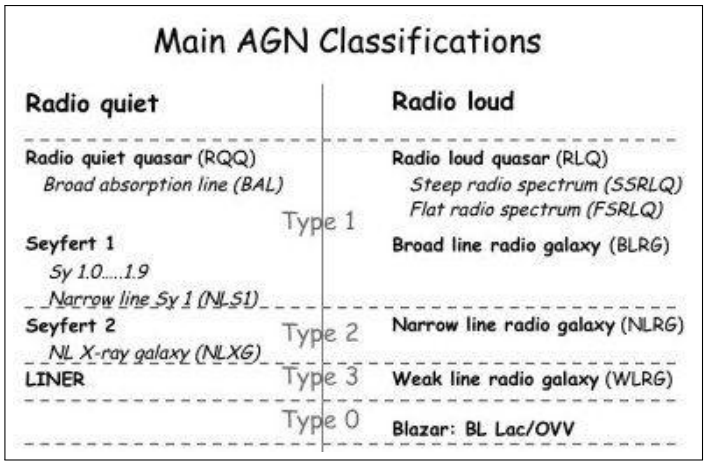

Figure 2.2: Classification labels used for Active Galactic Nuclei (Tadhunter, 2008).

1. AGNs with the broad permitted lines emerging from hot, high-velocity gas that is near the black hole are **Type 1 AGNs**. In the radio-quiet group, these include the Seyfert 1 galaxies and the higher-luminosity radio-quiet quasars. The radio-loud Type 1 AGN are the Broad-Line

Radio Galaxies (BLRG) at low luminosities and radio-loud quasars at high luminosities.

2. AGNs with only narrow emission lines are **Type 2 AGNs**. They have a weak continuum and only narrow emission lines. That means either they do not have any high-velocity gas or the line of sight to such gas is obscured by a thick torus. Radio-quiet Type 2 AGN include Seyfert 2 galaxies at low luminosities, as well as the narrow-emission-line X-ray galaxies. Likely candidates for their high-luminosity are the infrared-luminous IRAS AGN (Sanders et al., 1988; Wills et al., 1993). Radio-loud Type 2 AGN are the Narrow-Line Radio Galaxies (NLRG).

3. **Type 3 AGNs** are the lower luminosity AGNs. They include the Low-Ionization Nuclear Emission-line Regions (LINERs) in the radio-quiet version while the radio-loud counterpart are the Weak-Line Radio Galaxies (WLRGs).

4. Those AGNs showing rapid variability at optical wavelengths are labelled as **Type 0 AGNs**. They include Blazars and OVVs.

The behavior of an AGN can be basically categorised by three major properties - luminosity, broad line strength in its spectra and radio loudness. Keeping these three important features in mind, AGNs classification can be more clearly and compactly summarized in a 3-Dimensional diagram as shown in Figure 2.3 -

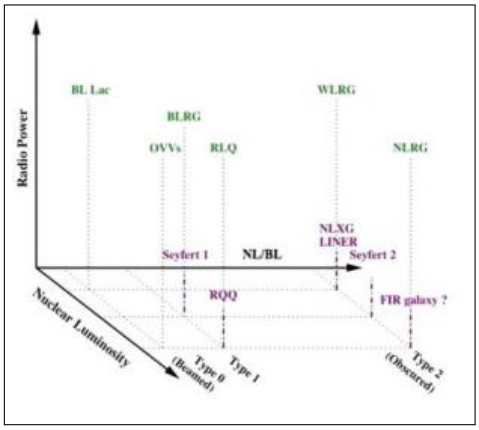

Figure 2.3: 3-dimensional Classification Scheme for Active Galactic Nuclei (Tadhunter, 2008).

2.4 Unified Model of AGNs

According to the Unified Model of AGNs, these classification schemes as presented in Section 2.3 are dominated by the orientation of the AGN with respect to the line of sight of an observer, and not due to some basic intrinsic physical properties. The Unified Model proposes that all AGNs have the same physical characteristics but are being looked at from a different point of view.

2.4.1 Historical Perspective

The idea of an Unified Model for AGNs has stayed around since 1977 and was developed in both radio and optical bands. For optical, Rowan-Robinson (1977) argued for all Seyferts being the same object differing only in the dust opacity surrounding its optical core. Antonucci (1984) made the first sketch of a circumnuclear torus. In the radio band, the development towards a Unified Picture began when Cohen et al. (1977) discovered that the radio jet is moving out at very high speed from an AGN. Thus Beaming Effect came into picture and a relation between FSRLQ and SSRLQ could be established.

At the end of 1980s, astronomers were aware of two distinct mechanisms causing anisotropy - (a) Beaming by a relativistic jet and (b) Obscuration by an optically thick torus. Barthel scheme (Barthel, 1989) combined both of them and the present Unification Model was formed. It started to gain popularity by the mid-80s (see reviews by Lawrence, 1987; Antonucci, 1993; Urry and Padovani, 1995).

Although recently the Unified Model has gained immense popularity and wide acceptance, but it is not completely proved and established yet. There are several open questions and controversies - Singal (1993) raised doubts if viewing angle of relativistic jet can actually unify radio-loud objects. Wilson (Colbert & Bland-Hawthrone) suggested that the dichotomy of radio power is intrinsic and it depends on the angular momentum of the central black hole. Whether the Unification Scheme seems to be the right approach is still open for debate.

2.4.2 AGN Structure from the Unified Model

The Unified Model of AGNs suggests all AGNs to have the same fundamental ingredients as its components. A schematic picture of an AGN is present in Figure 2.4 :

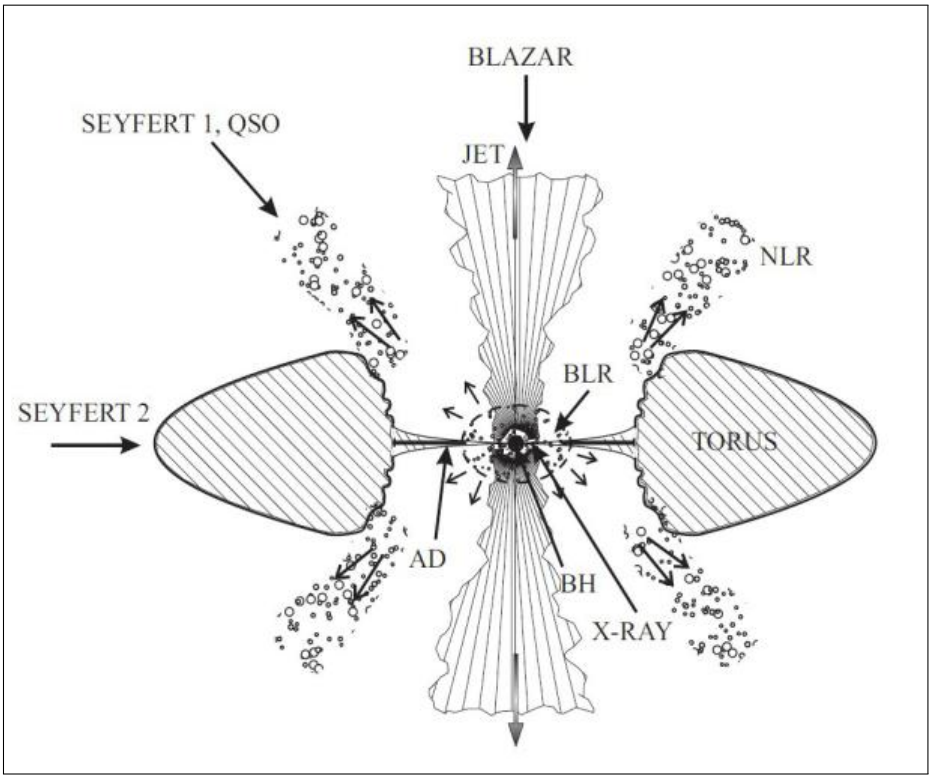

Figure 2.4: The Structure of an AGN where AD is Accretion Disk, BH is Black Hole, BLR implies Broad Line Region and NLR is Narrow Line Region (Jovanović & Popović, 2009).

According to the Unified Model of AGNs, the basic components that we expect to be present in all AGNs are -

- **Supermassive Black Hole** at the central-most region of the AGN with mass ranging from 10^{6-10} $M_{\odot}$ (Kaspi et al., 2000; Peterson et al., 2004).
- **Accretion Disk** that is formed by the material close to the central black hole. The accretion disk transports matter inwards and angular momentum outwards which heats the disk up. It radiates with a peak

in the optical-ultraviolet waveband. This is the energy source at the heart of the AGN - the central engine.

- **Broad Line Region (BLR)** is closer to the black hole comprising of high-velocity gas. It is a compact region, with small dimensions ranging from a couple of light days up to couple of light weeks (Kaspi et al., 2000; Peterson et al., 2004). This region has a higher density ($n > 10^9 cm^3$) and hence there are no forbidden lines coming from the BLR. The broad lines coming from this region are often variable in response to the continuum variability. This unique property can be used to do Reverbation Mapping (Blandford & McKee., 1982, Peterson, 1988, Netzer & Peterson, 1997) in order to find the mass of the central black hole.
  Earlier it was assumed to be consisting of clouds moving in Keplerian orbits around the central black hole. The modern view however is different and it is believed to be comprising of the gas from the accretion disk residing either just above the disk or in the disk wind. It has a very complex structure and most likely it consists of two or more separated subregions (Popović et al., 2004; Ilić et al., 2006; Bon et al., 2009).

- **Narrow Line Region (NLR)** consists of a low-velocity gas - the NLR extends even up to 1 kpc far from the central source (Peterson et al., 2004). This region is less dense ($\sim 10^3 cm^{-3}$) and have temperatures ranging from 10,000 to 20,000 K. These conditions are optimal for producing the forbidden lines. They are spread out further from the center and the dusty torus. Hence the NLR is always in view, so narrow lines will be seen even if the broad-line emitting gas is obscured.

- **Obscuring Torus** represents the gas and dust which being optically thick can hide the broad line region for certain orientations. This torus accounts for the strong infrared emission coming from AGNs.

- **Relativistic Jets** are present in all Radio-Loud AGNs. These jets are basically highly collimated and fast outflows that emerge in opposite directions from close to the disk and extend outwards for some kpc or Mpc

2.4.3 Arguments supporting the Unified Model

Few arguments for Orientation Unification scenario supporting the Obscuration Hypothesis :

- Antonucci & Miller (1985) found **hidden polarized broad lines** in the Type 2 Seyfert NGC 1068 and suggested that "the continuum and broad-line regions are located inside an optically and geometrically thick disk. Continuum and broad-line photons are scattered into the line of sight by free electrons above and below the disk." More examples like NGC 1068 have been found by Miller & Goodrich (1990) , thereby making this evidence more and more powerful.

- While Seyfert 1s show a star-like bright nuclei with a powerful featureless continuum that is variable on time-scales of weeks, the **Seyfert 2s have a featureless continuum** with weak or non-existant broad lines which do not vary. Even the Seyfert 2s that display polarized broad lines have a weak featureless continuum with the same polarization as the broad lines. The one and most obvious implication of this is the presence of something obscuring an observer's direct view of Seyferty2 nuclei so that only the scattered light from the AGN is visible.

- The **OH megamaser structure** detected in the nucleus of a Seyfert 1 AGN named Mrk 231 is best modelled as the inner wall of a rotating torus with obscuration angle of 60 degrees (Klockner et al., 2003).The detected CO emission can be considered as the outer radius.

- There were **suggestions for alternate theories** like the two types of Seyferts representing evolutionary stages in which the Sy1 nucleus switches off to produce the Sy2 state once the BLR gas has de-excited (Roy et al., 1994; Penston & Perez, 1984). But the space density of Seyferts is almost 2:1, with Seyfert 2 being more in number. Such a ratio can not be explained by switched-off Seyfert 1s as their predicted NLR excitation properties are different from the observed ones.

- **NLRs are sometimes cone-shaped** (Pogge, 1989; Evans et al., 1991; Evans et al., 1994) which is specially evident in well-resolved cases. Ionizing radiation seems to be roughly collimated before emerging into the NLR, which suggests the presence of an obscuring torus

or some prebeaming phenomenon by the accretion or its atmosphere (Kriss et al., 1994).

- The **X-ray spectrum** of the Seyfert 2s seems to have large absorbing columns compared to the Seyfert 1s (Mushotzky, 1982; Pounds et al., 1990).

- The optical-UV continuum flux needed to ionize the Seyfert 2 NLR is much larger than that seen directly. This is known as the **Photon-Deficit problem** (Neugebauer et al., 1980; Binette et al., 1993). This can be successfully explained by invoking anisotropic absorption around the continuum source.

- Moreover, HST imaging of the radio galaxy NGC 4261 at 5429 Åreveals a thin extended disk of obscuration (Jaffe et al., 1993). VLBA observations of the nucleus of NGC 1068 (Seyfert 2) at 8.4 GHz reveals a small elongated structure, probably an ionized disk of $\sim$ 1.2 pc (Gallimore et al., 1997) that radiates a free-free continuum or scattered light.

2.4.4 Arguments criticizing the Unified Model

Listed below are few strong points against the Orientation-based Unification Models :

- There are **problems regarding the Polarization Levels** as in the most of the Seyfert 2s, the continuum is seen in direct light while the broad lines are just seen in polarized light which can not be explained clearly with Unification Models. Also, the continuum is polarized at a lower level compared to the broad lines (Miller & Goodrich, 1990; Tran, 1995).

- Few **Seyferts change type in a very short timescale**, which is too fast to be explained by a cloud moving into our line of sight. Such events encouraged the proposal of considering Seyfert 2s as switched-off Seyfert 1s (Roy et al., 1994; Penston & Perez, 1984).

- It is not common to have a **scattered BLR in the Seyfert 2s** (Cid Fernades & Terlevich, 1995). But going by the Unification Model one

expects more frequent detection of the polarized scattered light from BLRs of Seyfert 2s.

- Though we see many Seyfert 2s, finding a narrow line QSO is not so easy. This curious **absence of radio-loud counterpart of Seyfert 2** can be explained by a modified unification scheme of a Receeding Torus Model (Hill et al., 1996).

- In the Unification Model Scenario, we can not fit in the **Weak Line Radio Galaxies** (WLRGs) with either anisotropy or beaming effect (Tadhunter, 2008). Moreover, the **status of BLRGs** is not clear under this Unification Scheme.

- Moreover, we assume that the obscuration in AGNs is by a compact torus made of gas and dust and the distribution of Interstellar Medium (ISM) remains fixed over the complete lifetime of an AGN. But the high resolution **observation reveals much extended ISM distribution** in the form of dust lanes. Moreover, making these assumptions questionable, we have found direct kinematic evidence for outflows in the few AGNs (Nesvadba et al., 2008).

The Unification Scheme hence can successfully explain many AGN characteristics and properties but some questions remain. It is still too simplified but it is the best explanation we have for developing a common model for an AGN.

Chapter 3

AGN Spectroscopy

3.1 Spectroscopy in Astrophysics

Astronomical spectroscopy has been invited since 1814 when Joseph von Fraunhofer recorded the first-ever astronomical spectrum and observed absorption lines in a diffracted beam of sunlight. Gustav Kirchoff and Robert Bunsen's experiments in the mid-19th century gave one the initial clues to understand the Fraunhofer's lines. With the arrival of 20th century came better and deeper understanding of these lines, thanks to the immense advancements in the quantum mechanics.

Electromagnetic radiation is the main carrier of information from all the extra-solar objects. The light emitted by the astronomical objects is the main source of almost all the useful knowledge we have gained till now about them. The most detailed analysis of these message-carrier electromagnetic radiation is done by the use of spectroscopy. It is basically the measurement of the radiation intensity as a function of wavelength. These spectra provide a very useful and efficient tool to explore the farthest of astronomical objets and extract informations about their physical properties. Knowledge of atomic and molecular physics is the key to interpret any astronomical spectra.

Many general things about the emitting object can be inferred from these spectra and the strengths, positions and the widths of the spectral lines -

- **Chemical Composition** - By determining which atoms are produc-

ing which transitions, we can list the composition of astronomical objects with a detailed information about the ions and molecules present there.

- **Abundance of the species** - Strength of a transition determines the number of atoms undergoing that transition. So, to find abundance of a particular species we just need to know the intrinsic strength of the transition being observed.

- **Physical Environment of the Region** - The different states involved in the transitions for one particular atom lead us to the informations on the degree of excitation and hence the temperature and density of the environment prevailing in that region. Moreover, emission line profiles and their broadening sheds light on the pressure and density of the emitting/absorbing gas. Pressure broadening is broadening of the lines due to collissions while the doppler broadening arises because of the thermal random motion of emitters.

- **Motion and Velocity of the Component Gases** - The motion of the species with respect to the observer is manifested on spectra as a change in the line position. This line shift in the wavelength is called Doppler shift and it gives an idea of the motion and velocity of the object with respect to an observer.

- **Magnetic Field** - Splitting of spectral lines - whenever present - and the degree of separation between the component of the splitted spectral line (Zeeman Effect) sheds light on the strength of the magnetic field whenever present.

3.2 Spectrum of a Galaxy - Normal and Active

The spectrum of a galaxy is the composite spectrum of all its components - the spectra from the billions of stars that it contains, the star-forming HII regions, other gases in a number of molecular clouds etc. Generally the continuum in the spectra is a result of all the black-body spectra coming from individual stars ranging over a distribution of temperatures. The atoms and molecules in stellar atmospheres and the cold gas in ISM absorbs these lines at specific wavelengths and absorption lines are formed in galaxy spectra.

On the other hand, emission lines are produced by the hot ionized gas surrounding the energetic and high-mass young stars.

Elliptical galaxy spectra are characterized by strong absorption lines due to metals and absence of emission lines due to the absence of young stars and gas. **Spiral galaxy** spectra, on the other hand, are characterized by strong emission lines owing to the heated gas surrounding hot young stars. They also have a few absorption features due to the older stellar population contained in them. **Irregular galaxy** spectra also have strong emission lines because of the hot young stars and surrounding HII regions.

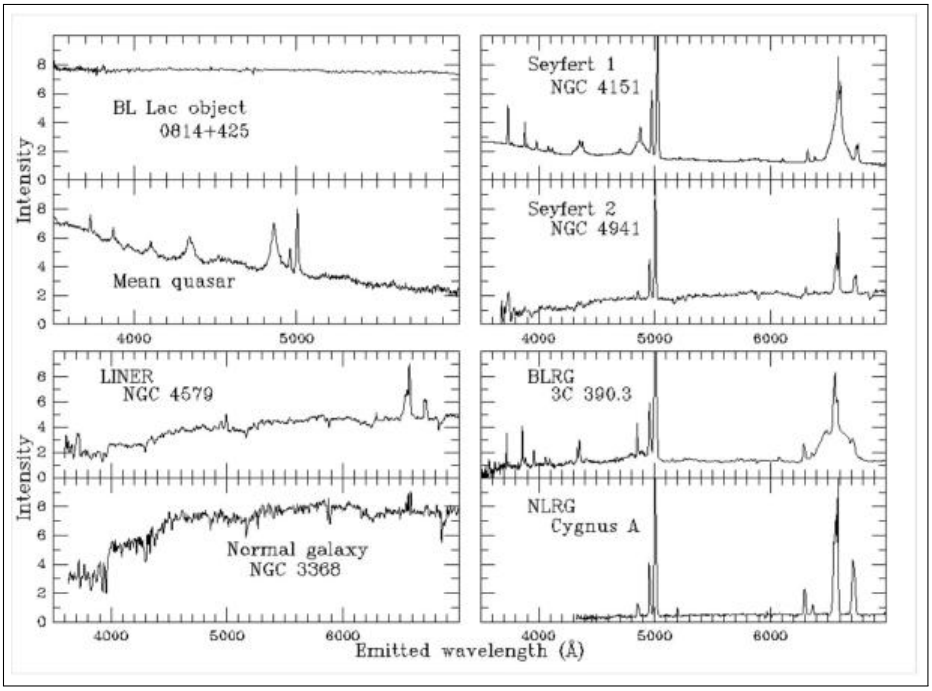

Figure 3.1: Different kinds of normal and active galaxy spectra (Credit: Bill Keel) - NGC 4941 and NGC 4579 are from observations by Keel in Keel (W. C.). The "mean quasar" spectrum is from a composite generated in Francis et al. (1991). The spectra for 0814+425 and 3C 390.3 are from Lawrence et al. (1996). Cygnus A spectra was published by Owne et al. (1990).The normal-galaxy spectrum of NGC 3368 is from the spectroscopic atlas of galaxies produced by Rob Kennicutt.

Active Galaxies have more powerful radiation and are characterised by very strong and bright emission lines relative to a low intensity continuum.

Moreover, the Spectral Energy Distributions (SED) of normal galaxies peak at optical wavelengths while the SEDs of active galaxies emit across a wide range of wavelengths. In addition this, unlike the normal galaxies, an Active Galaxy spectrum is variable - with a broad range of variability from hours to years. The spectra of different AGNs have different behaviour (see Figure 3.1).

Various classes of AGNs have their own trademark spectra. **Seyfert 1** galaxies have both narrow and broad emission lines in their optical spectra. On the other hand, **Seyfert 2** galaxies have only narrow emission lines (Khachikian & Weedman, 1974). A **Quasar** spectrum is similar to that of a Seyfert but they have weak or no stellar absorption features, the narrow emission lines are weaker than the broad lines and the bumps of Fe II emission are more prominent.

The **Radio Galaxies** can also be divided in two types according to their spectra and their counterparts in Seyferts can be identified accordingly - **BLRGs** having both broad and narrow emission lines like Seyfert 1s and **NLRGs** containing only narrow lines like that of the type 2 Seyferts.

BL Lacertae objects have virtually featureless continuum with rapid large-amplitude optical variability in flux and polarization and with strong and variable radio emission (Bregman, 1990).

3.3 Continuum in AGN Spectra

AGNs have a complex continuum spectra (Spectral Energy Distribution - SED, see Figure 3.2) that can be loosely approximated as a power law of the form $F_\nu \propto \nu^{-\alpha}$ with α ranging from 0 to 1. Although this power law assumption is reasonable enough, it shows some additional features like the **Big Blue Bump** at wavelength shortwards of $\sim$ 4000 Å which extends till $\sim$ 1000 Å. High-energy end of this feature is in the X-ray region and is called **Soft X-ray excess**. There is another smooth bump at wavelengths longward of $\sim 1\mu$m and is referred to as the **IR Bump**. In the vicinity of $\sim 1\mu$m is a local minimum. For the radio-quiet AGNs, the SED decreases sharply at low energies starting from the **Millimeter break**.

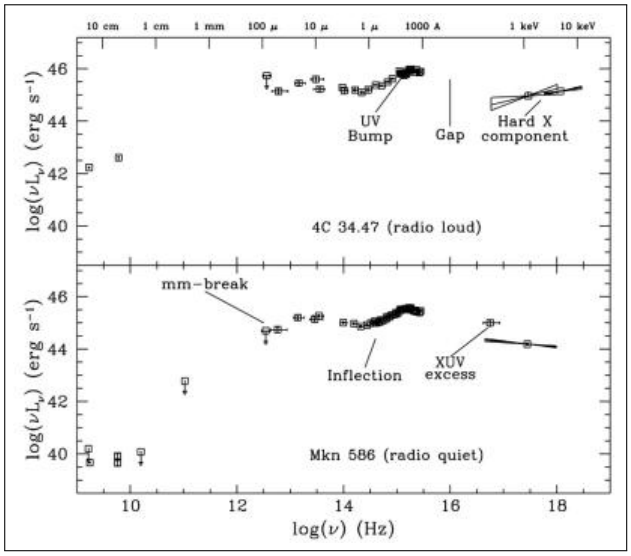

Figure 3.2: The typical AGN SED showing all its major features (Elvis et al., 1994)

3.3.1 AGN Continuum in the UV-optical range

The most prominent feature in the continuum of these wavelength ranges is the above-mentioned Big Blue Bump which is thought to be a thermal emission in $10^4 - 10^6$ K. Many authors consider it to be the emission from Accretion Disk (Shields, 1978; Malkan & Sargent, 1982). For an accretion disk surrounding a 10^8 $M_\odot$ Black Hole and accreting at Eddington Rate, the expected emitting wavelength is $\sim$ 100 Å and hence the continuum in this wavelength range helds special promises for investigating evidence of an accretion disk structure.

But a thin accretion disk as source of UV-optical continua is questionable due to several reasons like the simultaneity of the UV and optical continuum. This opens up many other possible explanations for the source of continuum at this λ range. Barvainis (1993) suggested that the UV-optical continuum represents an optically thin Bremmstrahlung emission rather than the optically thick black body emission. Malkan & Sargent (1982) showed that both these explanations fit the observed SED quite well. But all these models have their own limitations and the origin of the UV-optical continuum is still debatable.

3.4 Emission lines in AGN Spectra

Emission lines in AGN spectra can be divided into two types - permitted and forbidden lines. The permitted lines or the recombination lines result from free electrons recombining with mostly hydrogen nuclei and cascading down to the ground state while the forbidden line emission is typically excited by collisions in the NLR. The forbidden lines have extremely low transition probabilities and are emitted by atoms undergoing transitions that are normally not allowed by the LS selection rules of quantum mechanics. The permitted line emission is seen from both the BLR and NLR whereas forbidden line emission is typical for only NLR conditions.

3.4.1 Informations from emission lines

A spectral line is described by the position, width and line strength or intensity.

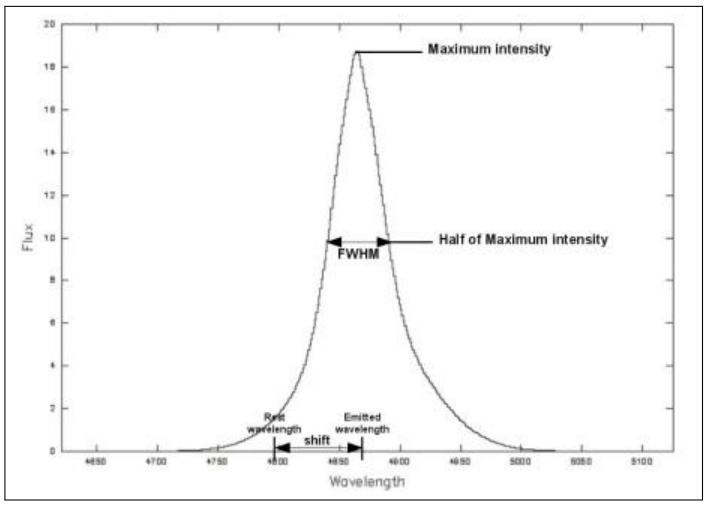

Figure 3.3: Different Line Parameters shown on a Hβ Balmer line - position (emitted wavelength), intensity, shift and full width at half maximum (FWHM)

The **line position** is basically the central wavelength where it is emitted - it helps to determine the Doppler shift and hence the motion of atomic species with respect to the observer. The width of a spectral line is most commonly expressed as the **Full Width at Half Maximum** (FWHM) and it is the line width when its strength is half of the total intensity. Another

important line parameter is the **Equivalent Width** (EW). The EW of a spectral line is again a measure of the line area on a intensity-vs-wavelength plot. It is measured by forming a rectangle with a height equal to that of the continuum emission, and finding the width such that the area of the rectangle is equal to the area in the spectral line. **Line flux** or strength is determined by the area under the line shape which basically is the integral of it's energy versus wavelength.

Emission line profiles provide important clue to the dynamics of the emission region. Lines are broadened due to several other mechanisms. Their broadening pattern and strength gives one an insight to the physical processes causing the broadening.

Asymmetry in line sheds light on anisotropy in the line emission, existence of inhomogeneities and outflow processes in the emission region, etc. The origin of these asymmetries are thought to be arising either due to Anisotropic line emission from radially moving clouds or due to a velocity difference between the centroids of the different emission regions (Corbin, 1995).

These line parameters depend on physics, geometry and kinematics of the emitting regions. Intrinsically, there is a very small natural width of every emission line owing to the quantum mechanical uncertainity in energy levels with finite lifetime. This **natural broadening** of a line is very small.

In high density environments, there is **collissional broadening** of the line. The collision of neighbour particles with the emitting particle shortens the characteristic time for the emission process and increases the uncertainty in the energy emitted. This results in broadening of the line. Another process resulting into line broadening is the thermal **Doppler broadening**. This is caused by the relative velocities of different atoms with respect to the observer. When temperatuure of the gas is high, the velocity distribution of the gas becomes wider. Thus the line profile broadens. Hence by analysing the broadening of a line, we can estimate the temperature, pressure and density of the emitting region.

Size and structure of the BLR can be obtained by observing delayed response of emission lines to variations in the continuum by the process called **Reverberation Mapping** (Blandford & McKee., 1982; Peterson, 1988; Netzer & Peterson, 1997).

The forbidden lines are very efficient in providing basic informations about the physical environment of the NLR. The intensity ratio of the [SII] $\lambda\lambda 6716, 6731$ or [OII] $\lambda\lambda 3726, 3729$ doublet can be used to estimate the electron density of the NLR while intensity ratio of lines arising from the same ion but having different excitation potentials like the [OIII] $\lambda\lambda 4363, 4959, 5007$ triplet or [NII] $\lambda\lambda 5755, 6548, 6583$ intensity ratios gives the NLR temperature. The typical value of NLR temperature is $\sim$ 16000 K (Koski, 1978). Moreover, by plotting different line ratios we can distinguish between Seyferts, LINERs and starbust galaxies (Baldwin et al., 1981; Veilleux & Osterbrock, 1987). These are the famous BPT diagrams.

3.4.2 The UV and Optical emission lines in AGNs

The spectrum of an AGN has several strong, broad emission lines in the optical and UV band (see Figure 3.4).

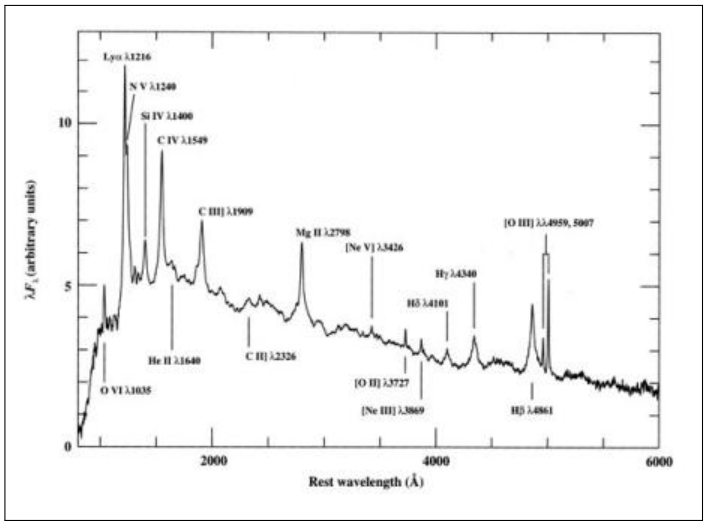

Figure 3.4: A quasar composite spectra with emission features labeled by ions (Francis et al., 1991).

In this thesis, we will be doing detailed analysis of these wavelength ranges of AGN spectra. Here we describe the most prominent line emissions in these wavelength ranges, that will be analysed further in this thesis.

- Balmer lines (Hβ, Hγ, Hδ) and Mg II λ 2798 are few of the most prominent emission lines in this range.
- The region between Hβ and Hγ is covered by a very broad spectral feature owing its origin to number of weak blended Fe II lines combined with He II λ 4686. A similar Fe II blend is also seen at λ longward of Hβ (Osterbrock, 1977).
- Forbidden lines are generally absent in broad-line spectra. In contrast, NLR spectra allow many forbidden transitions owing to its low density and we find many forbidden lines like [O II] $\lambda\lambda$ 3726,3729; [O III] $\lambda\lambda$4363,4959,5007; [N II] $\lambda\lambda$ 5755,6548,6583, etc.
- From $\sim 2000\mathring{A}$ to $\sim 4000\mathring{A}$ lies another strong blended feature consisting of the blended Fe II emission lines and Balmer continuum emission (Wills et al., 1985) and is termed as the Small Blue Bump (see Figure 3.5).

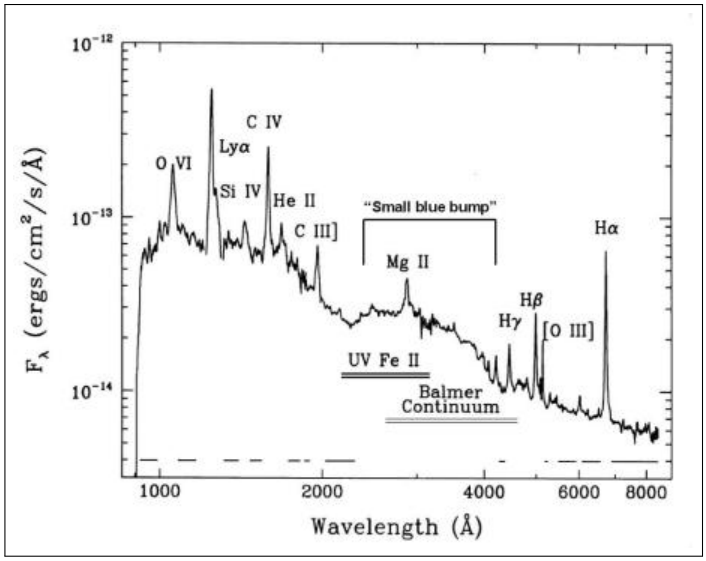

Figure 3.5: The Fe II blend and Balmer continuum comprising the Small Blue Bump from 2000 Å to 4000 Å in Seyfert 1 Mrk 335 (Zheng et al., 1995).

3.5 Spectral Property Correlations in AGNs

3.5.1 Need for Correlation between spectral properties

One can obtain physical parameters of an AGN and it's emission line regions by exploring it's spectrum - spectral line features like widths, shifts and fluxes of different lines arising due to transitions of different atoms, continuum properties, clues for the density and temperature of different regions, informations on polarizations and magnetic field, radio strength and X-ray properties, black hole masses, etc.

These observed properties are believed to be controlled by a few physical parameters. Which parameters are the most influencial ones is still a doubtful question. It is interesting to find some connections between these observables and the physical processes as that would help in answering many open questions regarding physical and kinematic properties of the AGN emission regions and their geometry.

3.5.2 Few important correlations

In order to understand the physics of line-emitting regions, many attempts have been made till now to find correlations and trends among different observable properties of AGNs and relate these correlations to some physical processes and parameters (Boroson & Green, 1992; Gaskell, 1985; Baldwin, 1977; Dong et al., 2009; Kovačević et al., 2010; Popović & Kovačević, 2011). The former of these two goals have been achieved by many but the later is an area which has not yet been successfully explored.

Few of these interesting trends and correlations are -

1. Boroson & Green (1992) have tried to find correlation between many spectral properties of AGNs and have discovered a very interesting correlation - as the Equivalent Width (EW) of Fe II increases, EW [O III] and FWHM Hβ decreases. These correlations are related to what they have termed as EV1 (Eigenvector 1) in Boroson & Green (1992). The physical cause of EV1 is yet to be understood.

2. Another such interesting correlation is known as the Baldwin Effect (Baldwin, 1977) - as the continuum luminosity increases, most of the

emission lines show a decrease in their EWs. Origin of the Baldwin Effect is also not yet understood clearly. However recently, quite interestingly there is a proposal of the Baldwin Effect to be related to EV1 (Dong et al., 2009; Kovačević et al., 2010).

3. There are interesting correlation between kinematic properties of the Fe II lines and the Balmer Line ILR component (Marziani and Sulentic, 1993; Popović et al., 2004; Kovačević et al., 2010) suggesting that the ILR (Intermediate Line Region) is the emission line region of the Fe II lines too.

These correlations, if analysed properly can lead us to a much better and deeper understanding of the emission regions and the geometry of the AGNs. But for that one needs to find the physical causes of these correlations. There have been many suggestions regarding the possible influencial properties, a few strong suggestions are :

- Eddington Ratio (Boroson & Green, 1992; Baskin & Laor, 2004)
- Black Hole Mass (Boroson, 2002)
- Inclination Angle (Miley and Miller, 1979; Wills & Browne, 1986; Marziani et al., 2001)

But as mentioned in the Introduction, there are many questions yet to be answered regarding the cause behind these correlations. Nevertheless, these investigations have the potential to take us to the next breakthrough in the area of AGNs and provide us with new informations on the geometry, physics and kinematics of different regions in AGNs.

Chapter 4

Sample and Method of Analysis

4.1 Sample Source - SDSS

We have taken spectra for our sample from SDSS (Sloan Digital Sky Survey) 7th Data Release (Abazajian et al., 2009). SDSS, in work since April 2000, is one of the most influential surveys in the Astronomical History of mankind. It has two concurrent surveys - photometric and spectroscopic.

It has a CCD camera with wide-field imaging to image the sky in five optical bands and two spectrographs - one covering a wavelength range of 3800 Å to 6150 Å and the other from 5800 Å to 9200 Å. The spectral resolution ranges from 1850 to 2200. This telescope covers more than a quarter of the sky and contains more than 930,000 galaxies and more than 120,000 quasars. SDSS is an open data source and all its images, spectra and other resources are open for general public, amature astronomers and scientific educators (Szalay et al., 2003). The advantage of using SDSS for AGN emission-line studies is that it allows one to have a large and uniformly selected sample.

The telescope dedicated for SDSS is a 2.5 meter altitude-azimuthal telescope located in the Apache Point Observatory, New Mexico (York et al., 2000). It is equipped with a 120-megapixel camera which is used to image 1.5 square degrees of sky at a time. The telescope also contains a pair of spectrographs capable of measuring more than 600 spectra in a single

observation. To manage the enormous and high-speed data flow from the telescope, a custom-designed set of software pipelines have been created.

The data is then reduced and within a week or two of the observation, the reduced data is made available to the SDSS astronomers for validation and analysis. These SDSS published data are made available to everyone after one year of observation. This data can be accessed via the SkyServer on the internet (http://skyserver.sdss.org/). SDSS data has a high spectral resolution. The spectral wavelength coverage is large. They have a good photometric calibration since each SDSS multifiber observation contains numerous standard stars and can be individually calibrated. And it has huge database sorted out nicely in order to find specific data with one simple search form.

4.2 Sample Selection

4.2.1 Specifications for Selection

For our work, we needed a good quality sample consisting of AGNs with the following specific properties :

1. High Signal to Noise Ratio (S/N $>$ 25)
2. Redshift Range of 0.4 to 0.6 so as to cover most of the Balmer series (Hβ, Hγ and Hδ), Mg II emission lines and the optical and UV FeII lines in the spectral range
3. High Redshift Confidence (zConf $>$ 0.95)

4.2.2 SQL Method to Select Samples

All the information of the SDSS is stored in a database. To search for objects with specified properties from the huge database of SDSS, we can send some queries requesting for information. The most effective way to do so is by directly submitting an SQL (Structured Query Language) query to the SDSS database server.

To find all the quasars with the above mentioned criteria, the SQL given in Figure 4.1 has been used.

```
SELECT SpecObj.SpecObjID, SpecObj.plate, SpecObj.mjd, SpecObj.fiberID, SpecObj.z,
SpecObj.sn_0

FROM SpecObj
JOIN SpecLine as L1 ON SpecObj.SpecObjID = L1.SpecObjID
JOIN SpecLine as L2 ON SpecObj.SpecObjID = L2.SpecObjID
JOIN SpecLineNames as LN1 ON L1.LineId = LN1.value
JOIN SpecLineNames as LN2 ON L2.LineId = LN2.value

WHERE LN1.name = 'Hb_4863'
and LN2.name = 'MgII_2799'
and L1.ew > 0
and L2.ew > 0
AND SpecObj.z between 0.407 and 0.643 and
SpecObj.zConf > 0.95 and
SpecObj.sn_0>25 and
specObj.specClass = 3
```

Figure 4.1: The SQL format used to search for SDSS Quasars fulfilling our specific requirements .

We extracted 333 quasar spectra with these criteria.

4.2.3 The Subsample

Within our sample we tried to make a subsample containing all the spectra with negligible stellar contribution. This was achieved by selecting all the spectra with the absorption lines CaK 3934 Å, Mg 5177 Å and Hδ 4102 Å having Equivalent Width less than 1 Å. The SQL run to extract these spectra is shown in Figure 4.2.

121 spectra out of our sample of 333 featured in this subsample list.

Of these 121 spectra, 83 were common with the sample list of Kovačević et al. (2010) where they have analysed optical Fe II line emission in a sample of AGN spectra with negligible stellar contribution. We have chosen these 83 spectra and have added 17 more spectra from the rest of our sample to see the differences between these two and also to have an unbiased sample.

Thus, 100 spectra were finally taken for our analysis.

```
SELECT SpecObj.SpecObjID, SpecObj.plate, SpecObj.mjd, SpecObj.fiberID, SpecObj.z,
SpecObj.sn_0

FROM SpecObj
JOIN SpecLine as L1 ON SpecObj.SpecObjID = L1.SpecObjID
JOIN SpecLine as L2 ON SpecObj.SpecObjID = L2.SpecObjID
JOIN SpecLine as L3 ON SpecObj.SpecObjID = L3.SpecObjID
JOIN SpecLine as L4 ON SpecObj.SpecObjID = L4.SpecObjID
JOIN SpecLine as L5 ON SpecObj.SpecObjID = L5.SpecObjID
JOIN SpecLineNames as LN1 ON L1.LineId = LN1.value
JOIN SpecLineNames as LN2 ON L2.LineId = LN2.value
JOIN SpecLineNames as LN3 ON L3.LineId = LN3.value
JOIN SpecLineNames as LN4 ON L4.LineId = LN4.value
JOIN SpecLineNames as LN5 ON L5.LineId = LN5.value

WHERE LN1.name = 'Hb_4863'
and LN2.name = 'MgII_2799'
and LN3.name = 'K_3935'
and LN4.name = 'Mg_5177'
and LN5.name = 'Hd_4103'
and L1.ew > 0
and L2.ew > 0
and L3.ew > -1
and L4.ew > -1
and L5.ew > -1
AND SpecObj.z between 0.407 and 0.643 and
SpecObj.zConf > 0.95 and
SpecObj.sn_0>25 and
specObj.specClass = 3
```

Figure 4.2: The SQL format used to search for a subsample of quasars with negligible stellar contribution .

4.3 Preparing the SDSS Spectra

De-redshifting, reddening corrections and the continuum subtraction of the spectra were done using the DIPSO plotting package. [1]

The redshift values and correction values for reddening were taken from the database of SDSS Skyserver.

[1]DIPSO is a plotting package with many basic astronomical applications incorporated in it. (see http://www.starlink.rl.ac.uk/docs/sun50.htx/sun50.html)

4.3.1 Continuum Subtraction

Continuum subtraction was done seperately for the optical and the UV range as we analysed both these wavelength ranges separately.

Continuum Subtraction in the Optical Range

To subtract the continuum in the optical range, we first drew the continuum level by using continuum windows given in the paper of Kuraszkiewicz et al. (2002). These continuum windows are at wavelengths without any emission line features. The windows that we used in the optical range are 3010-3040 Å, 3240-3270 Å, 3790-3810 Å, 4210-4230 Å, 5080-5100 Å, 5600-5630 Å and 5970-6000 Å. The continuum level is determined by interpolating between these points (see Figure 4.3). For the subtraction purpose we used the DIPSO software.

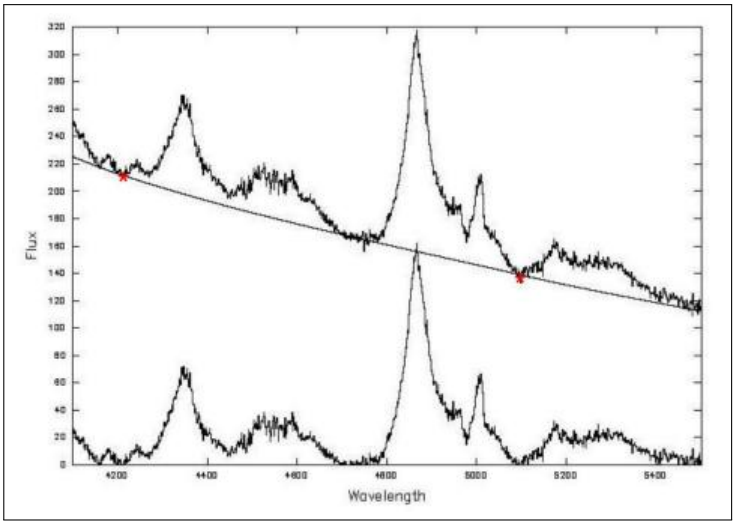

Figure 4.3: The continuum subtraction in the optical part of the QSO spectrum SDSS J210001.25-071136.34 using DIPSO software. The two continuum windows given in this wavelength range are shown as asterisks. The same spectrum has been shown prior to and after the subtraction of the continuum (the spectrum at the bottom)

The same procedure has been used to remove the continuum contribution from the optcal range of all 100 spectra in our sample.

Continuum Subtraction in the UV Range

To subtract the continuum from the UV part of the spectra by using only continuum windows is tricky because of the complex shape of the continuum which is a combination of the power law, Fe II pseudo-continuum and the Balmer continuum (Grandi, 1982). Moreover, to cover the Fe II lines in both optical and UV range, we have selected our sample spectra to be within the spectral range: 2900 Å - 5500 Å. This leaves us with less continuum windows than what is required to reproduce the continuum level effectively. There have been a number of models suggested by different authors to fit the continuum in the UV range considering all the possible contribution (e.g. Tsuzuki et al., 2006). But there is no one satisfactory model for it yet and trials to find the perfect continuum fit still continues (Sameshima et al., 2011).

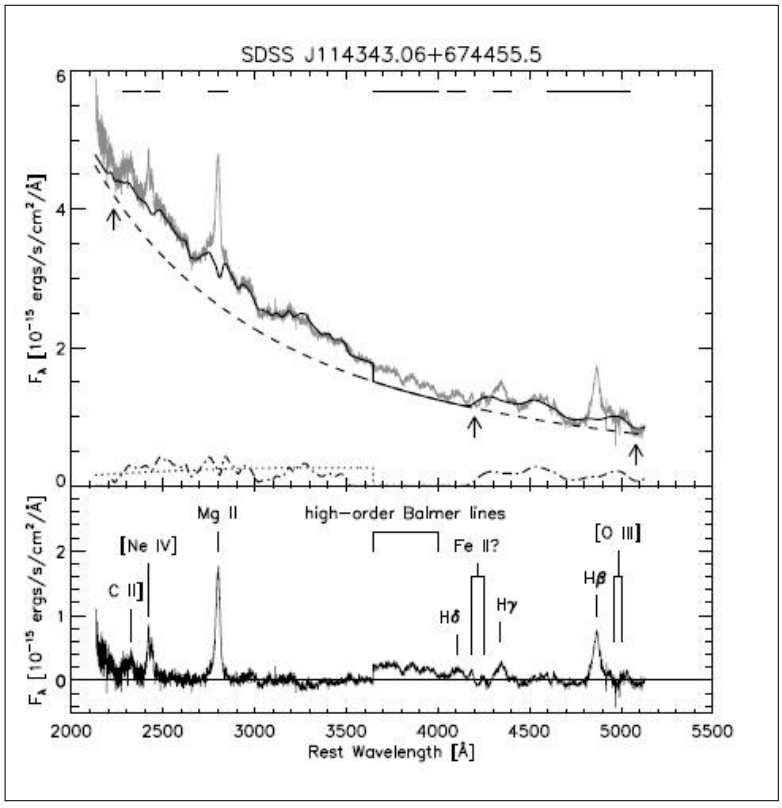

Figure 4.4: Continuum subtraction in UV part of a sample QSO Spectra (Sameshima et al., 2011).

As evident from the Figure 4.4, there are still modifications needed in the continuum model as we can see a non-physical discontinuity near $\sim 3600\mathring{A}$ after the Balmer edge. We tried to make a model which we could use for fitting spectra within the 2900 Å to 5500 Å range (with less number of continuum windows than needed). And we try to make a good fit near the Balmer edge ($\sim 3646\mathring{A}$).

Our model consists of a Power law, the Balmer continuum ($\lambda < 3646\mathring{A}$) and high order Balmer lines (n=3-400) with $\lambda > 3646\mathring{A}$.

- **Power Law Continuum** - Power law continuum is simply given as

$$F_{\lambda}^{cont} = F_{5100}\left(\frac{\lambda}{5100}\right)^{\alpha}$$

  It has the power-law index α and the scaling factor F_{5100} as the free parameters

- **Balmer Continuum** - Balmer continuum produced by a uniform temperature, partially optically thick cloud is given in Grandi (1982) as

$$F_{BaC}B_{\lambda}(T_e)\left[1-\exp\left\{-\tau_{BE}\left(\frac{\lambda}{\lambda_{BE}}\right)^{3}\right\}\right]$$

  where $B_{\lambda}(T_e)$ is the Planck function at electron temperature T_e

$$B_{\lambda}(T) = \frac{2hc^2}{\lambda^5}\frac{1}{e^{\frac{hc}{\lambda k_B T}}-1}$$

  and τ_{BE} is the optical depth at Balmer edge ($\lambda = 3646\mathring{A}$). This formula has been frequently used by many authors to fit the Balmer continuum (Kurk et al., 2007; Dietrich et al., 2003). This same formula has been used by us to estimate the strength of the Balmer continuum.

- **High order Balmer lines** - This is one additional component we have included to fit the UV-optical continuum more accurately. We are fitting them by one Gaussian with the same width and shift as H_γ. The relative intensites for Balmer lines with $n < 50$ are taken from the paper Storey & Hummer (1995) while the relative intensities for $50 < n < 400$ are calculated using the approximate formula:

$$\frac{I_1}{I_2} = \frac{b_1(T, N_e)}{b_2(T, N_e)} \left(\frac{\lambda_2}{\lambda_1}\right)^3 \frac{f_1}{f_2} \cdot \frac{g_1}{g_2} \cdot e^{-(E1-E2)/kT}$$

An example of the continuum subtraction in the UV part of the spectra using our model can be seen below in Figure 4.5.

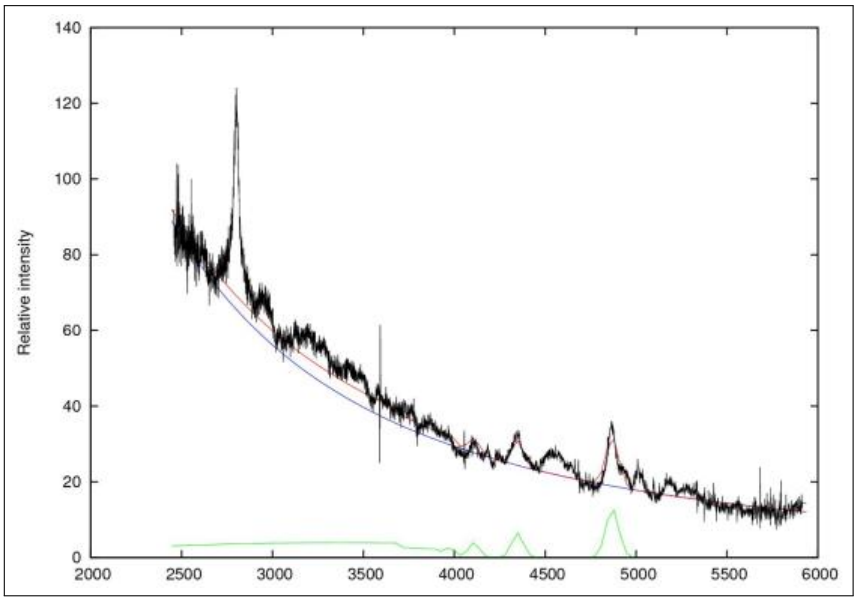

Figure 4.5: Continuum subtraction in the UV part of SDSS J223500.74-101216.83 spectrum using our model. Here the bold blackline shows the observed spectra. The green line in the bottom composes of the Balmer continuum with the high order Balmer lines. The blue line shows the power law continuum and the red line is the addition of both - representing the total UV continuum.

So we conclude that the intensity of the Balmer continuum near Balmer edge (~ 3646 Å) may be well estimated using fitting result for the intensity

of prominent Balmer lines. The fit near Balmer edge can be improved by including high order Balmer lines with n=3-400 for $\lambda > 3646$ Å in our model. The calculated intensity of the Balmer continuum combined with one more continuum window (~ 3000 Å) should be enough to determine the UV pseudocontinuum in 2900 Å- 5500 Åwavelength range.

4.4 Line Fitting Procedure

We intended to study the emission line properties of the AGN spectra and investigate their correlations to extract some information about the physical properties of the emission line regions of the AGNs. For this purpose, we fitted all the emission lines with Gaussians of different shifts and widths. The Fe II lines need special treatment as they are often many in number and form blended features. To fit the Fe II lines we have used our own template. The fitting has been done seperately for the optical and the UV part to make it less cumbersome.

4.4.1 Fitting the optical Fe II ($\lambda\lambda 4100 - 5500\mathring{A}$) lines

As mentioned above, the fitting of the Fe II line profile is complex as it consists of numerous overlapping lines with different intensities for various transitions. For example, the Fe II model calculated by Bruhweiler & Verner (2008) using CLOUDY code produces 344,035 atomic transitions. These lines often form a broad blended feature which can not be fitted simply using single Gaussians and a seperate empirical iron template is needed to fit these iron features better and more accurate (Vestergaard & Wikes, 2001).

These templates are defined mainly by the line width and the line strength. The relative strengths of the lines in the Fe II multiplets are the same in all objects. But due to the presence of numerous lines, the list of Fe II lines used and their relative intensities differ for different models (Veron-Cetty et al., 2004; Bruhweiler & Verner, 2008). Values of oscillator strengths in different atomic data sources also differ (Fuhr et al., 1981; Giridhar & Ferro, 1995).

Theoretically many authors have worked on the iron templates (Bruhweiler & Verner, 2008; Verner et al., 1999; Sigut & Pradhan, 2003 etc.),

which has been complemented by different analytic empirical models. The empirical iron template applied in Boroson & Green (1992) has been formed by removing all lines which are not Fe II, from the spectrum of I Zw 1. Similarly, Veron-Cetty et al. (2004) constructed an Fe II template by identifying the broad and of narrow Fe II lines and measuring their relative intensitites in the I Zw 1 spectrum. On the other hand, Dong et al. (2008) used a template having one intensity parameter for the broad Fe II lines and another for the narrow ones.

These existing empirical and theoretical Fe II models have good fits for the Fe II lines in NLSy1 but show discrepancies in the spectra with broader H_β lines. Hence we use the optical multi-gaussian Fe II template given in Kovačević et al. (2010) consisting of 50 Fe II emission lines (see Figure 4.7) with the addition of 15 more Fe II lines in the extra spectral range being considered in this analysis (Shapovalova et al., 2012) :

1. Majority of the strong multiplets dominant in the optical part ($\lambda\lambda 4100-5500$) whose lines can be clearly identified in AGN spectra and which have one of the three specific lower terms of their transitions: F, S, G or P - we have taken into account 65 such lines and have grouped them according to the lower term of their transition (F, S, G or P)

    - F group - Blue shelf of the iron template (4400-4700 Å) with 19 lines which are mainly multiplets 37 and 38 .
    - S group - Fe II emission covering the H_β and [O III] region in addition to some emission from the red Fe II bump (5150-5400). This group has 5 lines in multiplets 41, 42 and 43 .
    - G group - Red bump of the iron shelf (5150-5400 Å) with 11 lines from multiplets 48 and 49 .
    - P group - The transition arising from the group with lower level 4p, consisting of 15 lines from multiplets 27 and 28 .

2. 15 more lines selected from Kurucz database7 [2] which presumably originate from higher levels and are emitted around $\sim 4450\mathring{A}, \sim 4630\mathring{A}, \sim 5130\mathring{A}$ and $\sim 5370\mathring{A}$. Their relative intensities were measured from I Zw 1 (Veron-Cetty et al., 2004). These extra lines are represented in

[2] http://www.pmp.uni-hannover.de/cgi-bin/ssi/test/kurucz/sekur.html

the bottom plot of Figure 4.6 with a dotted line. There are indications of processes like self-fluorescence, continuum fluorescence etc., which can excite the Fe II lines with higher energy of excitation (Verner et al., 1999; Hartman & Johansson, 2000) and produce these lines but their origin is not yet well-known.

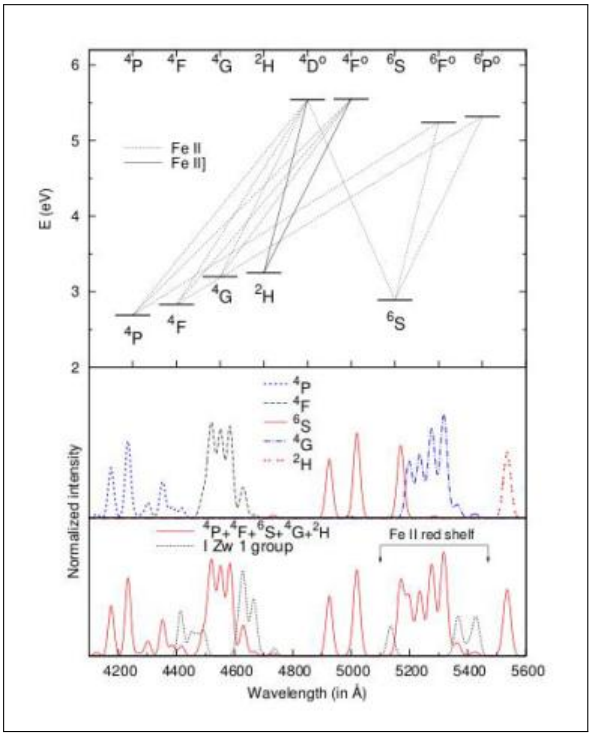

Figure 4.6: The top level shows the strongest Fe II transitions in the 4100-5500 Å region. Middle plot has the lines separated into five groups according to the lower level of transition: F (dashed), S (solid), G (dash-dotted), H (two-dashed) and P (dotted). The bottom panel showcases the lines from these five line groups (solid line) and lines measured from I Zw 1 - represented with dots (Shapovalova et al., 2012).

Each emission line profile in the model is represented by a Gaussian described by the line width, shift and intensity. The width and shift are taken to be the same for all iron lines as they are expected to originate in the same region.

So we describe our optical iron template with eight free fitting parameters

- one parameter for width, another for shift, five parameters for intensity (for the F, S, G, P line groups and for the high excitation group) and the seventh parameter is the excitation temperature needed to calculate the relative intensities within F, S, G and P line groups (see Kovačević et al., 2010; Shapovalova et al., 2012).

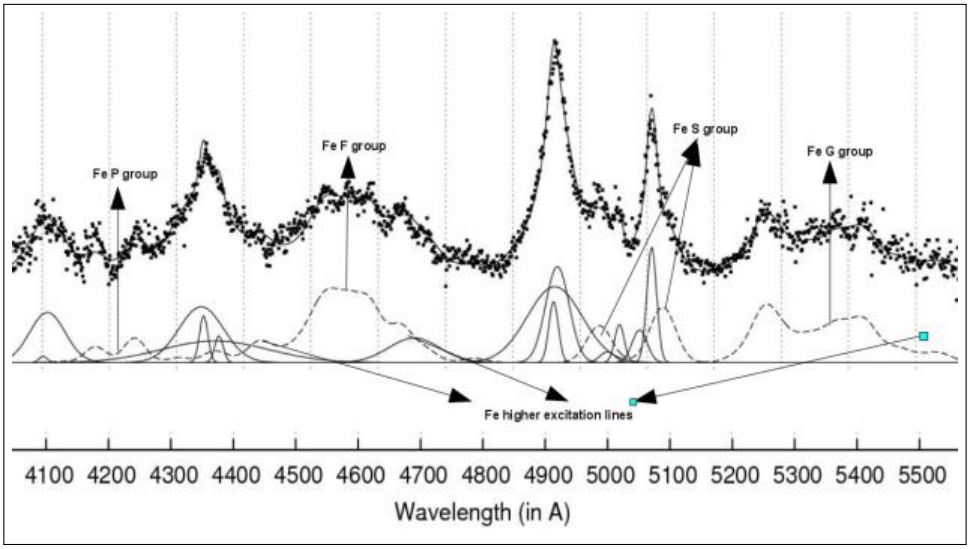

Figure 4.7: An example of multi-gaussian fitting of an spectrum in optical range (4100-5500 Å) highlighting the Fe II template - The dashed line showed in the bottom represents all the optical Fe II lines with marked sub-groups while the solid lines represents the Gaussian components of each Balmer line.

4.4.2 Fitting the UV Fe II lines

For the UV template of the Fe II lines, we have considered the contribution of 33 Fe II lines from multiplets 60, 61, 62, and 63 near the red and blue wing of Mg II λ2798 (see Popović et al., 2003). The atomic data for the line strength has been taken from the NIST web site which is a partner of VAMDC project. The line intensity ratio within a multiplet has been assumed to be proportional to the ratio of corresponding line strengths (Kovačević et al., 2010) .

Like the optical iron template, we have again assumed the Fe II emission to originate from the same region and hence have the same width and shift.

4.4.3 Spectral emission lines fitting

We assume the emission line profiles can be fitted with number of Gaussians. Each such line profile is considered to be a composite of contributions from different emitting regions.

Components of most of the broad emission lines are hypothesized to come from two or more emission regions (Brotherton et al., 1994; Popović et al., 2004; Ilić et al., 2006; Bon et al., 2009; Kovačević et al., 2010).

Thus each emission line is a sum of gaussians with different parameters - shift from the laboratory transition wavelengths, widths and intensities. These parameters reflect the physical conditions and kinematics of the respective emission sub-region. Few of the most prominent lines in this wavelength range which have been used extensively for our studies have been noted below.

Fitting of the UV part

The most prominent line in UV spectral range - the Mg II λ2800 Å line, is a doublet (Mg II $\lambda\lambda 2795, 2803$ Å). We see it as one line because they are too close. We fit this line with one Gaussian in core, which is actually sum of two Gaussians in core of two lines, and the same for the wings. So each component of the fitted Mg II line is convolution of 2 Gaussians (Tsuzuki et al., 2006).

We fit these lines with only two Gaussians instead of four, because we want to simplify the procedure and their flux ratio is not constant (like for OIII) (the same is done in Sameshima et al. (2011)). In this UV spectral range, we have also fitted the UV Fe II lines as described above (see Figure 4.8) .

This part of the spectrum was fitted with 12 free parameters - 6 of them considering the intensity, widths and shifts for two broad and intermediate Mg II components and the other 6 for the width, shift and intensity (for multiplets 60, 61, 62 and 63) of the iron lines in the UV.

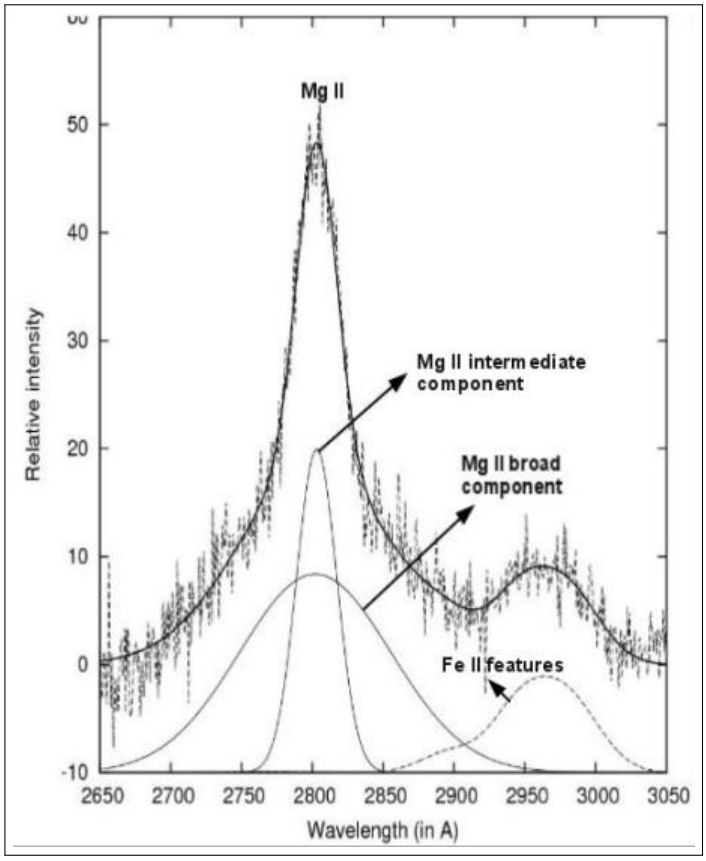

Figure 4.8: The two components of the Mg II λ2800 Å line with the Fe II features in the UV spectra range

Fitting of the optical part

Balmer lines are normally thought to be coming from two regions - NLR and BLR. But the complex broad emission lines are often impossible to be correctly represented by only one single Gaussian component.

Many authors assume these broad lines to be emitted from two parts of BLR - a 'Very Broad Line Region' (VBLR) and a kinematically different 'Intermediate Line Region' (ILR) (Brotherton et al., 1994; Corbin & Boroson, 1996; Popović et al., 2004; Hu et al., 2008; Kovačević et al., 2010) . In our analysis, we have also assumed the Balmer lines to be coming from three kinematically different emission regions - NLR, ILR and VBLR.

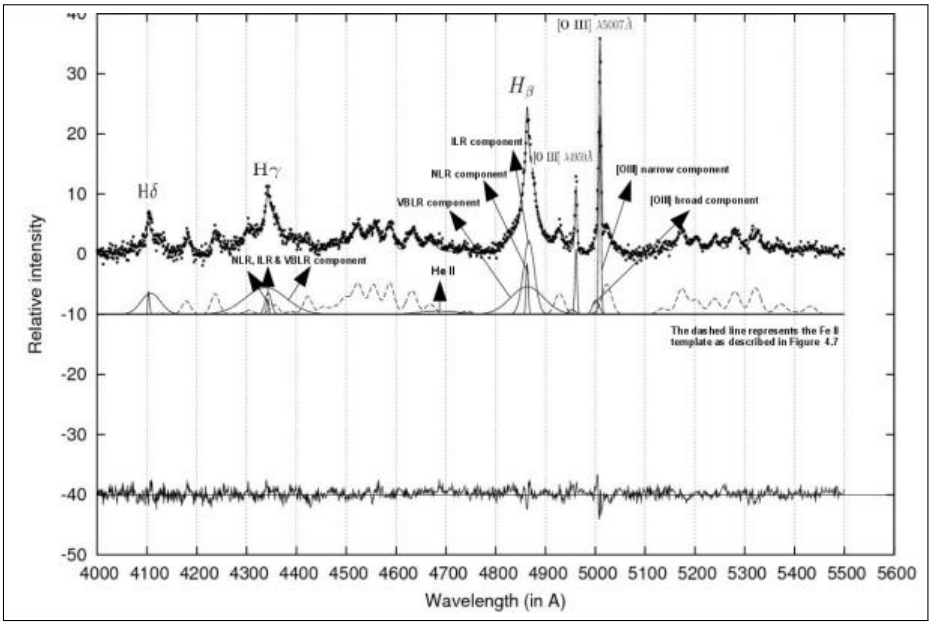

Figure 4.9: Line fitting in optical spectral range - The SDSS observed spectrum of SDSS J020039.16-084555.01 (dots) and the best fit (solid line) where Balmer lines are fitted with the sum of three Gaussians representing emission from the NLR, ILR, and VBLR, lines of the [O III] $\lambda\lambda$4959,5007 doublet are fitted with two Gaussians each, He II λ4686 is fitted with one broad Gaussian and the Fe II lines are fitted with a template denoted by a dashed line here.

The forbidden [O III] $\lambda\lambda 4959, 5007\mathring{A}$ doublet originates from the same lower energy level. In addition to this, beause they are strongly foridden, they should have negligible optical depth. Thus they can be assumed to have the same emission line profile with same width and same shift. Moreover, their intensity ratio can be taken as 2.99 (Dimitrijević et al., 2007). The [O III] lines have been fitted either with one gaussian or with two gaussians in case of significant asymmetry (Popović et al., 2004; Ilić et al., 2006).

As the narrow forbidden lines and the narrow components of the broad permitted emission lines should be theoretically originating from the same NLR, we have taken the same values for shifts and widths of the Gaussians of all NLR originated components. The He II $\lambda 4686\mathring{A}$ line is fitted with one broad gaussian.

An example of a fitted spectrum in optical range by our multi-gaussian fit can be seen in Figure 4.9.

4.4.4 χ^2 Minimization Routine

The spectral fitting in the optical 4100-5500 Å range was performed by applying a χ^2 minimization routine (Popović et al., 2004) to obtain the best fit. The UV range was fitted separately with a multi-gaussian fitting method described in Popović et al. (2003). The optical part of the spectra for the whole sample was fitted twice with two slightly different minimization routines with changed parameters.

Original fitting procedure

This is the multi-gaussian fitting procedure as described the latest in Kovačević et al. (2010).

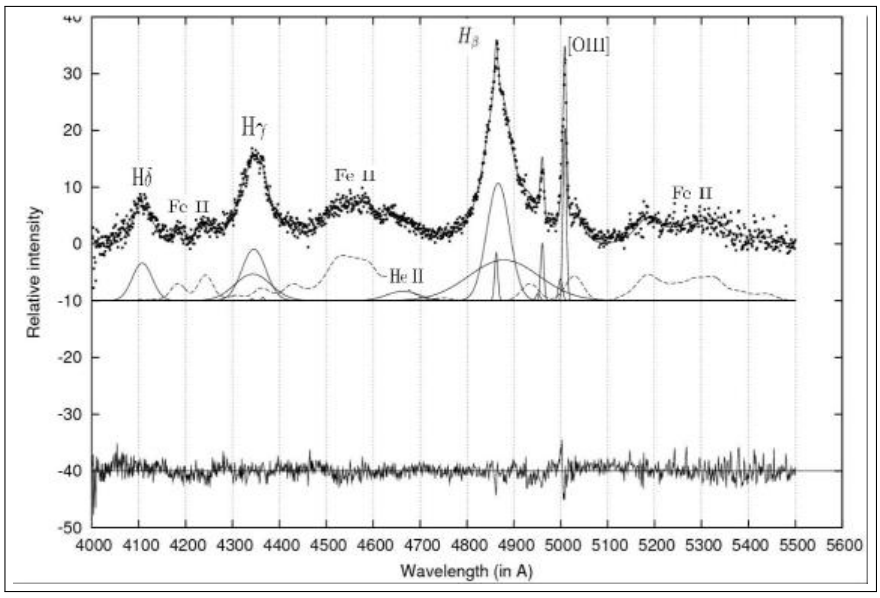

Figure 4.10: The SDSS observed spectrum (dots) and the best fit with original fitting programme (solid line) where Balmer lines are fit with the sum of three Gaussians representing emission from the NLR, ILR, and VBLR, lines of [O III] $\lambda\lambda$4959,5007 doublet are fitted with two Gaussians each, He II λ4686 is fitted with one broad Gaussian and the Fe II lines are fitted with a template denoted by a dashed line.

We first fitted the optical range of the spectra ($\lambda\lambda 4100\mathring{A} - 5600\mathring{A}$) with 36 free parameters to cover the width, shift and intensities of various lines in that wavelength range along with few more physical parameters like temperature. In this analysis, we had kept the widths and shifts of various Balmer line components (like the VBLR components of all Balmer lines, the NLR width and shifts of the Balmer lines) to have different values (see Figure 4.10).

Fitting with fixed Balmer line widths and shifts

In the original fitting model we had separate parameters for the widths and shifts of different Balmer line components. After completing the sample fitting, we found many spectra where the shifts and widths of the NLR, ILR, and VBLR components of Hβ are highly correlated with the shifts and widths of the NLR, ILR, and VBLR components of Hγ and Hδ.

But several others had a highly redshifted Hβ VBLR component compared to the other two Balmer lines in our spectral range (Hγ and Hδ) and hence showed disagreement with these correlations of line parameters as it can be seen in Figure 4.11.

Therefore we introduce some constraints assuming that Balmer lines and their components are originating in the same region and hence should have the same widths and shifts. This reduced the number of parameters in our new programme from 36 to 31. We re-fitted all the 100 spectra again with this new programme.

We normally expect the various components of different Balmer lines to originate from the same region - e.g. VBLR Hβ, VBLR Hγ and VBLR Hδ should originate in the same emission region and hence portray similar physics and dynamics. Thus it is theoretically more acceptable to have the shifts and widths of all NLR (or ILR or VBLR) components of Balmer lines (Hβ, Hγ and Hδ) to be the same.

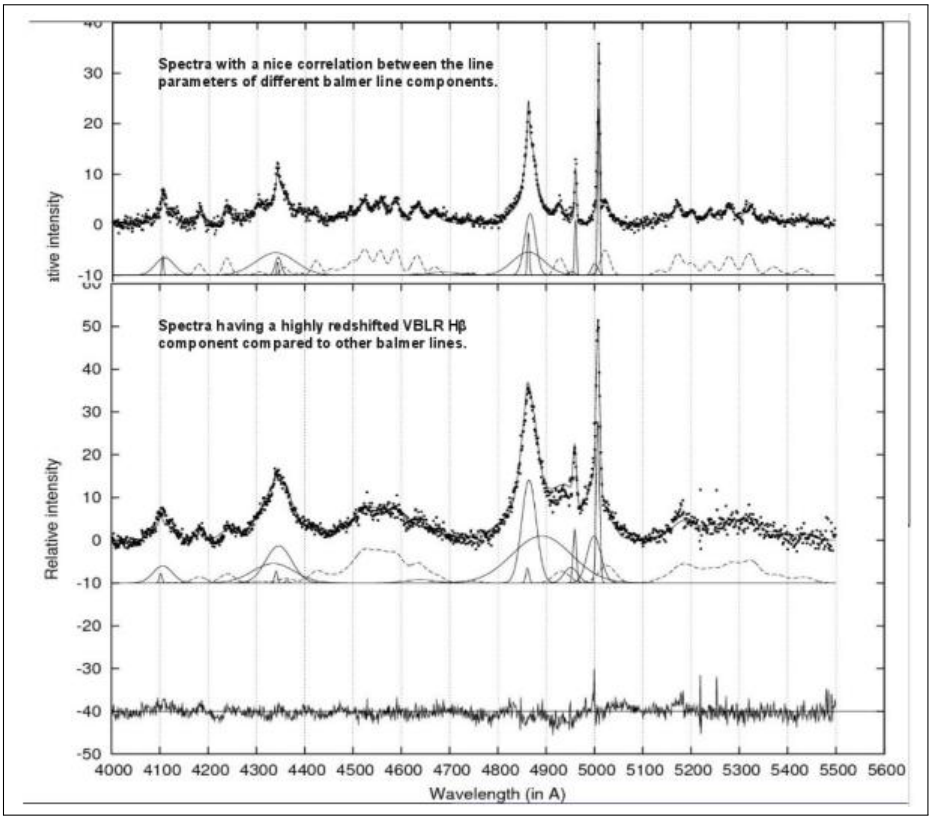

Figure 4.11: Both the spectra here are fitted with our original fitting programme with different width and shift values for different components of Hβ, Hγ and Hδ. The spectrum at the top shows good correlations between the line parameters of NLRs, ILRs and VBLRs of the respective Balmer lines. The spectrum on the bottom plan is an example where the width and shift of Hβ VBLR is very much different from widths and shifts of Hγ and Hδ VBLR.

As mentioned above, not all spectra have shown a nice correlation between these parameters. But with our new programme, we could get a good fit for almost all spectra. Comparison of an AGN spectrum being fitted first by our original programme and then by the new programme can be seen in Figure 4.12.

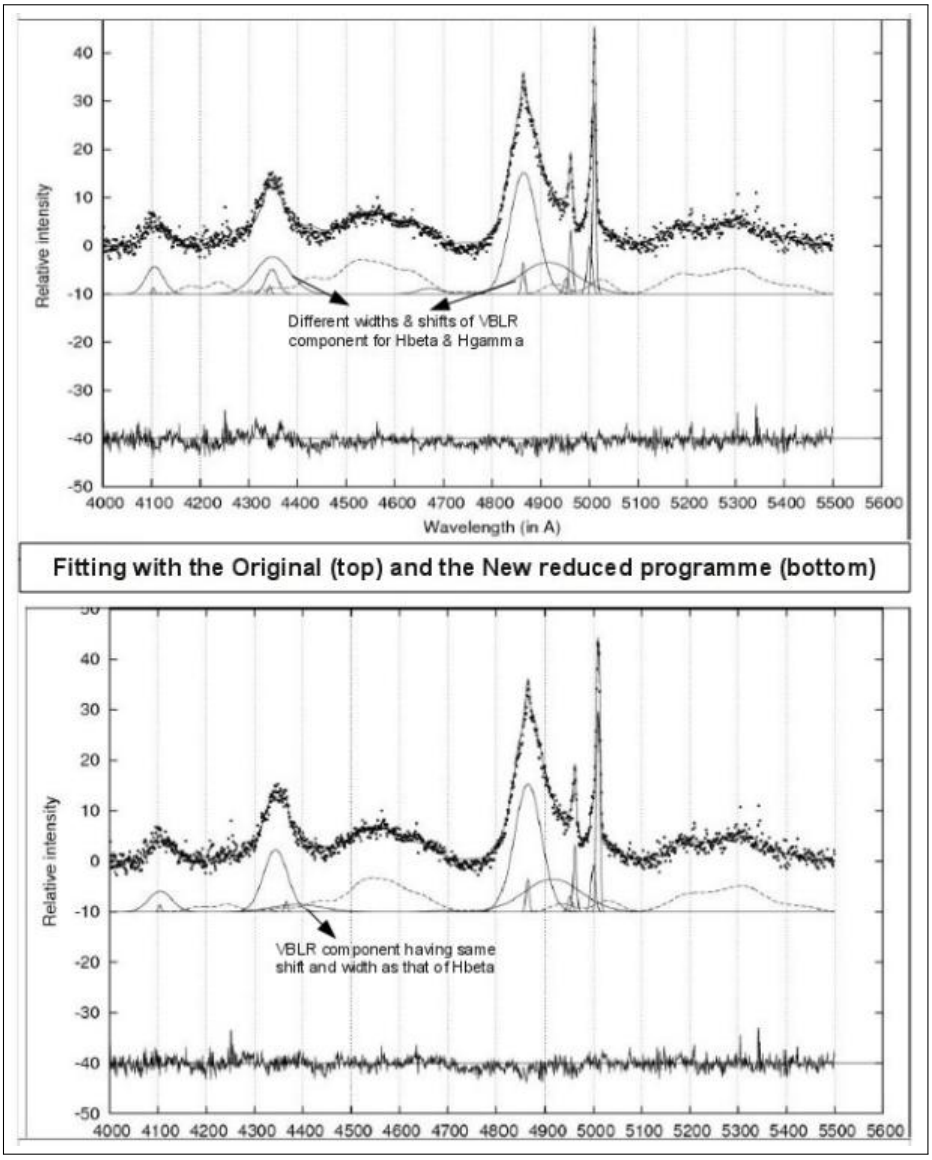

Figure 4.12: A comparison for the two fitting programmes on the same AGN spectrum - the observed spectrum is shown in dots, the upper panel shows the multi-gaussian fit of it with our original programme considering different width and shift parameters VBLR, ILR and NLR components of the Hβ, Hγ and Hδ lines, the plot at the bottom represents the fit with the new programme where we have introduced the same width and shift parameters for NLR, ILR and VBLR of all the Balmer lines.

4.5 Line parameters obtained from the best fit

By running the χ^2 minimization routine (Popović et al., 2004), we obtain the best fit for given spectrum and extract line parameters from the spectrum. The following parameters are further analysed.

Luminosity of emission lines

Luminosities were calculated using the formulae given in Peebles, 1993 considering the cosmological parameters to be $\Omega_M = 0.27, \Omega_\Delta = 0.73, \Omega_k = 0$ and Hubble constant as 71 km s^1 Mpc^1.

Continuum Luminosity

The average value of the continuum flux is measured between $\lambda\lambda 5095 - 5100$ and $\lambda\lambda 5100 - 5105$ and is taken for the calculation of the continuum luminosity at 5100 Å.

Line Width and Shift

We obtained the parameters for shifts and widths (for all emission lines) directly from the fit.

Excitation Temperature

The excitation temperature needed to obtain the relative intensities within F, S, G and P line groups is given as one of the parameters from our Fe II template.

Line Equivalent Widths

To measure the Equivalent Width (EW) of the lines, we first estimate the continuum by subtracting all fitted lines from the observed spectra and then adding the line of interest to the continuum (see Figure 4.13). Then the lines are normalized to the continuum level and their flux is measured (see Figure 4.14). This gives us the value for the EW.

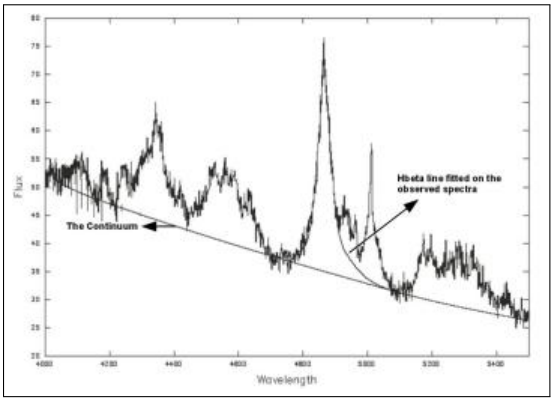

Figure 4.13: Example of measuring Equivalent Width of the Hβ line on SDSS J131840.21+000735.28 - Observed SDSS spectrum with fitted continuum and Hβ line.

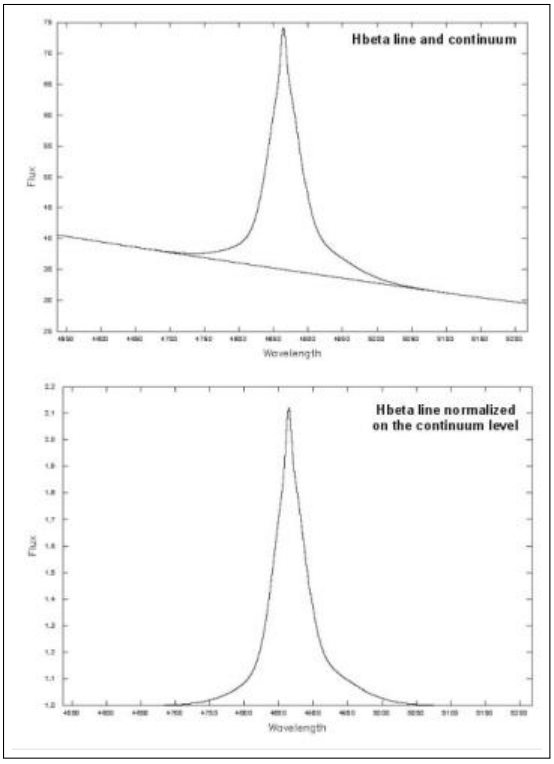

Figure 4.14: Example of measuring Equivalent Width of the Hβ line on SDSS J131840.21+000735.28 - Top: Hβ line and the continuum, Bottom: Hβ line normallized to the continuum level.

Line FWHM

The broad component of the Balmer line is assumed as a sum of the VBLR and ILR components. The fitted broad Balmer line is then normalized to unity and the full width at half of the maximum intensity is measured. This gives the value of FWHM for the line (see Figure 4.15).

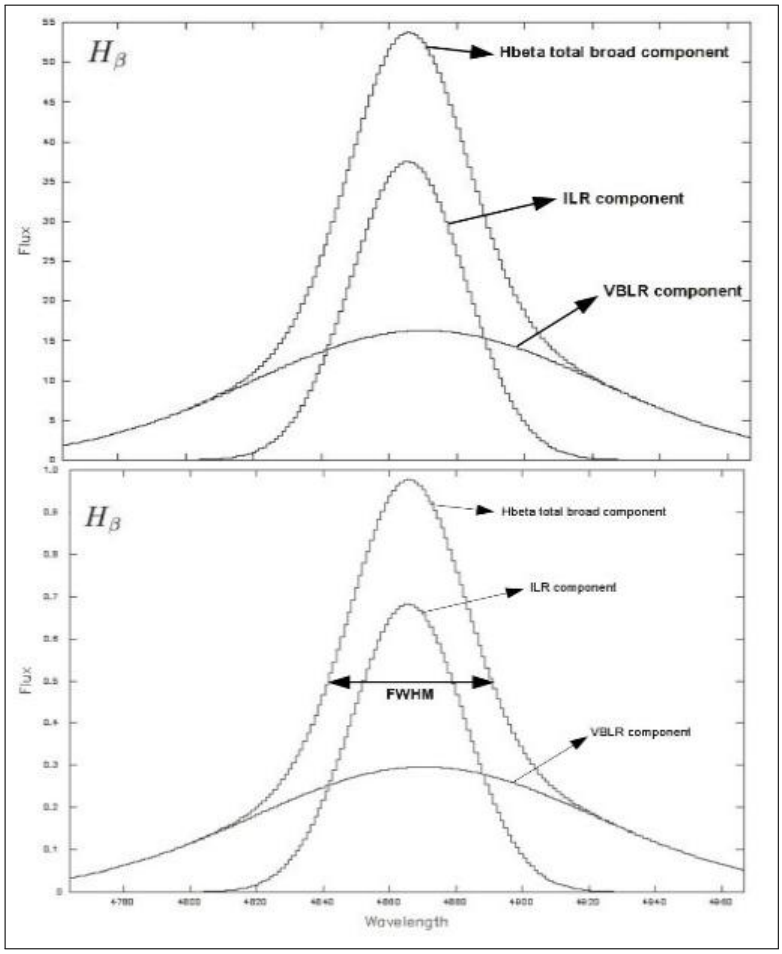

Figure 4.15: Example of measuring FWHM of the Hβ line on SDSS J113615.14+103430.94 - Top: The broad Hβ line is fitted by adding the ILR and VBLR components, Bottom: The complete broad line is then normallized to unity and the width of the line at intensity 0.5 is calculated as the FWHM of the line.

Chapter 5

Results

We have investigated correlations between different UV/optical emission line and continuum properties. We fitted a sample of 100 AGNs in the UV/optical range.

Note here that 15 of 100 spectra from the sample, have a fitting problem near 2650 $\mathring{A}$ since it seems that continuum is not well subtracted below the Mg II line. The possible reason for that may be that there are some additional Fe II lines in that part, which we did not take into account properly in the fitting procedure. Additionally, 16 spectra have good fitting in the optical, but could not be fitted well in the UV because of a strong absorption in Mg II and strong noise.

For the rest 69 AGNs, the fittings are reasonably good and furthermore we will explore correlations for these 69 AGNs.

5.1 Kinematical Parameters of Emitting Regions

The line widths and shifts obtained from our best fit were used to extract informations about the kinematical relations among different emission regions. The width is assumed to be connected to the degree of Doppler effect caused by the motion of emission clouds. The Line shift, on the other hand, is assumed to be a measure of the systematic motion of the emission regions with respect to the host galaxy.

Further we outline the major results of the multigaussian fitting.

5.1.1 Connection between Balmer and Fe II emission regions

The average value for the Fe II (optical) width, for the sample, is $\sim$ 2050 km/s, while the average values for the Balmer line (Hβ,Hγ and Hδ) widths are $\sim$ 300 km/s for the NLR, $\sim$ 1900 km/s for the ILR component and $\sim$ 4570 km/s for the VBLR component. Even before looking at the correlations, it is obvious that the averaged Fe II width is much closer to the average widths of the Balmer ILR components as compared to that of the NLR and VBLR components (see Figure 5.1) .

Relationships among the widths of the Fe II and various Blamer components are also presented in Figure 5.1. We do not see much of a correlation between the kinematic properties of the emission clouds of the Fe II lines with Balmer NLR and VBLR components.

But as shown by the Pearson correlation values, the correlation between the Fe II width and the width of Balmer ILR is very strong and significant (r = 0.75, P = 1e-13).

We also performed the same analysis for the Fe II lines in UV. There was no obvious similarities between Balmer line component average widths which are $\sim$ 4570 km/s for the VBLR component, $\sim$ 1900 km/s for the ILR component and $\sim$ 300 km/s for the NLR component, as compared to the average width of Fe II (UV) lines, which is $\sim$ 2900 km/s.

Moreover, as shown in Figure 5.2, we found no correlation between the kinematical properties of the Balmer line components and the UV Fe II lines. The Pearson correlation values for Balmer VBLR component and Fe II UV width are r = 0.22, P = 0.05; for ILR Balmer component and Fe II UV width are r = 0.28, P = 0.18 and for widths of Balmer NLR and UV Fe II are r = 0.01, P = 0.91.

As obvious from the above mentioned values, altough slight but there is still a trend of the width component of Fe II UV with Balmer ILR component width but there is no trend whatsoever with the NLR and VBLR components.

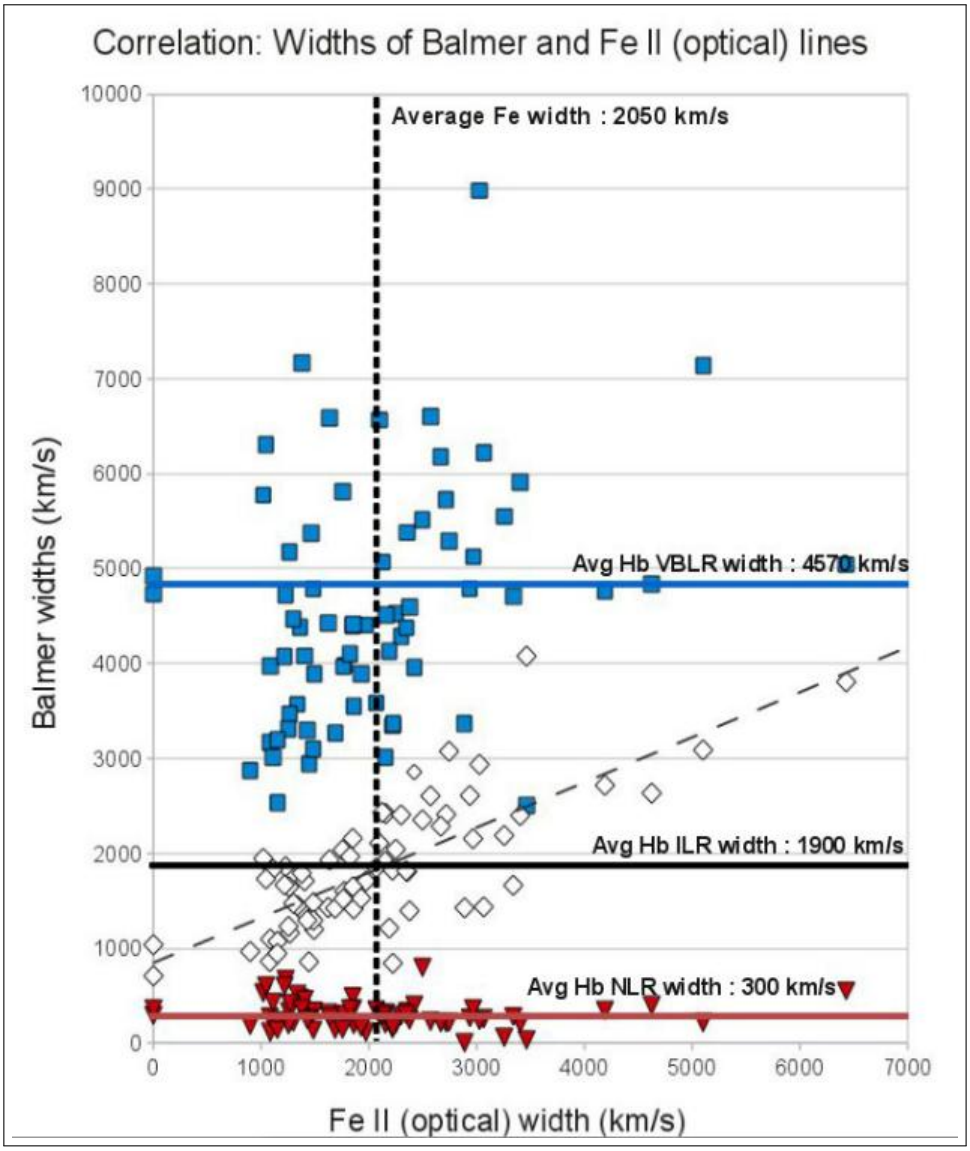

Figure 5.1: Widths of the Balmer line components are compared with the widths of the Fe II (optical) lines. On the X-axis are the widths of FeII and on Y-axis are the widths of the Balmer line components : squares show VBLR data, open diamonds represents ILR components and inverted triangles are giving the NLR data. There is a good correlation (dashed line) between the kinematic properties of the emission region of the optical Fe II lines and ILR Balmer lines.

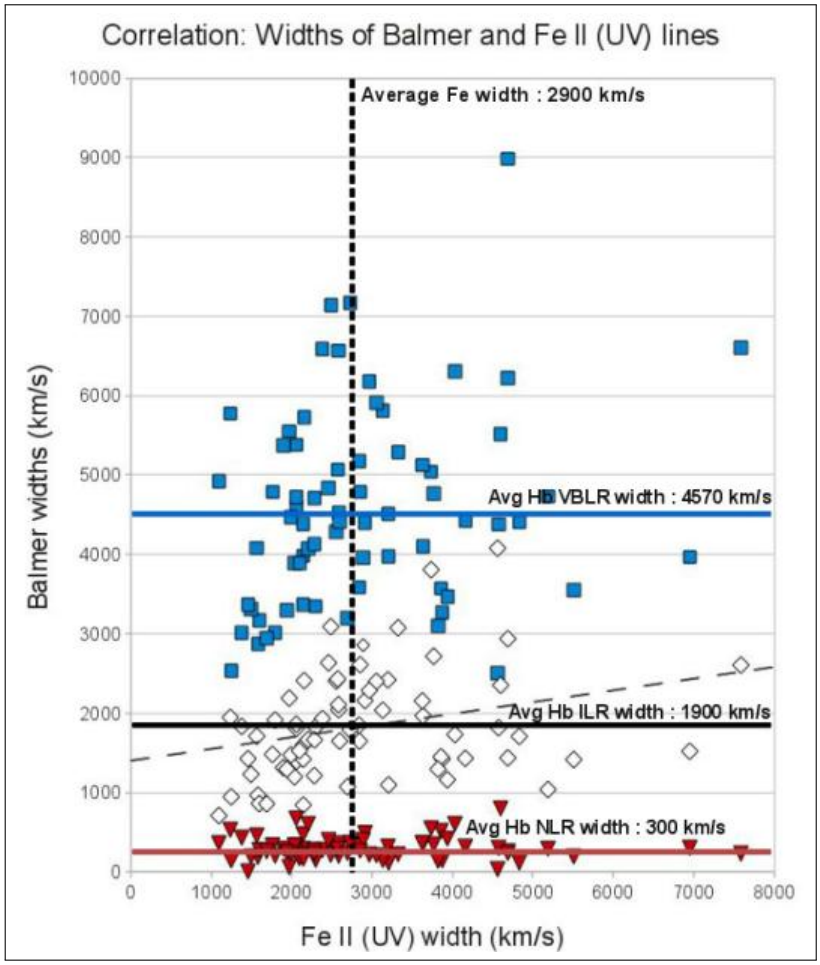

Figure 5.2: Widths of the Balmer line components are compared with the widths of the Fe II (UV) lines. On the X-axis are the widths of Fe II and on Y-axis are the widths of the Balmer line components. No correlation was seen between the kinematic properties of the emission region of Fe II UV lines and the Balmer lines components, although a slight trend was shown by the ILR components with Fe II (UV) widths The notation is same as in Figure 5.1.

The correlation analysis for the shifts of the Balmer lines and Fe II optical as well as UV lines showed no significant correlations (Figure 5.3). Even the average shift values were not similar between any of the components. The values for average shifts are - Balmer VBLR $\sim$ 1400 km/s, Balmer ILR $\sim$ 150 km/s, Balmer NLR $\sim$ 200 km/s, Fe II optical lines $\sim$ 450 km/s and Fe II UV lines $\sim$ 1530 km/s.

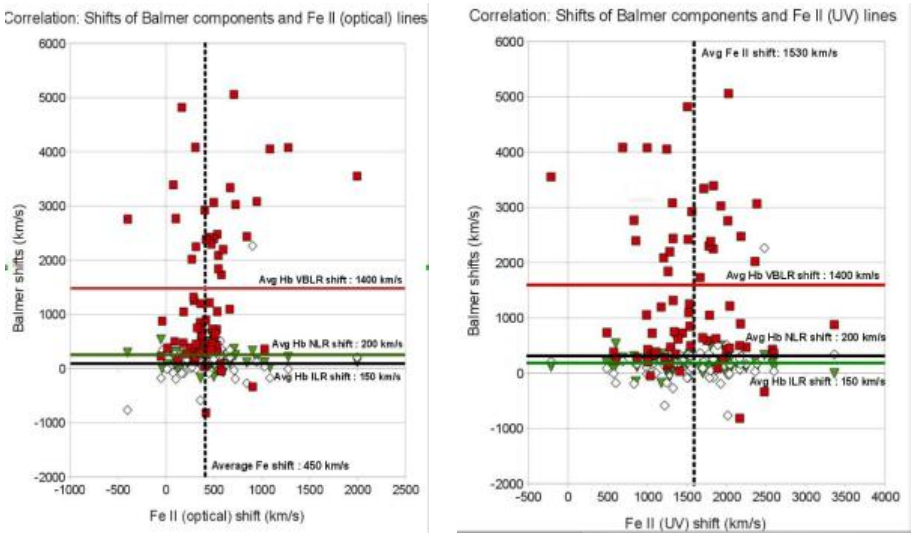

Figure 5.3: The same as in Figure 5.1 and 5.2 but for shifts of the Balmer and Fe II lines. The left panel shows the relations with Fe II optical shifts while the right panel demonstrates the shifts of Balmer line components and Fe II UV lines. The notation is the same as in Figure 5.1

5.1.2 Kinematic relations between Mg II and Fe II emission regions

The Mg II emission line, as mentioned before in Section 4.4.3, is fitted with two gaussians - one broad component and an intermediate component.

Exploring the widths and shifts of these two Mg II components and the Fe II optical as well as Fe II UV Lines, we saw that neither of the Mg II components show a correlation with the widths and shifts of Fe II lines in the UV range.

But there is a high correlation (r = 0.69, P = 1E-11) between the widths of Mg II intermediate component and optial Fe II line widths (Figure 5.4). Moreover, the average value of intermediate component width of Mg II ($\sim$ 1600 km/s) is highly similar to the optical Fe II width ($\sim$ 2050 km/s), while the average width of Mg II broad component was significantly higher ($\sim$ 9200 km/s).

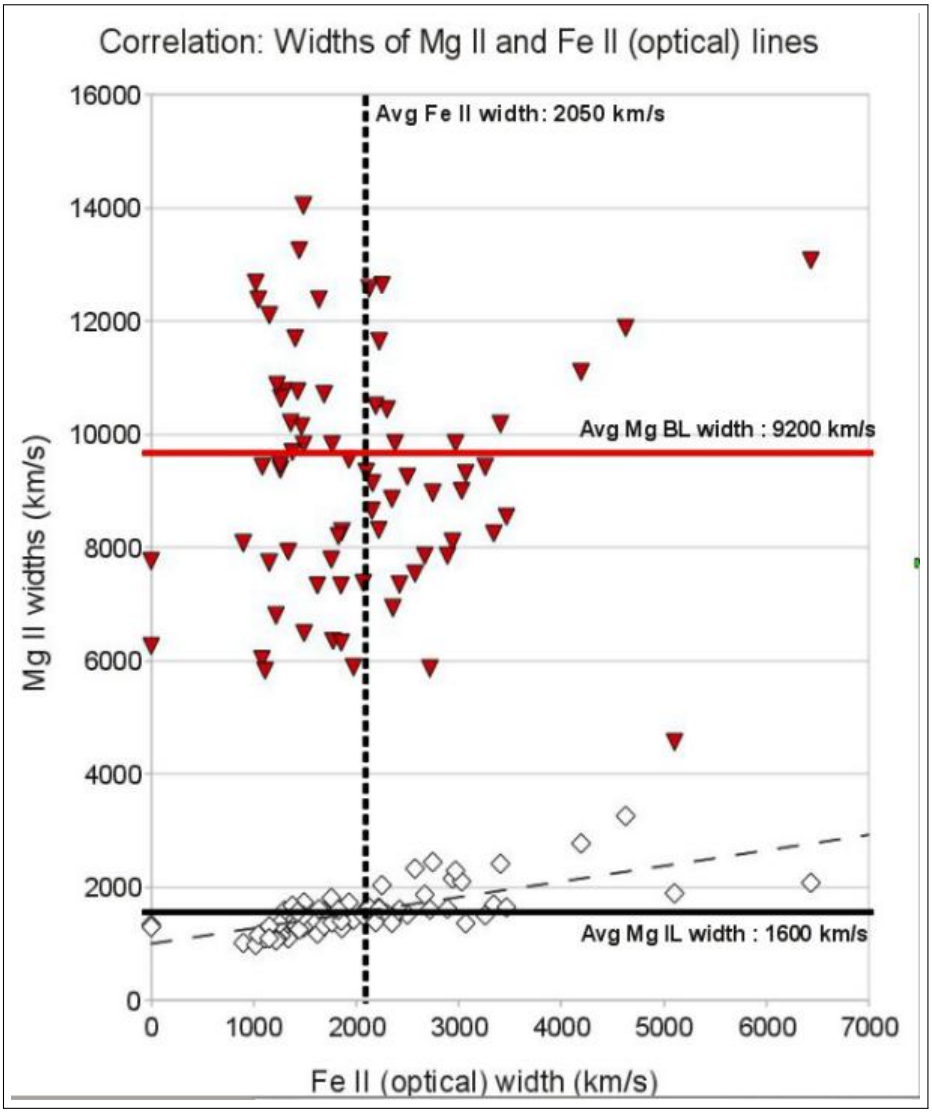

Figure 5.4: Widths of the Mg II line components compared with the widths of the Fe II (optical) lines. On the X-axis are the widths of Fe II and on Y-axis are the widths of the Mg II components. Filled triangles show the Mg II broad component and open diamonds represent the data from Mg II intermediate component.

No such strong relationships were found between the UV Fe II widths and Mg II broad line widths (Figure 5.5).

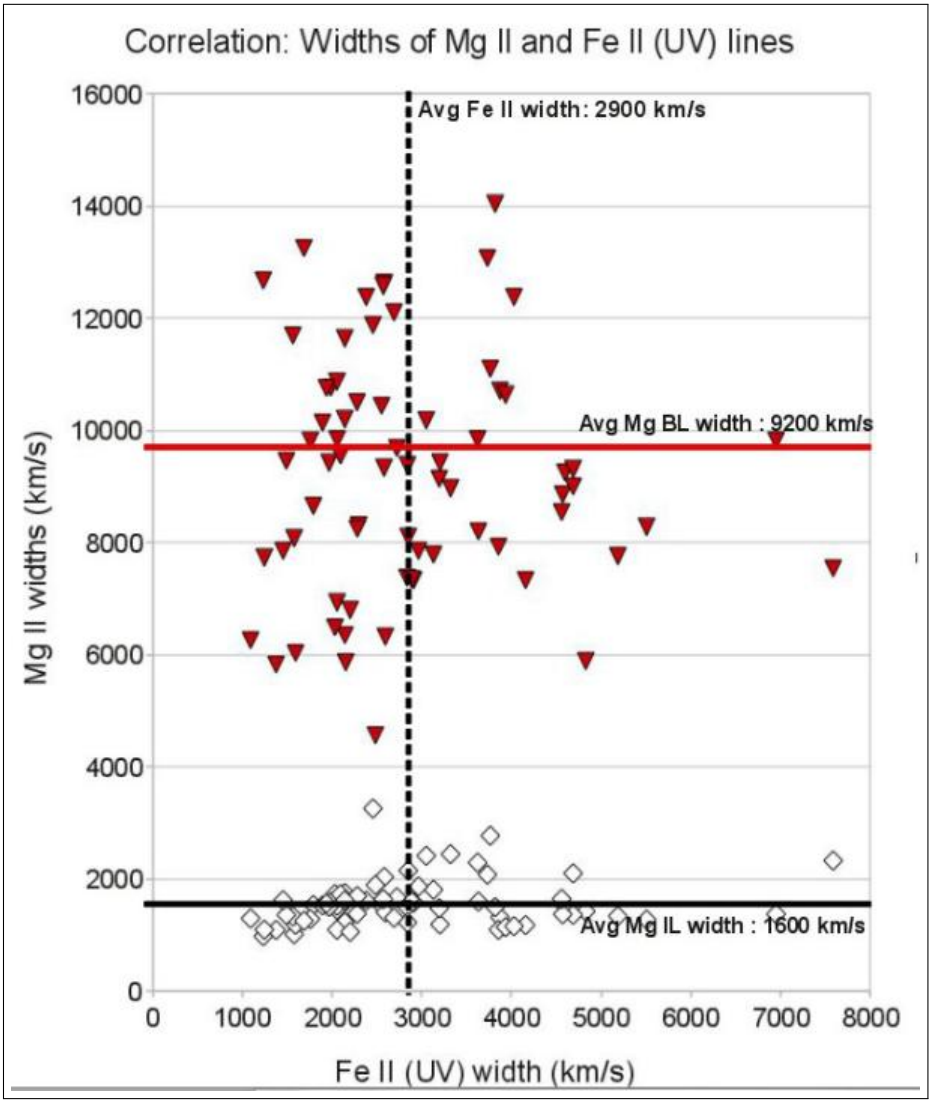

Figure 5.5: The same as in Figure 5.4 but for UV Fe II lines

For the shifts between Fe II lines in the UV as well as the optical band and the components of Mg II, we again saw no significant correlation (Figure 5.6, 5.7).

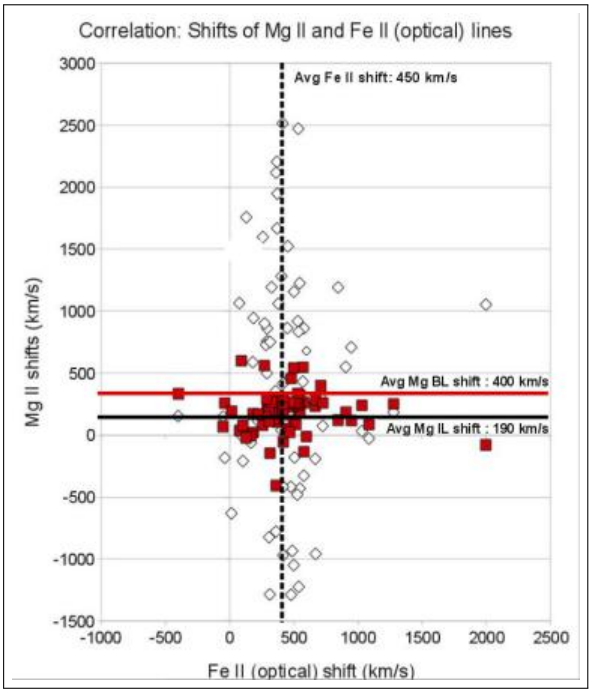

Figure 5.6: The same as in Figure 5.4, but for shifts

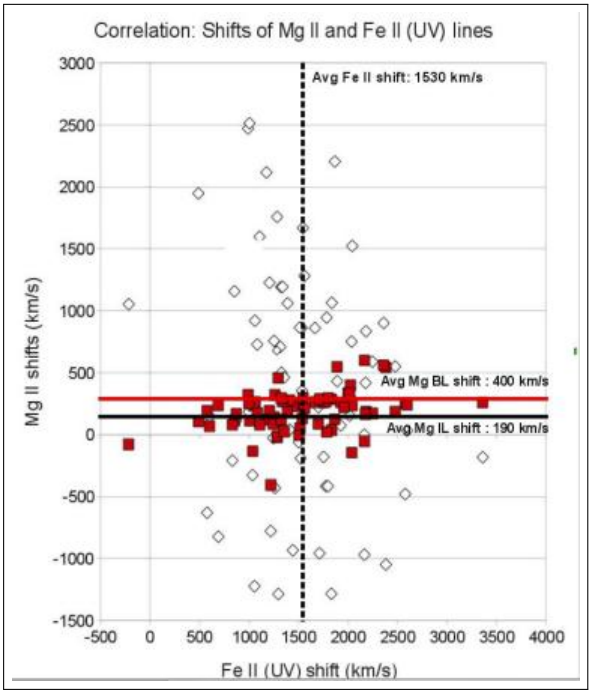

Figure 5.7: The same as in Figure 5.5, but for shifts

5.1.3 Optical and UV Fe II lines

No correlation was found between the widths and shifts of Fe II lines in optical and in UV. We get Pearson values of r = 0.18 and P = 0.124 for the line widths correlation of optical and UV lines, showing no relationship in the kinematic properties of the emission regions of Fe II lines in optical and the regions emitting Fe II in UV (Figure 5.8).

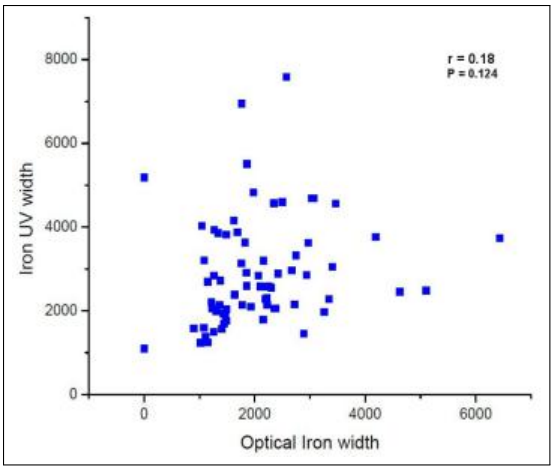

Figure 5.8: The widths of the UV iron (Fe II) lines with respect to the widths of the optical iron lines.

We also looked for the correlations between the shifts of the Fe II lines in optical and UV but there was no correlation (r = -0.19, P = 0.1169) at all between these properties (see Figure 5.9).

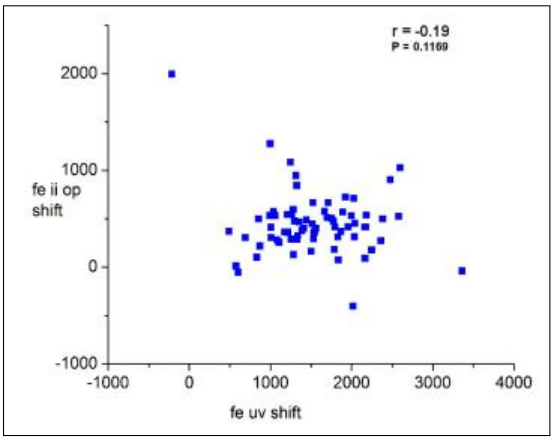

Figure 5.9: The shifts of the optical vs the UV widths of iron (Fe II) lines.

5.1.4 Kinematical relations between the Mg II and Balmer Line Emitting Regions

We looked for correlations between widths and shifts of the Mg II components in the UV range and the Balmer Hβ line components. We assumed in the fitting procedure that the widths and shifts of the Balmer lines (Hβ, Hγ and Hδ) are the same. The only effective correlations were found between the Mg intermediate component widths and widths of the ILR (r = 0.61, P = 1E-8) and VBLR (r = 0.38, P = 8E-4) components of Hβ (Figure 5.10).

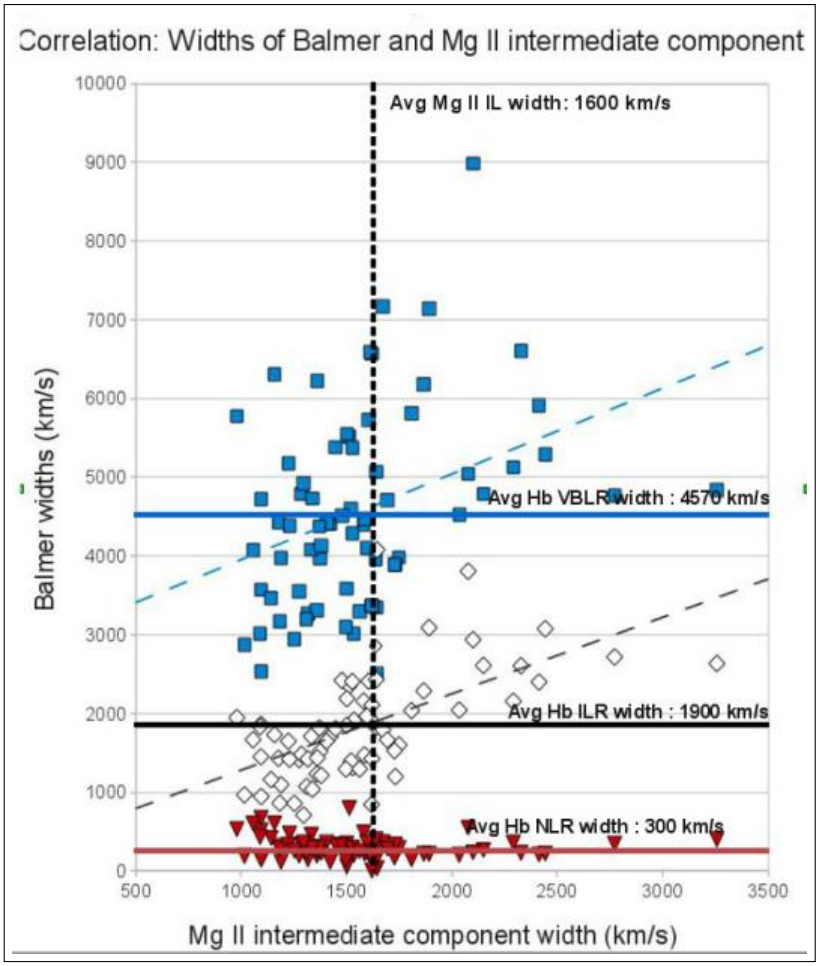

Figure 5.10: Widths of the Balmer lines compared with the width of the Mg II intermediate component - squares showing data of broad Hβ component, diamonds representing the ILR data and triangles giving the NLR component of Hβ. The correlations are shown by the dashed lines.

There is no correlation between the widths of Mg II broad component and widths of any of these Balmer components. Moreover, the averaged value of Mg II broad component was found to be much higher ($\sim$ 9200 km/s) in comparison with the widths of Balmer line components (VBLR $\sim$ 4570 km/s, ILR $\sim$ 1900 km/s and NLR $\sim$ 300 km/s) (Figure 5.11).

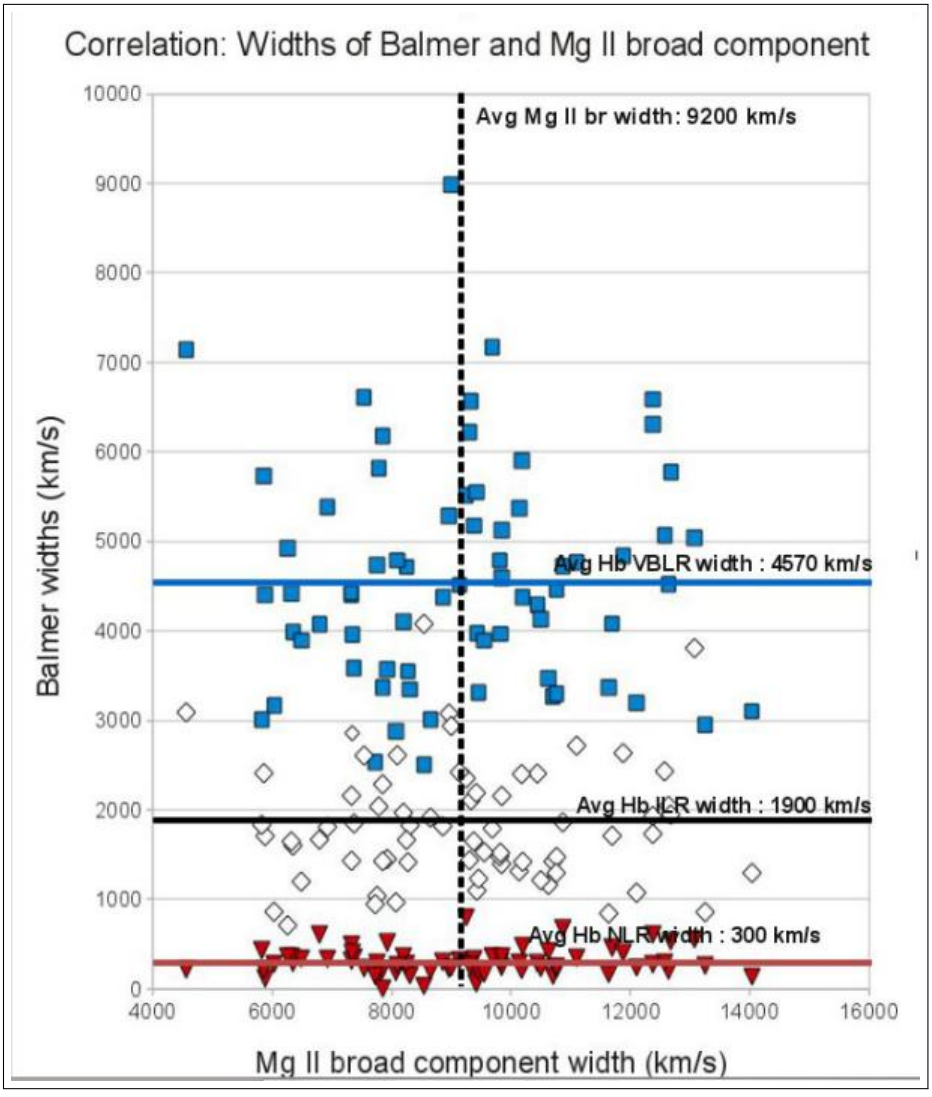

Figure 5.11: The same as in Figure 5.10 but for the broad component of Mg II

The same analysis was carried out for the correlations between the shifts of the UV/optical lines.

Although no high correlation was seen among the shifts of the components (Figure 5.12, 5.13), we found the averaged value of the shifts of Mg intermediate component ($\sim$ 190 km/s) to be highly similar to the average shifts of NLR and ILR components of Balmer lines ($\sim$ 200 km/s and $\sim$ 150 km/s respectively).

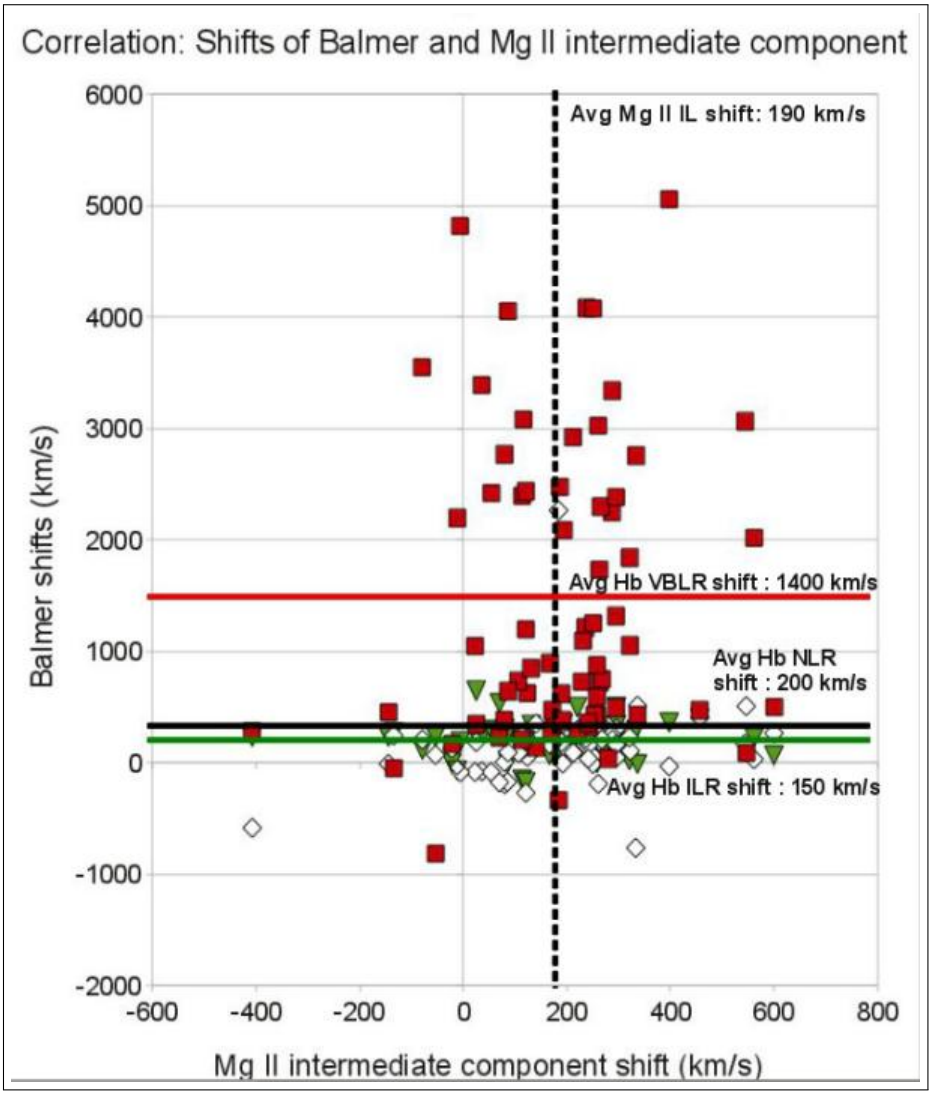

Figure 5.12: The same as in Figure 5.10, but for line component shifts.

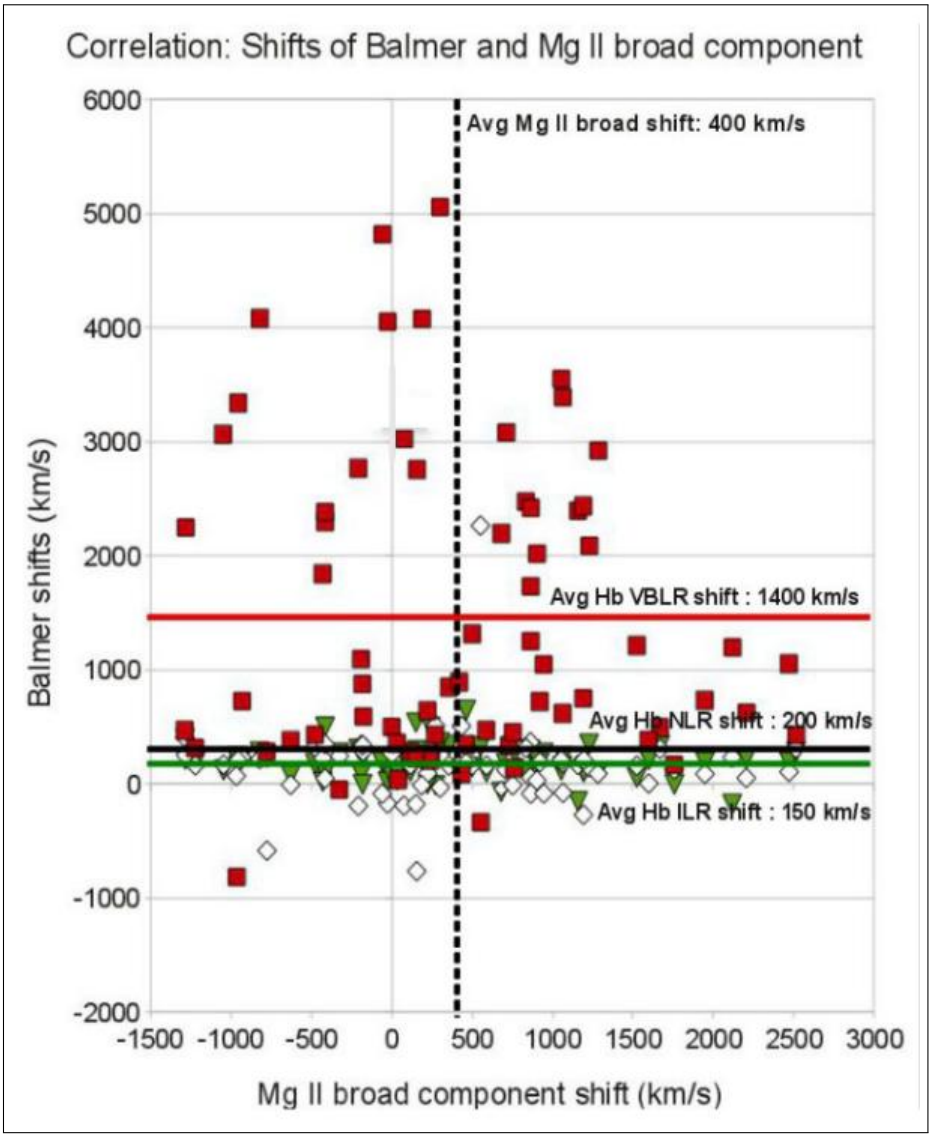

Figure 5.13: The same as in Figure 5.11, but for the component shifts

5.1.5 Correlation between widths and shifts of Fe II lines

We found a significant correlation between the width and the shift of the Fe II lines in UV, with pearson values : r = 0.51, P = 6e-6 (see Figure 5.14)

There was a strong enough correlation even between the width and the shift of the optical Fe II lines (r = 0.46, P = 5e-5). (see Figure 5.15)

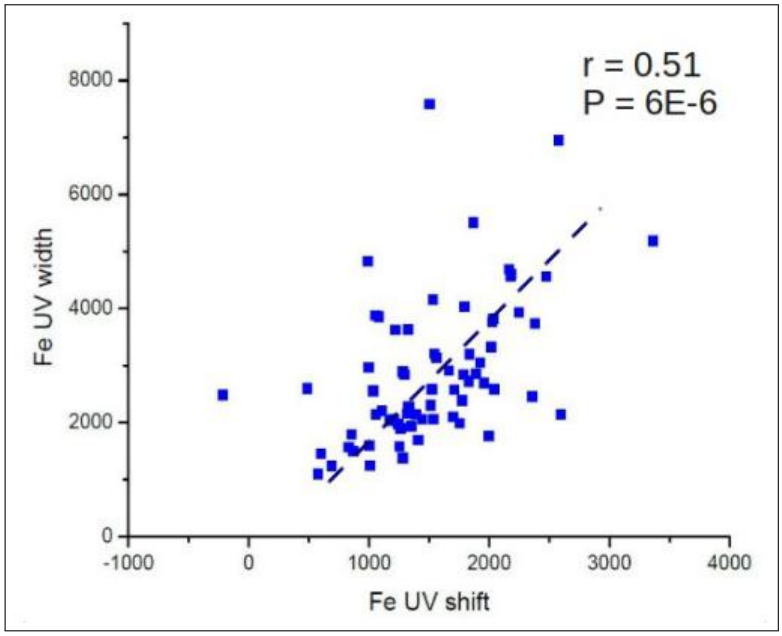

Figure 5.14: The widths vs shifts of Fe II (UV) lines. Both these line parameters are given in km/s.

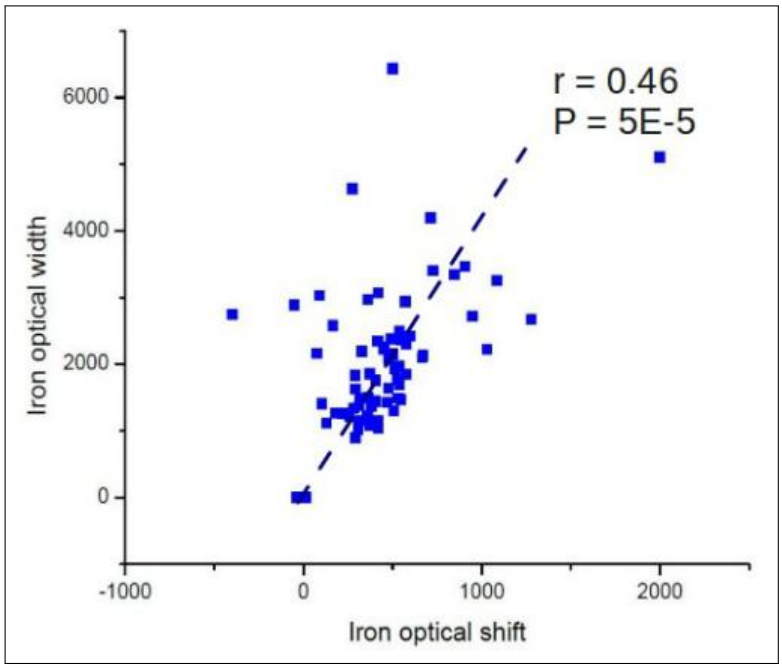

Figure 5.15: The widths vs shifts of the optical Fe II lines. Both the width and the shift are given in the units of km/s.

5.2 Correlation between the intensities of emission lines

We analysed the line intensities of the various components of different emission lines in order to find some relationships. Line intensity, basically, is the flux on the wavelength where we have a line maximum. It is the flux on the specific wavelength where the line is peaked. Line intensities in the following analysis will always be given in 10^{-17} erg cm^{-2} s^{-1} Å^{-1}

5.2.1 Correlation between Balmer and Mg II line strengths

The line intensities of both the broad and the intermediate components of Mg II lines were seen to be highly correlated with the line intensities of all the components of Hβ, Hγ & Hδ (Figure 5.16).

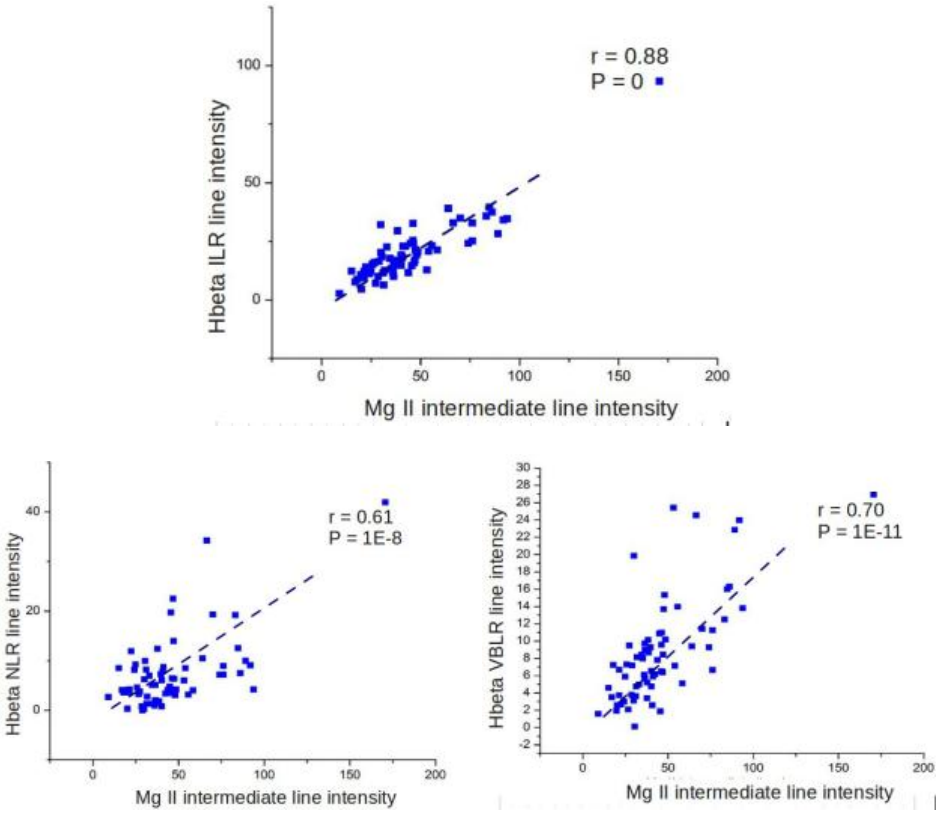

Figure 5.16: Correlations between intensities of Mg II intermediate component and the three (NLR, ILR, VBLR) component of Hβ. All the line intensities are given in units of 10^{-17} erg cm^{-2} s^{-1} Å^{-1}

The Mg II intermediate component has higher correlation with the Hβ ILR (r = 0.88, P = 0) component as compared to the correlation with the NLR (r = 0.61, P = 1E-6) and VBLR (r = 0.70, P = 1E-11) intensities.

The same trend was observed with the line intensities of Hγ and Hδ too, with higher significance for correlation with the ILR component intensities as compared to that of VBLRs and NLRs (Figure 5.17).

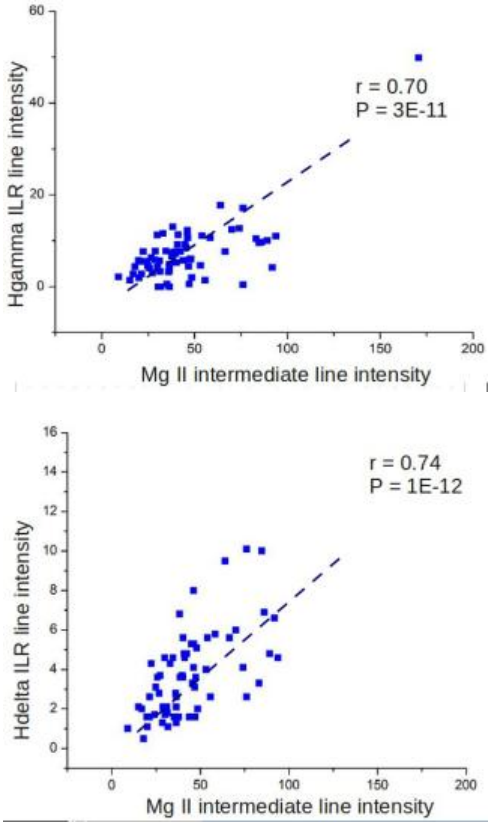

Figure 5.17: Correlations between intensities of Mg II intermediate component and the intermediate components of Hγ and Hδ. The line intensities are given in units of 10^{-17} erg cm^{-2} s^{-1} Å^{-1}.

A correlation was not found between the line intensities of Balmer line components and the broad component of Mg II. Even for Fe II line intensity, no correlation was found with the Balmer line and Mg II line components.

5.2.2 Correlation between different Balmer line intensities

The fluxes of the NLR, ILR and VBLR components of the different Balmer lines (Hβ,Hγ and Hδ) were analysed.

Correlations among the VBLR component intensities of different Balmer lines returned very high Pearson values. We got for Hβ vs Hγ (r = 0.85, P =0), Hδ vs Hβ (r = 0.84, P =0) and Hγ vs Hδ (r = 0.80, P =2E-16). The same trend was observed also in the correlations among the ILR component intensities of the three different Balmer lines - Hβ vs Hγ (r = 0.80, P =1E-16), Hδ vs Hβ (r = 0.55, P =1E-6) and Hγ vs Hδ (r = 0.68, P =1E-10). These are illustrated in figures 5.18 and 5.19. Even the intensities of the NLR components of the respective lines showed good correlations.

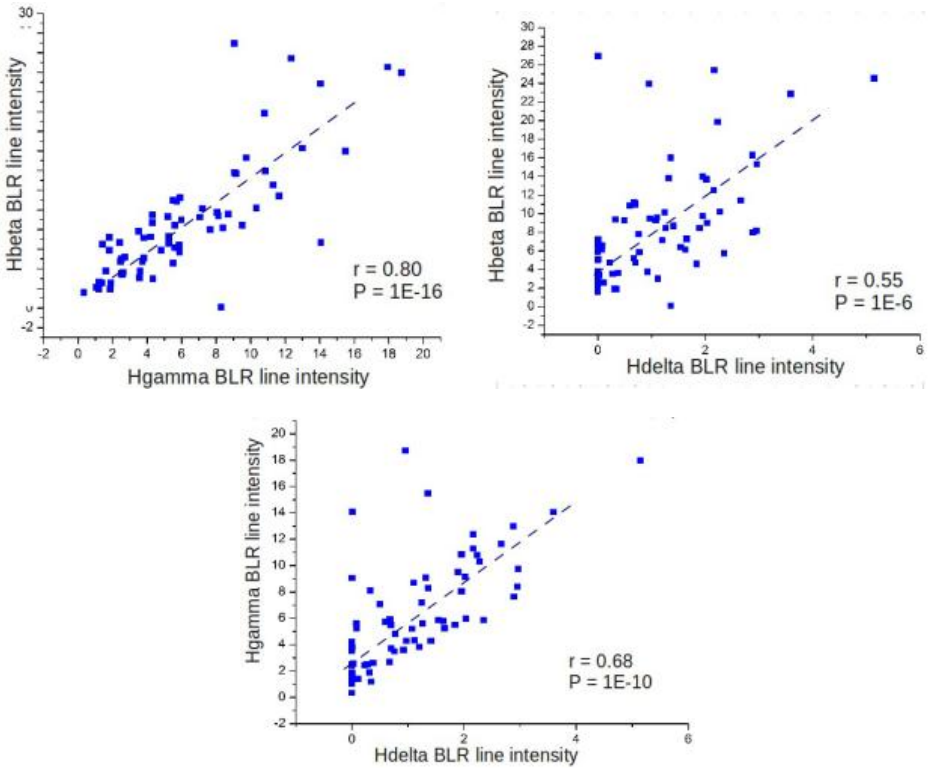

Figure 5.18: Correlations among the VBLR component intensities of different Balmer lines can be seen here. Very high correlations were found between their intensities.The line intensities are given in units of 10^{-17} erg cm^{-2} s^{-1} Å^{-1}.

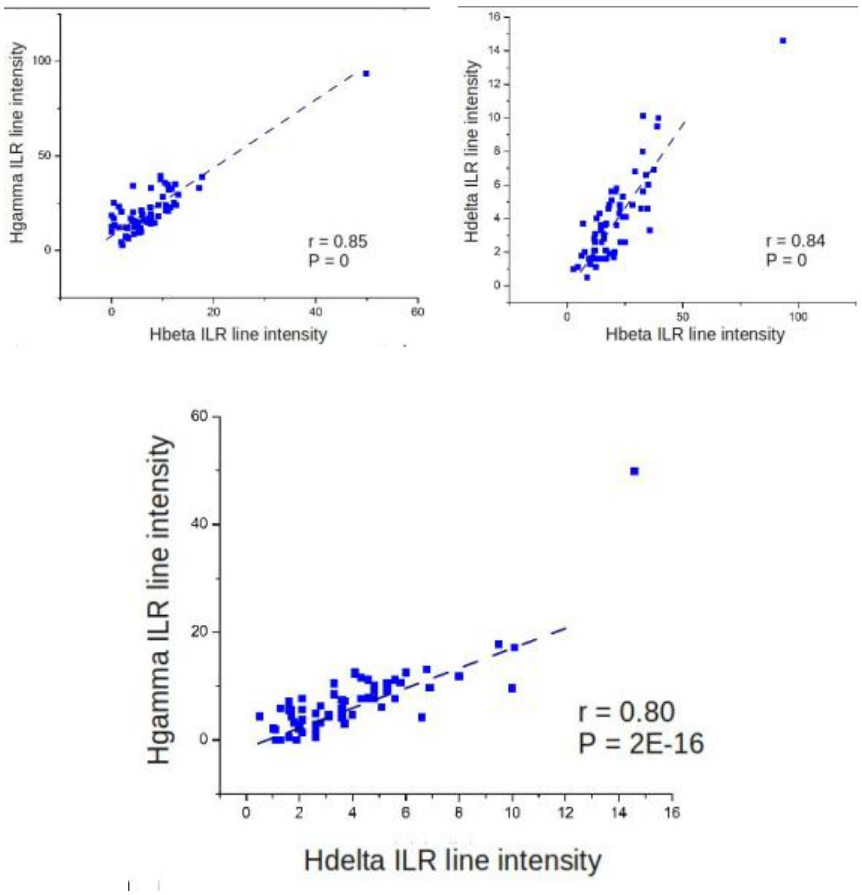

Figure 5.19: Correlations among the ILR component intensities of different Balmer lines. The line intensities are given in units of 10^{-17} erg cm^{-2} s^{-1} Å^{-1}.

5.3 Correlation with the EWs of emission lines

Many correlations were tried out between the Equivalent Widths of emission lines and their ratios, for different emission lines from the analyzed spectral range.

A few very interesting correlations were found for the two ratios - EW [O III]/ EW Fe II (optical) and EW [O III]/ EW Hβ ILR with many other optical and UV emission lines, although the reason behind this significance is not yet understood.

5.3.1 Relations with EW [O III]/ EW Fe II (optical)

We saw a high correlation for the ratio EW [O III]/ EW Fe II (optical) and EW [O III] (r = 0.82, P = 1E-14) (see Figure 5.20) and thus a significant anti-correlation for the same ratio with EW Fe II (optical) (r = -0.56, P = 7E-6) (Figure 5.21).

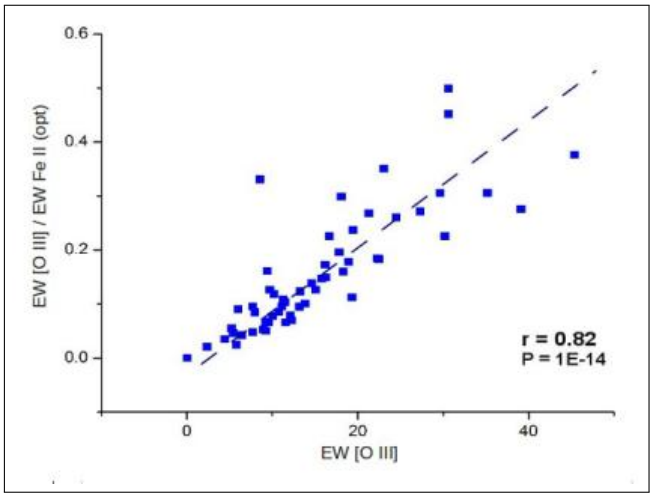

Figure 5.20: The EW [O III] / EW Fe II (opt) presented against EW [O III]. The Pearson corr coefficients are also given. The EWs are in Å.

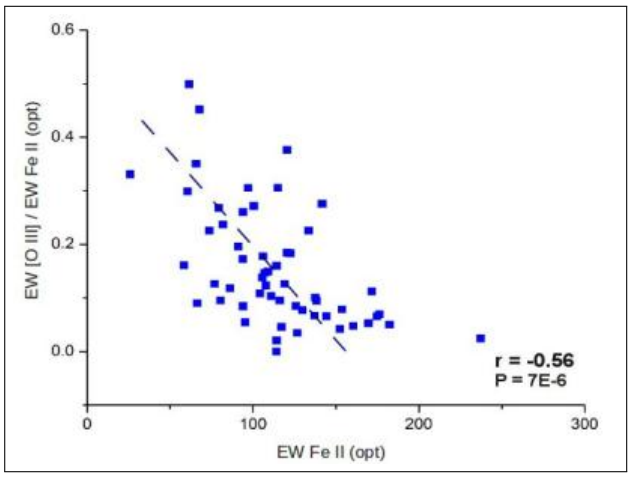

Figure 5.21: The EW [O III] / EW Fe II (opt) presented against EW Fe II (opt). The Pearson corr coefficients are also given. The EWs are in Å.

A high correlation was also seen between the logarithmatic of the ratio EW [O III]/ EW Hβ (NLR, ILR and VBLR) components and log of EW [O III]/ EW Fe II (optical), with the most significant relationship being the one with Hβ ILR component (Figure 5.22).

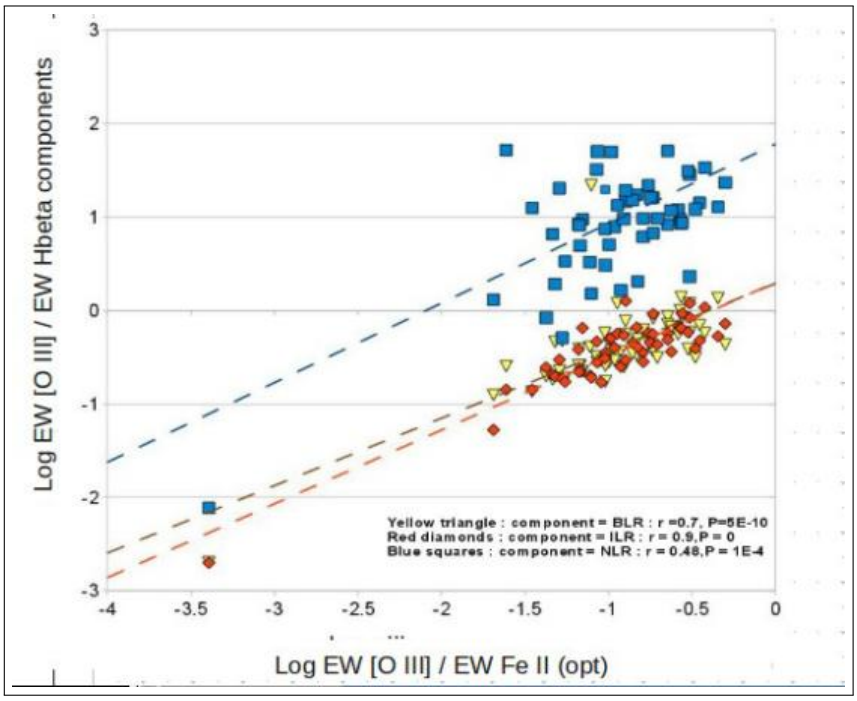

Figure 5.22: The log of EW [O III] / EW Hβ components presented against the log of EW [O III] / EW Fe II (opt) . The Pearson corr coefficients are specified for all the Hβ components. EWs are in Å.

5.3.2 Relations with EW [O III]/ EW Hβ ILR

As shown in the Figure 5.22, log of EW [O III]/ EW Hβ components have good correlations with the log value of the ratio EW [O III]/ EW Fe II (optical). The highest correlation component was obtained between log of EW [O III]/ EW Hβ ILR component and log of EW [O III]/ EW Fe II (optical) with Pearson corr coefficient values : r = 0.9, P = 0. The pearson values showed some significance even for log of EW [O III]/ EW Hβ VBLR vs log of EW [O III]/ EW Fe II (optical) with r = 0.7, P = 5E-10 and log of EW [O III]/ EW Hβ NLR vs log of EW [O III]/ EW Fe II (optical) with Pearson values of r = 0.4, P = 1E-4.

The ratio of EW [O III]/ EW Hβ ILR also shows a very high significance correlation with EW [O III] (Figure 5.23).

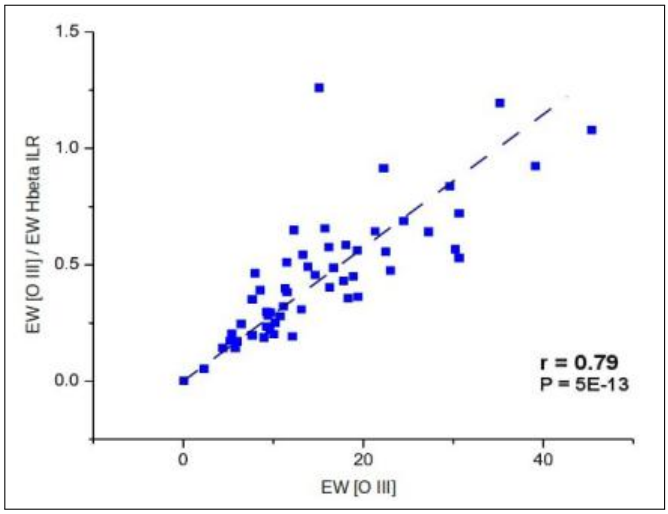

Figure 5.23: The log of EW [O III] / EW Hβ ILR presented against EW [O III]. The Pearson corr coefficients are also specified. EWs are in Å.

There was also a correlation between the EW [O III] / EW Fe II (opt) vs EW [O III] / EW Hβ ILR as shown in Figure 5.24. We saw pearson coefficient values of r = 0.62 and P = 3E-7.

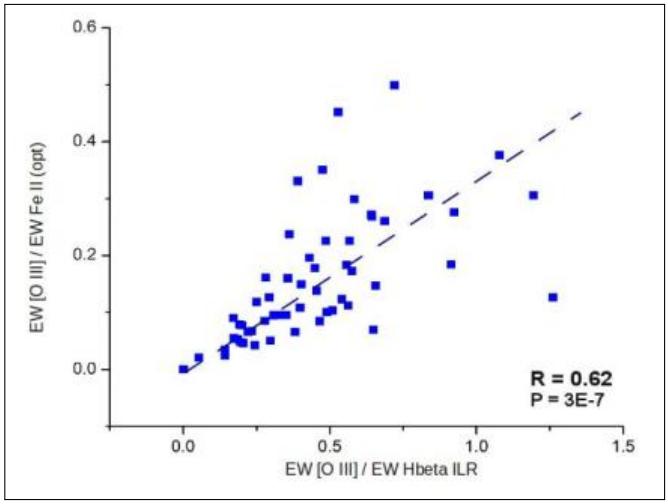

Figure 5.24: The ratio of EW [O III] / EW Fe II (opt) presented against EW [O III] / EW Hβ ILR. The Pearson corr coefficients are also specified.

Chapter 6

Discussion

We have investigated the physical and kinematical characteristics of the different line emission regions in a sample of AGNs by analysing their line parameters and their correlation with the spectral features of other emission lines in the optical and UV wavelength ranges. Some analysis of the results we have obtained and few observations about the sample spectra are discussed here.

6.1 Origin of Emission Lines

6.1.1 Distances of Emission Regions from the Black Hole

From the widths of different emission lines and considering the typical mass of the central black hole of an AGN to be 10^8 $M_\odot$, we can estimate the distance of the line emission regions from the central black hole by taking the simple virial relation. We assume that for the stability of an emission cloud (mass m) moving around the central black hole (mass M) with velocity V km/s at a distance of R meters; it's centripetal force must equal the Gravitation pull towards the black hole :

$$\frac{mV^2}{R} = \frac{GMm}{R^2} \tag{6.1}$$

where G is the gravitational constant: 6.67 x 10^{-11} m^3 kg^{-1} s^2.

Thus we get the distance of the emission cloud from the central black hole (R) as

$$R = \frac{GM}{V^2} \tag{6.2}$$

where the line width gives a reasonable first estimate of the velocity of the lines emission regions.

After looking at the various distances (see Figure 6.1), we figured that the Mg II broad component is emitted closest to the black hole, followed by the Hβ BLR component. They are closely persued by the Fe II UV emission region, which seems to lie in between the VBLR and ILR emission regions. Further out from the black hole comes the intermediate line components of both Mg II and Hβ lines. The emission line regions of Fe II optical components lie very close to the intermediate line emission regions. As it is well known, the furthest from the center is the NLR emitting the narrow lines in a spectra.

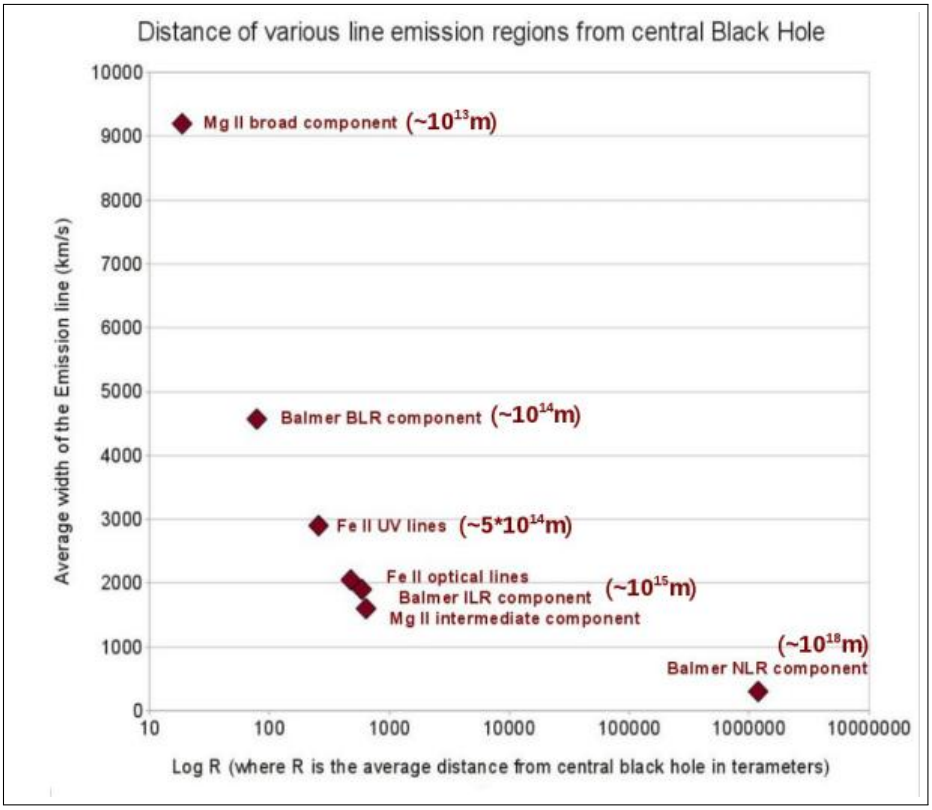

Figure 6.1: The estimated averaged distances of emission line regions from the central black hole, where the mass of black hole is taken as 10^8 $M_\odot$

6.1.2 Optical Fe II emission regions

To get ideas about the location of the optical Fe II emission region, we explored the kinematics of that region and compared the widths and shifts of the optical Fe II, Balmer and Mg II line components. We found that the correlation between the widths of the optical Fe II and Balmer ILR component is significantly higher (r = 0.75, P = 1e-13) than for the VBLR and NLR (see Figure 5.1). Moreover, the average width of the optical Fe II ($\sim$ 2050 km/s) is very close to the average value of the width of the ILR component of Balmer lines ($\sim$ 1900 km/s).

In addition to it, although there was no significant correlation between the Fe II widths and the width of the Mg II broad component, we found a strong correlation (r = 0.69, P = 1E-11) between the widths of the Fe II lines in optical and the intermediate component of the Mg II emission lines (Figure 5.4).

Thus, we observed indication of Fe II emitting region being located in the ILR i.e. the emission region of the intermediate lines which may be the transition region from a torus to the BLR.

This has been proposed earlier by Marziani and Sulentic (1993) and Popović et al. (2004). Few other authors have also noted that the optical Fe II emission arise from a region which lies in the outer parts of the BLR (Gaskell et al., 2007; Hu et al., 2008; Kuehn et al., 2008; Popović et al., 2009; Kovačević et al., 2010).

6.1.3 Regions emitting Fe II in UV

One interesting result regarding the the Fe II UV lines is the very high redshift that they feature (see Figure 6.2).

The Fe II UV lines in most of our spectra were highly redshifted - most of them in the range of 500 - 2500 km/s with an average of $\sim$ 1530 km/s.

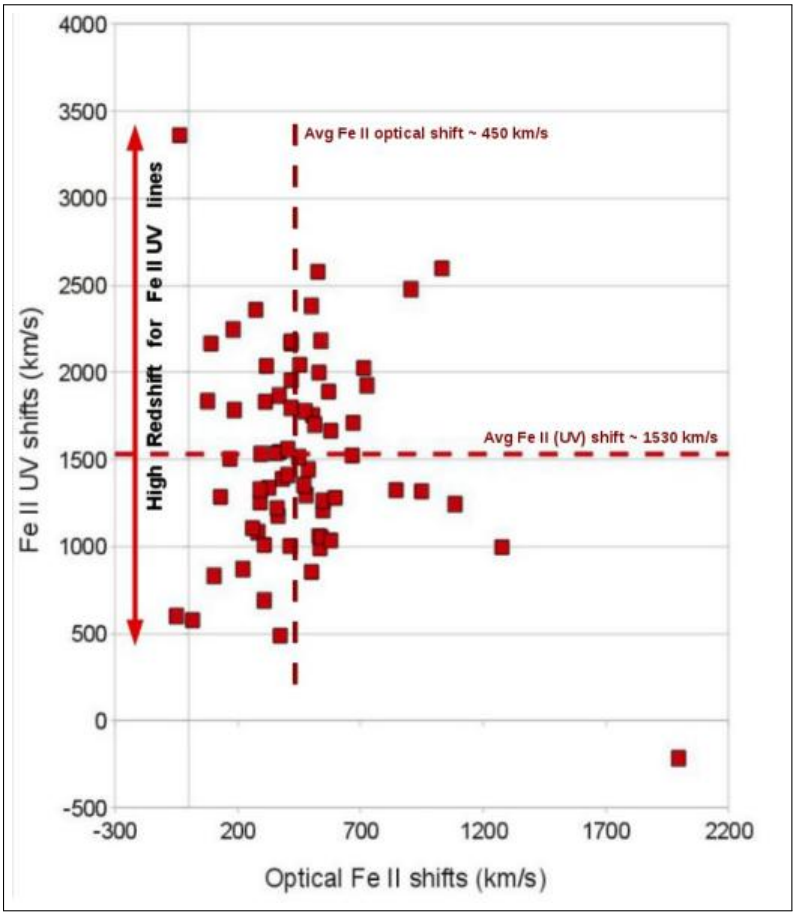

Figure 6.2: Fe II UV shifts vs Fe II optical shifts : the Fe II lines in UV have a high redshift range as compared to the optical Fe II lines

Moreover, we correlated the kinematical parameters (widths and shifts) of the Fe II (UV) lines with the same parameters of the Mg II line components and components of the Balmer lines. No kinematical relationship were found between the emission regions of Fe II UV lines and the Balmer or Mg II line components, though the average width of the Fe II in UV ($\sim$ 2900 km/s) was slightly closer to the average value of the width for the ILR component of Balmer lines ($\sim$ 1900 km/s) as compared to that of NLR and VBLR. There was also no correlation between the emission region of the optical Fe II lines and the region emitting Fe II in UV. Even with the shifts of these lines, we did not catch any relationship. So we conclude that the emission region of the Fe II UV lines is different from these other lines considered in our analysis.

6.2 Highly redshifted Broad component of Hβ

One of the interesting results from the investigation is a highly redshifted VBL component in Hβ that is often seen in so called Pop 1 objects (Sulentic et al., 2009) .

Normally we expect an emission line profile to be such that it has the NLR component in the center taking care of the line core with the BLR component covering for the line wings (see Figure 6.3)

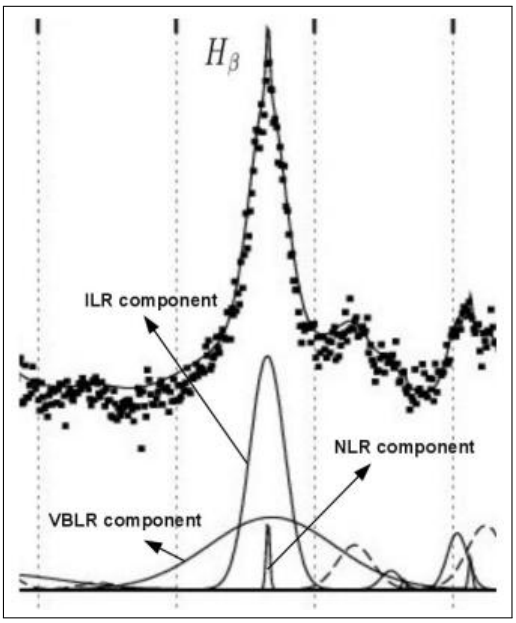

Figure 6.3: Classical Hβ fitting with its NLR, ILR and VBLR components

But in almost half of the spectra from this sample (especially the spectra with line width $>$ 4000 km/s), it was seen that the VBLR component of Hβ is unusually highly redshifted compared to the NLR and ILR Hβ components. The high redshift range of the VBLR components as compared to that of the ILR and NLR components can be seen in Figure 6.4.

This can be a real physical asymmetry, but no justification could be ascribed by us to this strange behaviour yet, and this should be studied in more details in the future work.

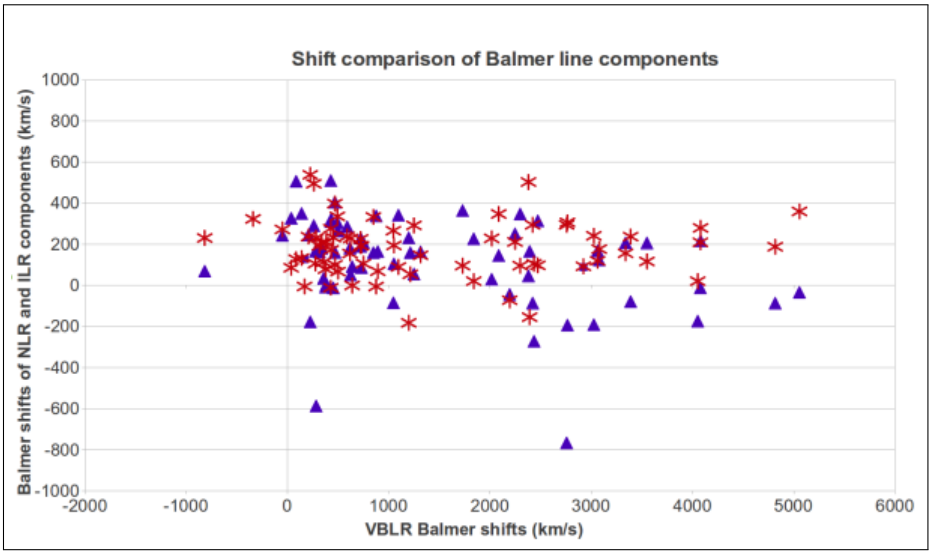

Figure 6.4: Shifts of Hβ VBLR (in x-axis) plotted against the shifts of Hβ NLR (red asteriks) and Hβ ILR component (blue triangles).

This highly redshifted VBLR component might even be artificial and it is normal to suspect that we are missing few other lines under the Hβ and [O III] emission lines, which are present but their importance has been underestimated in our analysis. This wavelength range from $\sim$ 4900 Å to $\sim$ 5100 Å is generally complicated due to the presence of numerous emission lines - most of the contribution coming from Hβ broad component, the forbidden [O III] doublet and few iron lines. But there can be additional contributions from more iron lines or may be even weaker helium lines.

6.3 Broad [O III] component

The [O III] $\lambda\lambda 4959, 5007 \mathring{A}$ lines are typical forbidden lines in a quasar spectra. Normally, forbidden lines have extremely low transition probabilities and are emitted only in some ideal emission environments like low density plasma with optimal temperature. The NLR provides such conditions to let these forbidden lines arise while these lines are absent in the Broad line spectra.

The [O III] $\lambda\lambda 4959, 5007 \mathring{A}$ being a forbidden line should have only a narrow component in it's emission line profile. But sometimes, as shown in

Figure 6.5, it has been observed that the line profile shows some contribution from the broad region too (Popović et al., 2004; Ilić et al., 2006; Kovačević et al., 2010).

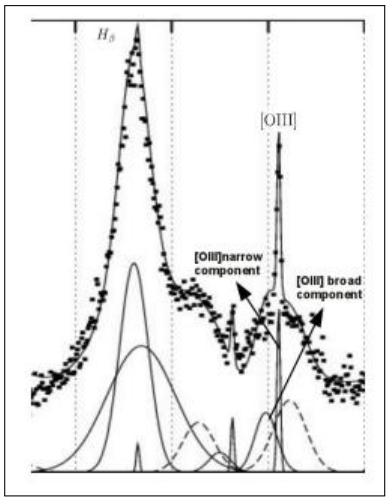

Figure 6.5: Fitting of the forbidden [O III] doublet showing both the narrow and the 'broad' components.

The broad line component of [O III], in our analysis is generally seen to be between ∼20 km/s and ∼3500 km/s and mostly they are observed to be blue-shifted (98 out of 100 spectra showed this trend). In very few cases, this broad [O III] component seemed to have a width more than ∼ 1000 km/s, which is generally not expected.

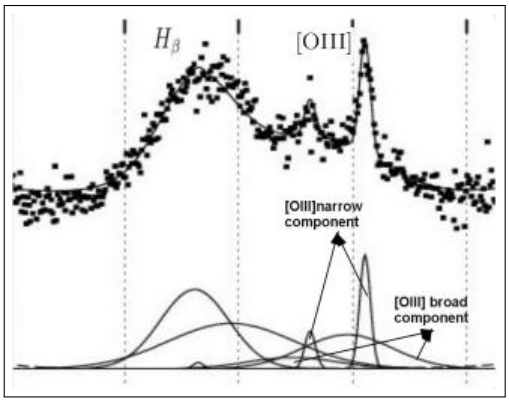

Figure 6.6: An unusual quasar spectra with a broad [O III] component having width of ∼ 3330 km/s

The spectrum presented in Figure 6.6 has such broad [O III] component, which is physically prohibited. This seemingly broadened component might be a result of blending of many different narrower gaussians which are [O III] emissions coming from different outflowing regions differing slightly in their shifts. All these gaussians add up to produce one final single gaussian which can be seen in the QSO spectra as one broad component.

Chapter 7

Conclusions

This master thesis is a part of a project to investigate relationship between the UV and optical line emitting regions. The complete sample has 333 AGNs and here we did a test work on a subsample of 100 AGNs.

We took the 100 spectra from SDSS DR7 and corrected them for redshift and reddening. Then we fitted all of them with multi-gaussian procedure considering each emission line to be composite of contributions from different emission regions having different physical properties. It was also assumed that all the Balmer lines (Hβ, Hγ and Hδ) originate at the same emitting regions and hence should have same widths and shifts for their constituent components. From the best fit obtained by χ^2 method, we extracted various line parameters as the widths, shifts, intensities of all the line components. We further calculated few other signatures of the emission lines like the FWHM, equivalent width, etc. The parameters obtained for different emission lines were then correlated to find connection between various line emitting regions.

Even a smaller number of AGNs can lead us to some valuable conclusions which probably will not be changed after analysis of the complete sample. A few of them are :

1. By comparing the widths and shifts of the Fe II, Balmer and Mg II line components, we found a high correlation between the widths of the Fe II optical lines and Balmer ILR component (r = 0.75, P = 1e-13). Moreover, the average width of the optical Fe II ($\sim$ 2050 km/s)

is very close to the average value of width for the ILR component of Balmer lines ($\sim$ 1900 km/s). We also found a strong relationship (r = 0.69, P = 1E-11) between the widths of Fe II optical lines and the intermediate component of the Mg II emission line, So we confirm an indication of Fe II emitting region being located in the ILR which has been earlier suggested by Marziani and Sulentic (1993), Popović et al. (2004), Kuehn et al. (2008) etc.

2. The distances of various emission regions from the central black hole were calculated by taking the mass of the central black hole to be 10^8 $M_\odot$ and by using the simple virial relation. As previously suggested in literature, this sample data confirms a stratification of emission regions in an AGN. The closest to the black hole were the Mg II broad component emission region, followed closely by the broad line region emitting Hβ. Further out from the black hole comes the intermediate line components of both Mg II and Hβ lines. The Fe UV emission region seems to lie in between the VBLR and ILR emission regions, while the emission line regions of Fe II optical components were found to lie very close to the intermediate line emission regions. The furthest from the center is of course the narrow line region.

3. We found some promising relationships between various emission line equivalent widths and their ratios. Eg. high correlations were found between EW [O III]/ EW Fe II (optical) and EW [O III] (r = 0.82, P = 1E-14) while an equally significant anti-correlation was seen for the same ratio with EW Fe II (optical) (r = -0.56, P = 7E-6). A good correlation was also spotted between log of the ratio EW [O III]/ EW Hβ components and log of EW [O III]/ EW Fe II (optical) with Hβ ILR component showing the closest relationship. This ratio of EW [O III]/ EW Hβ ILR also shows a very high significance correlation with EW [O III].

As we noted above, here we give investigation of a subsample of 100 AGNs and in the future we plan to fit the total sample of 333 spectra and extract line parameters. We plan to explore new correlations to find kinematic similarities or differences between Fe II lines in UV and optical, search for Baldwin effect in the Balmer, [O III], Mg II and Fe II emission lines and explore possible physical mechanisms behind these correlations.

Chapter 8

Appendix

8.1 Line parameters obtained from the best fit

8.1.1 Shifts of the lines in km/s

	SDSS name (SDSS J)	Redshit	NLR	Hb ILR	Hb BLR	Fe optical	Mg broad	Mg IL	Fe UV
1	014942.51+001501.73	0.552	96.555	364.719	1729.743	578.406	861.453	262.458	1665.366
2	033438.28-071149.03	0.634	54.69	159.777	1213.776	453.069	1524.189	235.563	2042.277
3	032205.05+001201.48	0.471	90.174	342.666	1096.311	667.008	-190.407	232.383	1521.48
4	112158.37+651716.20	0.502	228.684	52.014	623.598	368.277	2205.333	123.957	1866.063
5	163746.56+425449.66	0.544	194.7	105.828	1051.845	534.738	2471.961	322.566	990.168
6	004222.29-103743.70	0.423	292.314	55.977	1249.686	292.245	861.594	251.34	1531.44
7	020435.19-093155.02	0.623	336.132	306.411	493.599	369.579	1668.837	295.932	1544.079
8	020039.16-084555.01	0.431	133.527	350.37	140.079	290.973	757.494	140.556	1252.599
9	210001.25-071136.34	0.599	98.043	315.075	2473.017	536.646	834.915	185.829	2180.925
10	212619.66-065408.95	0.418	-154.146	166.08	2392.53	500.676	1157.721	113.844	852.588
11	223500.74-101216.83	0.553	193.083	190.524	723.264	531.099	920.451	264.114	1058.781
12	091957.60+510609.61	0.553	347.754	146.067	2086.986	545.544	1226.724	193.551	1206.732
13	093930.09+514103.62	0.605	276.258	310.71	427.305	412.548	2514.678	259.224	1003.926
14	105122.29+020736.63	0.599	21.141	227.619	1839.678	546.645	-430.557	320.823	1262.151
15	111507.66+023757.62	0.566	226.374	230.181	723.762	488.202	-933.714	229.353	1441.455
16	085334.25+434902.33	0.514	155.328	182.322	617.598	379.539	1060.929	189.876	1389.27
17	091625.40+471441.64	0.538	-10.839	510.696	428.184	530.841	270.867	336.54	1998.939
18	083010.51+321352.74	0.521	116.763	207.243	3550.602	1997.07	1053.489	-78.882	-215.502
19	112224.15+031802.59	0.474	192.381	162.834	315.54	538.194	-1223.391	242.622	1053.78
20	163746.56+425449.66	0.544	-181.662	232.458	1198.2	362.088	2117.436	120.789	1175.358
21	095000.74+483129.33	0.588	172.977	323.214	431.937	526.053	-479.127	253.467	2577.516
22	095257.15+050910.31	0.543	210.507	181.137	338.421	282.078	728.481	174.435	1081.992
23	115355.82+543528.40	0.440	398.508	406.05	468.459	478.089	-1287.129	457.155	1295.316
24	113615.14+103430.94	0.522	238.83	286.104	590.172	505.023	-179.544	258.381	1752.915
25	150257.98+502914.85	0.530	237.714	-78.216	3389.634	75.513	1064.925	36.261	1835.352
26	111357.36+425326.34	0.441	294.831	-85.2	2422.035	448.539	864.108	53.802	1512.306
27	135459.65+405218.24	0.473	306.843	-192.765	2765.817	103.392	-208.773	80.457	831.108
28	123734.47+444731.74	0.460	176.961	124.404	3079.488	947.145	708.939	116.892	1315.746
29	163746.56+425449.66	0.544	21.057	-172.857	4052.475	1085.787	-27.231	85.5	1243.806
30	141842.22+423343.34	0.420	272.613	243.768	-50.082	577.41	-326.997	-134.232	1035.114
31	073314.35+431049.04	0.500	279.978	217.593	4080.795	307.086	-823.113	237.3	689.796
32	112643.02+154554.87	0.434	266.454	-83.811	1046.616	185.682	945.174	22.665	1783.638

	SDSS name (SDSS J)	Redshit	NLR	Hb ILR	Hb BLR	Fe optical	Mg broad	Mg IL	Fe UV
33	095623.21+323621.71	0.526	100.827	161.058	469.239	179.955	588.858	171.342	2246.508
34	161916.55+334238.40	0.470	188.409	-85.92	4817.22	166.353	-60.801	-5.34	1502.622
35	114212.33+301613.39	0.481	193.266	86.952	730.767	371.616	1948.209	106.725	487.8
36	132115.86+284719.50	0.549	333.321	159.996	848.955	357.564	355.08	131.67	1535.097
37	122520.13+084450.78	0.535	93.234	89.412	2923.098	403.311	1282.122	212.676	1558.953
38	105157.24+375429.12	0.561	360.186	-33.207	5056.5	711.336	300	397.914	2025.354
39	161924.11+260907.30	0.628	86.181	327.384	37.275	403.23	40.821	279.648	1409.487
40	145450.03+111434.51	0.467	211.836	251.391	2247.669	312.729	-1284.366	286.392	1831.107
41	083332.92+164411.09	0.460	96.384	347.997	2298.84	475.494	-416.232	265.608	1776.243
42	094236.68+192541.22	0.539	209.712	4.233	382.836	258.861	1598.472	79.599	1105.746
43	103458.43+204912.23	0.516	106.401	166.782	276.72	220.173	115.071	170.133	869.799
44	114212.33+301613.39	0.481	156.642	207.342	3339.753	669.693	-957.342	288.207	1710.702
45	083010.51+321352.74	0.521	-4.815	128.52	169.233	128.937	1758.177	-21.78	1283.043
46	130357.42+103313.50	0.589	503.328	47.064	2380.89	417.183	-416.208	295.923	1796.691
47	074619.19+444707.87	0.601	0.225	92.016	639.786	514.167	222.078	86.445	1700.085
48	150527.60+294718.38	0.526	-71.562	-43.071	2194.746	597.654	679.923	-11.472	1279.956
49	083109.40+143448.94	0.565	241.704	-190.341	3025.86	725.124	74.85	260.814	1925.37
50	140356.15+080731.66	0.591	495.018	291.474	260.391	417.6	240.843	220.563	1955.559
51	154453.86+165710.12	0.518	105.522	-271.107	2435.598	845.025	1192.179	121.035	1324.02
52	154333.95+102231.90	0.486	106.542	208.557	750.198	326.559	1193.976	267.795	1337.4
53	130435.04+184749.04	0.641	232.761	-11.463	453.177	315.528	751.737	-144.504	2035.794
54	143222.85+184343.41	0.550	294.696	-765.465	2757.495	-401.115	154.311	333.24	2015.637
55	155821.86+120533.23	0.574	209.838	-10.995	4078.245	1276.779	185.049	250.629	996.195
56	160739.30+103555.69	0.458	146.88	163.575	1314.582	290.154	499.695	295.431	1326.513
57	095758.44-002354.0	0.595	128.004	506.994	86.001	570.051	432.303	546.513	1889.859
58	151722.51-003002.7	0.444	231.018	70.098	-816.936	416.67	-968.778	-53.493	2164.563
59	170533.69+644004.7	0.534	69.21	165.486	892.29	416.142	418.263	166.713	2176.722
60	171334.02+595028.3	0.615	67.458	264.855	499.17	90.972	0	600	2164.563
61	024240.31+005727.1	0.569	-5.007	338.991	876.366	-38.361	-182.253	258.447	3360.939
62	011132.32+133519.1	0.576	323.721	2264.781	-339.396	904.329	550.797	184.11	2476.806
63	024651.91-005930.9	0.467	237.516	245.814	207.579	308.262	232.572	113.208	1008.444
64	234440.03-003231.6	0.502	538.278	-176.925	225.234	-52.065	149.598	69.939	600.399
65	040148.98-054056.64	0.570	119.814	168.198	3063.255	499.062	-1048.491	543.81	2382.207
66	041210.17-051109.1	0.549	79.215	-7.449	376.521	13.794	-630.627	192.249	575.739
67	085559.00+005745.4	0.454	231.798	-585.705	283.548	360.21	-778.167	-407.328	1218.54
68	094443.08+580953.2	0.562	229.329	30.627	2016.78	272.523	901.551	561.627	2359.539
69	122806.90+670844.1	0.443	113.622	35.436	357.534	1030.479	32.901	241.584	2597.679

8.1.2 Widths of the lines in km/s

SDSS name (SDSS J)	NLR	Balmer ILR	Balmer BLR	Mg broad	Mg IL	Fe optical	Fe UV
014942.51+001501.73	494.463	2159.406	4401.081	7329.66	1581.027	2912.04	2912.04
033438.28-071149.03	201.825	2045.076	4523.082	12639.114	2034.435	2584.449	2584.449
032205.05+001201.48	299.439	2108.466	6569.517	9332.064	1619.91	2581.728	2581.728
112158.37+651716.20	195.012	1416.36	3548.448	8274.06	1274.964	5508.72	5508.72
163746.56+425449.66	116.541	1709.097	4406.409	5883.138	1422.516	4830.993	4830.993
004222.29-103743.70	313.191	1432.188	4426.041	7329.66	1176.744	4159.767	4159.767
020435.19-093155.02	116.433	1097.973	3975.15	9429.24	1188.777	3205.506	3205.506
020039.16-084555.01	188.367	967.788	2875.386	8073.024	1015.242	1580.175	1580.175
210001.25-071136.34	799.305	2353.83	5515.587	9249.516	1512.855	4599.135	4599.135
212619.66-065408.95	203.76	1915.062	3012.639	8651.973	1534.845	1794.18	1794.18
223500.74-101216.83	289.62	1602.012	3984.18	6348.21	1748.724	2145.819	2145.819
091957.60+510609.61	335.799	1809.48	5380.857	6926.829	1448.211	2058.768	2058.768
093930.09+514103.62	278.64	862.491	3169.278	6032.379	1182.828	1596.162	1596.162
105122.29+020736.63	294.606	1314.852	5371.821	10137.567	1527.801	1896.489	1896.489
111507.66+023757.62	243.705	1396.095	4597.068	9842.913	1520.793	2059.698	2059.698
085334.25+434902.33	475.863	1421.16	4380.378	10196.736	1229.253	2143.986	2143.986
091625.40+471441.64	340.515	1481.925	4786.662	9811.461	1285.674	1761.501	1761.501
083010.51+321352.74	215.097	3090.615	7139.472	4561.512	1891.17	2486.514	2486.514
112224.15+031802.59	145.722	1424.016	3265.908	10704.936	1316.439	3874.581	3874.581
163746.56+425449.66	341.091	1199.703	3893.898	6487.815	1731.48	2035.323	2035.323
095000.74+483129.33	302.112	1521.345	3965.778	9823.485	1374.096	6951.993	6951.993
095257.15+050910.31	514.584	1451.511	3571.569	7928.016	1093.464	3857.415	3857.415
115355.82+543528.40	354.369	1850.058	3586.167	7372.158	1500.096	2838.234	2838.234
113615.14+103430.94	222.522	1474.935	4465.845	10764.006	1584.705	1990.254	1990.254
150257.98+502914.85	319.161	2420.775	4511.316	9136.743	1477.851	3197.724	3197.724
111357.36+425326.34	152.07	1825.926	3348.105	8308.533	1640.922	2298.618	2298.618
135459.65+405218.24	459.387	1711.911	4079.685	11694.066	1332.642	1565.997	1565.997
123734.47+444731.74	212.874	2411.214	5731.488	5861.877	1604.766	2155.539	2155.539
163746.56+425449.66	60.636	2190.414	5548.335	9419.307	1501.119	1969.842	1969.842
141842.22+423343.34	286.314	2406.996	4289.628	10441.821	1527.027	2554.332	2554.332
073314.35+431049.04	530.262	1948.011	5774.367	12676.026	979.401	1236.9	1236.9
112643.02+154554.87	329.958	1649.076	5175.312	9377.034	1223.82	2842.638	2842.638

SDSS name (SDSS J)	NLR	Balmer ILR	Balmer BLR	Mg broad	Mg IL	Fe optical	Fe UV
095623.21+323621.71	420.51	1162.578	3469.266	10628.55	1141.758	3937.05	3937.05
161916.55+334238.40	229.449	2607.444	6607.116	7541.109	2327.319	7587.972	7587.972
114212.33+301613.39	358.671	1649.439	4416.675	6321.153	1404.477	2596.689	2596.689
132115.86+284719.50	672.441	1861.632	4722.399	10867.902	1094.157	2057.034	2057.034
122520.13+084450.78	148.629	2038.434	5813.373	7785.528	1808.079	3132.513	3132.513
105157.24+375429.12	345.84	2718.36	4767.042	11100	2771.85	3766.605	3766.605
161924.11+260907.30	258.537	859.134	2947.194	13251.651	1252.335	1689.525	1689.525
145450.03+111434.51	368.043	1792.641	7167.453	9685.917	1672.485	2724.75	2724.75
083332.92+164411.09	274.428	1932.957	6585.27	12376.446	1611.573	2382.867	2382.867
094236.68+192541.22	606.18	1668.723	4076.625	6792.195	1056.204	2204.496	2204.496
103458.43+204912.23	195.162	1231.509	3308.418	9457.314	1359.018	1493.952	1493.952
114212.33+301613.39	295.509	2431.953	5068.707	12572.427	1640.877	2573.736	2573.736
083010.51+321352.74	430.548	1834.308	3011.049	5825.658	1089.741	1378.77	1378.77
130357.42+103313.50	608.955	1732.608	6308.832	12376.446	1157.958	4030.776	4030.776
074619.19+444707.87	171.102	1528.62	3893.271	9552.978	1727.394	2096.373	2096.373
150527.60+294718.38	400.059	2858.112	3956.829	7342.077	1638.462	2889.867	2889.867
083109.40+143448.94	210.474	2400.483	5907.21	10178.718	2413.128	3053.157	3053.157
140356.15+080731.66	240.165	1074.741	3195.672	12103.389	1309.752	2693.316	2693.316
154453.86+165710.12	283.536	1665.102	4714.251	8249.631	1693.62	2284.716	2284.716
154333.95+102231.90	232.227	1214.652	4127.151	10500	1379.409	2281.341	2281.341
130435.04+184749.04	139.029	1296.066	3102.603	14037.36	1496.706	3820.719	3820.719
143222.85+184343.41	222.642	3076.761	5287.23	8962.557	2442.555	3323.502	3323.502
155821.86+120533.23	216.237	2287.227	6181.062	7850.511	1866.156	2966.148	2966.148
160739.30+103555.69	360.252	1968.255	4099.209	8199.12	1596.048	3633.951	3633.951
095758.44-002354.0	267.78	2611.257	4789.284	8096.916	2149.443	2851.908	2851.908
151722.51-003002.7	256.791	1437.855	6223.734	9306.138	1360.992	4689.486	4689.486
170533.69+644004.7	300.171	1817.724	4377.249	8858.604	1370.616	4573.392	4573.392
171334.02+595028.3	239.409	2938.191	8983.968	9000	2100	4689.486	4689.486
024240.31+005727.1	292.995	1039.416	4732.377	7756.626	1337.451	5188.413	5188.413
011132.32+133519.1	33.3	4079.568	2502.174	8542.896	1644.453	4561.596	4561.596
024651.91-005930.9	143.028	947.13	2537.073	7726.305	1094.913	1248.066	1248.066
234440.03-003231.6	4.077	1427.685	3372.339	7852.095	1620.051	1457.229	1457.229
040148.98-054056.64	553.275	3807.732	5043.639	13073.841	2077.038	3734.652	3734.652
041210.17-051109.1	362.559	711.066	4920.093	6259.821	1296.084	1094.97	1094.97
085559.00+005745.4	364.35	2156.187	5125.779	9846.597	2291.166	3625.032	3625.032
094443.08+580953.2	399.438	2635.614	4839.048	11878.581	3257.016	2458.536	2458.536
122806.90+670844.1	165.603	844.14	3371.961	11636.694	1618.836	2144.802	2144.802

8.1.3 EWs of the lines in Å

	SDSS name (SDSS J)	z	Fe UV	OIII EW	Hb NLR EW	Hb ILR EW	Hb BLR EW	Fe optical EW
1	014942.51+001501.73	0.552	1665.366	1.00491E+01	3.06213E+00	4.99484E+01	2.47393E+01	1.29739E+02
2	033438.28-071149.03	0.634	2042.277	1.07531E+01	2.15066E-01	3.86326E+01	3.83556E+01	1.25757E+02
3	032205.05+001201.48	0.471	1521.48	1.83092E+01	2.97798E+00	5.13108E+01	5.54934E+01	1.14271E+02
4	112158.37+651716.20	0.502	1866.063	0.00000E+00	0.00000E+00	0.00000E+00	0.00000E+00	5.12736E-01
5	163746.56+425449.66	0.544	990.168	2.96211E+01	1.04210E+00	3.54199E+01	5.03923E+01	9.68830E+01
6	004222.29-103743.70	0.423	1531.44	1.61847E+01	7.46341E-01	2.81116E+01	3.49160E+01	9.37025E+01
7	020435.19-093155.02	0.623	1544.079	5.41823E+00	8.26872E-01	2.64612E+01	2.96355E+01	1.17110E+02
8	020039.16-084555.01	0.431	1252.599	2.22696E+01	3.31203E+00	2.43696E+01	2.72116E+01	1.20378E+02
9	210001.25-071136.34	0.599	2180.925	1.02087E+01	6.19628E+00	4.07304E+01	2.80545E+01	8.62190E+01
10	212619.66-065408.95	0.418	852.588	9.70498E+00	6.62432E-01	3.30390E+01	1.26538E+01	7.68227E+01
11	223500.74-101216.83	0.553	1058.781	9.25697E+00	4.58320E-01	3.11613E+01	4.04901E+01	1.82329E+02
12	091957.60+510609.61	0.553	1206.732	4.41799E+00	3.55389E-01	3.12024E+01	3.25172E+01	1.26836E+02
13	093930.09+514103.62	0.605	1003.926	1.38461E+01	2.76531E+00	2.82138E+01	4.96826E+01	1.37577E+02
14	105122.29+020736.63	0.599	1262.151	4.54044E+01	1.34998E+00	4.21070E+01	7.95160E+01	1.20483E+02
15	111507.66+023757.62	0.566	1441.455	2.24935E+01	1.39824E+00	4.04216E+01	6.06827E+01	1.22329E+02
16	085334.25+434902.33	0.514	1389.27	1.11205E+01	3.66853E+00	3.45954E+01	4.33748E+01	1.16175E+02
17	091625.40+471441.64	0.538	1998.939	1.89119E+01	1.18819E+00	4.20379E+01	3.97940E+01	1.06131E+02
18	083010.51+321352.74	0.521	-215.502	0.00000E+00	0.00000E+00	0.00000E+00	0.00000E+00	5.98070E-01
19	112224.15+031802.59	0.474	1053.78	1.14986E+01	2.31975E-01	2.25490E+01	3.10855E+01	1.10924E+02
20	163746.56+425449.66	0.544	1175.358	1.57696E+01	9.16096E-01	2.40459E+01	4.75251E+01	1.07046E+02
21	095000.74+483129.33	0.588	2577.516	2.44973E+01	2.04550E+00	3.56403E+01	4.40617E+01	9.39443E+01
22	095257.15+050910.31	0.543	1081.992	6.42751E+00	7.71979E+00	2.61689E+01	3.23484E+01	1.52295E+02
23	115355.82+543528.40	0.440	1295.316	1.13114E+01	1.44169E+00	2.83629E+01	3.85662E+01	1.04162E+02
24	113615.14+103430.94	0.522	1752.915	1.46472E+01	9.70341E-01	3.21905E+01	4.23696E+01	1.05575E+02
25	150257.98+502914.85	0.530	1835.352	2.33672E+00	1.79100E+00	4.42410E+01	1.86794E+01	1.14262E+02
26	111357.36+425326.34	0.441	1512.306	2.13067E+01	2.27259E+00	3.31055E+01	2.12786E+01	7.92932E+01
27	135459.65+405218.24	0.473	831.108	7.66588E+00	3.99841E+00	3.90723E+01	1.67012E+01	1.60354E+02
28	123734.47+444731.74	0.460	1315.746	2.72886E+01	3.19183E+00	4.25010E+01	1.96215E+01	1.00451E+02
29	163746.56+425449.66	0.544	1243.806	5.78309E+00	1.12163E-01	4.07225E+01	2.28728E+01	2.37273E+02
30	141842.22+423343.34	0.420	1035.114	1.93325E+01	1.45269E+00	3.44185E+01	1.61412E+01	1.71654E+02
31	073314.35+431049.04	0.500	689.796	8.95862E+00	1.76014E+01	4.78500E+01	1.88264E+01	1.69648E+02
32	112643.02+154554.87	0.434	1783.638	3.91228E+01	4.55786E+00	4.23385E+01	4.68099E+01	1.41732E+02

	SDSS name (SDSS J)	z	Fe UV	OIII EW	Hb NLR EW	Hb ILR EW	Hb BLR EW	Fe optical EW
33	095623.21+323621.71	0.526	2246.508	1.22888E+01	1.30094E+00	1.89404E+01	5.54088E+01	1.76304E+02
34	161916.55+334238.40	0.470	1502.622	2.30390E+01	1.62536E+00	4.85276E+01	3.29506E+01	6.56677E+01
35	114212.33+301613.39	0.481	487.8	3.02240E+01	3.64612E+00	5.32684E+01	3.54999E+01	1.33644E+02
36	132115.86+284719.50	0.549	1535.097	1.62721E+01	8.03815E+00	4.03455E+01	3.34567E+01	1.08978E+02
37	122520.13+084450.78	0.535	1558.953	5.21497E+00	1.55688E+00	3.02089E+01	2.75800E+01	9.51411E+01
38	105157.24+375429.12	0.561	2025.354	1.66858E+01	3.28065E-01	3.42817E+01	2.36511E+01	7.37682E+01
39	161924.11+260907.30	0.628	1409.487	1.50790E+01	7.81543E-01	1.19546E+01	2.68208E+01	1.19075E+02
40	145450.03+111434.51	0.467	1831.107	1.78176E+01	1.85417E+00	4.13575E+01	5.71961E+01	9.10179E+01
41	083332.92+164411.09	0.460	1776.243	9.41282E+00	9.84239E-01	3.34084E+01	1.51693E+01	5.84060E+01
42	094236.68+192541.22	0.539	1105.746	3.51742E+01	1.52932E+01	2.94538E+01	2.93560E+01	1.15005E+02
43	103458.43+204912.23	0.516	869.799	9.25496E+00	1.88976E+00	3.95098E+01	3.60202E+01	1.37082E+02
44	114212.33+301613.39	0.481	1710.702	1.94484E+01	1.66640E+00	5.37286E+01	2.93405E+01	8.18616E+01
45	083010.51+321352.74	0.521	1283.043	1.21130E+01	8.02596E+00	6.32154E+01	5.56248E-01	1.53785E+02
46	130357.42+103313.50	0.589	1796.691	4.60863E-02	5.93645E+00	2.30345E+01	2.29156E+01	1.14062E+02
47	074619.19+444707.87	0.601	1700.085	7.69029E+00	3.91500E-01	2.19196E+01	4.44644E+01	8.03679E+01
48	150527.60+294718.38	0.526	1279.956	1.31352E+01	1.77843E+00	4.27425E+01	2.28719E+01	1.38329E+02
49	083109.40+143448.94	0.565	1925.37	3.06369E+01	1.32727E+00	4.25294E+01	7.11242E+01	6.13484E+01
50	140356.15+080731.66	0.591	1955.559	1.15419E+01	1.36779E+00	3.01924E+01	4.45823E+01	1.74738E+02
51	154453.86+165710.12	0.518	1324.02	1.80913E+01	5.85763E-01	3.09710E+01	4.70402E+01	6.04859E+01
52	154333.95+102231.90	0.486	1337.4	1.32870E+01	1.39355E+00	2.45122E+01	5.35746E+01	1.07865E+02
53	130435.04+184749.04	0.641	2035.794	7.97935E+00	2.49944E-01	1.71794E+01	2.49151E+01	9.40171E+01
54	143222.85+184343.41	0.550	2015.637	8.56105E+00	7.10621E-01	2.19111E+01	2.72390E+01	2.58907E+01
55	155821.86+120533.23	0.574	996.195	3.06459E+01	2.39364E+00	5.79331E+01	2.27229E+01	6.78085E+01
56	160739.30+103555.69	0.458	1326.513	9.58989E+00	1.18206E+00	4.35710E+01	2.47823E+01	1.44156E+02
57	095758.44-002354.0	0.595	1889.859	1.49052E+01	6.47471E-02	7.77444E+01	1.37659E+01	1.05637E+02
58	151722.51-003002.7	0.444	2164.563	1.14774E+01	2.41071E+00	1.78628E+01	3.69625E+01	1.44943E+02
59	170533.69+644004.7	0.534	2176.722	2.26897E+01	3.73204E+00	4.22058E+01	4.68241E+01	1.86473E+02
60	171334.02+595028.3	0.615	2164.563	3.13258E+01	1.69983E+00	2.16931E+01	3.70558E+01	3.81122E+01
61	024240.31+005727.1	0.569	3360.939	4.90412E+01	1.77166E+00	1.77519E+01	6.57070E+01	1.34715E-01
62	011132.32+133519.1	0.576	2476.806	1.10557E+01	1.61803E-01	4.05806E+01	2.05076E+01	7.87627E+01
63	024651.91-005930.9	0.467	1008.444	1.52598E+01	3.52227E+00	2.24171E+01	4.48033E+01	1.19109E+02
64	234440.03-003231.6	0.502	600.399	7.16238E+00	1.66890E-01	1.52582E+01	4.88733E+01	9.31212E+01
65	040148.98-054056.64	0.570	2382.207	5.98071E+00	9.63067E-05	3.50198E+01	2.05691E+01	6.62387E+01
66	041210.17-051109.1	0.549	575.739	1.68414E+02	2.12225E+00	1.34882E+01	9.15341E+01	2.70496E-01
67	085559.00+005745.4	0.454	1218.54	1.32003E+01	9.75956E-01	2.77246E+01	4.94989E+01	8.44811E+01
68	094443.08+580953.2	0.562	2359.539	3.06512E+01	3.23859E-01	2.84147E+01	3.00727E+01	7.04056E+01
69	122806.90+670844.1	0.443	2597.679	1.72312E+01	7.92148E-01	8.60357E+00	6.87082E+01	7.03756E+01

Bibliography

Abazajian, K., Jennifer K. Adelman-McCarthy, Marcel A. Ageros, Sahar S. Allam, et al. 2009, ApJS, 182, 543

Antonucci, R. R. J. 1984, ApJ, 278, 499

Antonucci, R. A. R. 1993, ARA&A, 31, 473

Antonucci, R. R. J., & Miller, J. S. 1985, ApJ, 297, 476

Baldwin, J. 1977, ApJ, 214, 679

Baldwin, J. A., Phillips, M. M., & Terlevich, R. 1981, PASP, 93, 5

Barthel P. D., 1989, ApJ, 336, 606

Barvainis, R. 1993, ApJ, 412, 513

Baskin, A. & Laor, A. 2004, MNRAS, 350, L31

Binette, L., Fosbury, R. A. E., & Parker, D. 1993, PASP, 105, 1150

Blandford R.D., & McKee C.F., ApJ, 255, 419, 1982

Boller, Th., Brandt, W. N., Fink, H. 1996, A&A, 305, 53

Bon, E., Bon, E., Popović, L. Č., Gavrilović, N., La Mura, G., & Mediavilla, E. G., 2009, MNRAS, 400, 924

Boroson, T. A. & Green, R. F. 1992, ApJS, 80, 109

Boroson, T. A. 2002, ApJ, 565, 78

Bregman, J. N. 1990, Astron. Astrophys. Rev., 2, 125

Brotherton, M. S., Wills, B. J., Francis, P. J., & Steidel, C. C. 1994, ApJ, 430, 495

Bruhweiler, F. & Verner, E. 2008, ApJ, 675, 83

Cid Fernandes, R. J., & Terlevich, R. 1995, MNRAS, 272, 423

Cohen, M., Hudson, H., O'Dell, S., & Stein, W. A. 1977, MNRAS, 181, 233

Corbin, M. R. 1995, ApJ, 447, 496

Corbin, M. R. & Boroson, T. A. 1996, ApJS, 107, 69

Della Ceca, R., Palumbo, G. G. C., Persic, M., Boldt, E. A., Marshall, E. E., & de Zotti, G. 1990, ApJS, 72, 471

Dietrich M., Hamann F., Appenzeller I., Vestergaard M., 2003, ApJ, 596, 817

Dimitrijević, M. S., Popović, L. Č., Kovaević, J., Daić, M., & Ilić, D. 2007, MNRAS, 374, 1181

Dong, X., Wang, T., Wang, J., Yuan, W., Zhou, H., Dai, H., & Zhang, K. 2008, MNRAS, 383, 581

Dong, X., Wang, J., Wang, T., Wang, H., Fan, X., Zhou, H., & Yuan, W. 2009

Elvis, M., Wilkes, B. J., McDowell, J. C., Green, R. F., Bechtold, J., Willner, S. P., 1994, ApJS, 95, p. 1-68

Evans, I. N., Ford, H. C., Kinney, A. L., Antonucci, R. R. J., Armus, L., & Caganoff, S. 1991, ApJ, 369, L27

Evans, I. N., Ford, H. C., Kriss, G. A., & Tsvetanov, Z. 1994, in ASP Conf. Proc. 54, The First Stromlo Symposium: The Physics of Active Galaxies, ed. G. V. Bicknell, M. A. Dopita, & P. J. Quinn (San Francisco: ASP), 3

Fanaroff, B. L., & Riley, J. M. 1974, MNRAS, 167, 31P

Fath E. A., 1908, Lick obs, Bull, 5, 71

Francis, P. J., Hewett, P. C., Foltz, C. B., Chaffee, F. H., Weymann, R. J., & Morris, S. L. 1991, ApJ, 373, 465

Fuhr, J. R., Martin, G. A., Wiese, W. L., & Younger, S. M. 1981, J. Phys. Chem. Ref. Data, 10, 305

Gallimore, J. F., Baum, S. A., & O'Dea, C. P. 1997, ApJ, 464, 198

Gaskell, C. M. 1985, ApJ, 291, 112

Gaskell, C. M., Klimek, E. S., & Nazarova, L. S. 2007, BAAS, 39, 947

Giridhar, S. & Ferro, A. A. 1995, RevMexAA, 31, 23

Grandi, S. A. 1982, ApJ, 255, 25

Hartman, H. & Johansson, S. 2000, A&A, 359, 627

Hill, G. J., Goodrich, R. W., & Depoy, D. L. 1996, ApJ, 462, 163

Hoyle, F., & Fowler, W. 1963, MNRAS, 125, 169

Hu, C., Wang, J.-M., Chen, Y.-M., Bian, W. H., & Xue, S. J. 2008, ApJ, 683, 115

Ilić, D., Popović L. Č, Bon. E, Mediavilla, E. G., Chavushyan V. S., 2006, MNRAS, 371, 1610.

Jaffe, W., Ford, H.C., O'Connell, R.W., Ferrarese, L.,& van den Bosch, F. 1993, Nature, 364, 213

Jovanović P.& Popović L.Č. 2009, chapter in the book "Black Holes and Galaxy Formation", Nova Science Publishers Inc, Hauppauge NY, USA, 249-294

Kaspi, S., Smith, P. S., Netzer, H., Maoz, D., Jannuzi, B. T., & Giveon, U. 2000, ApJ, 533, 631

Keel, W. C. 1983, ApJ, 269, 466

Khachikian, E. Ye., & Weedman, D. W. 1974, ApJ, 192, 581

Klockner, H.-R., Baan, W. A., & Garrett, M. A. 2003, Nature, 421, 821

Komossa, S. 2008, in Rev. Mex. Astron. Astrofis., 27, Rev. Mex. Astron. Astrofis. Conf. Ser., 32, 86

Kormendy, J., and Gebhardt, K. 2001, in American Institute of Physics Conference Series, Vol. 586, 20th Texas Symposium on relativistic astrophysics, ed. J. C. Wheeler & H. Martel, 363381

Koski, A. T. 1978, ApJ, 223, 56

Kovačević, J., Popović, L. Č., & Dimitrijevi, M. S. 2010, ApJS, 189, 15

Kriss, G. A., Tsvetanov, Z., & Davidsen, A. F. 1994, in ASP Conf. Proc. 54, The First Stromlo Symposium: The Physics of Active Galaxies, ed. G. V. Bicknell, M. A. Dopita, & P. J. Quinn (San Francisco: ASP), 281

Kuehn, C. A., Baldwin, J. A., Peterson, B. M., & Korista, K. T. 2008, ApJ, 673, 69

Kuraszkiewicz, J. K., Green, P. J., Forster, K., Aldcroft, T. L., Evans, I. N., & Koratkar, A. 2002, ApJS, 143, 257

Kurk J.D., Walter F., Fan X. et al., 2007, ApJ, 669, 32

Lawrence, A. 1987, PASP, 99, 309

Lawrence C. R. , J. R. Zucker, A. C. S. Readhead, S. C. Unwin, T. J. Pearson, & W. Xu, ApJ Suppl 107, 541, 1996

Leighly, K. M. 1999a, ApJS, 125, 297

Leighly, K. M. 1999b, ApJS, 125, 317

Leighly, K. M. 2000, NewAR, 44, 395

Lynden-Bell, D. 1969, Nature, 223, 690

Magorrian, J.,Tremaine, S.; Richstone, D.; Bender, R. et al. 1998, AJ, 115, 2285

Malkan, M., & Sargent, W. L. W. 1982, ApJ, 254, 22

Marziani, P., & Sulentic, J. W. 1993, ApJ, 409, 612

Marziani, P., Sulentic, J. W., Zwitter, T., Dultzin-Hacyan, D., & Calvani, M. 2001, ApJ, 558, 553

Miley, G. K. & Miller, J. S. 1979, ApJ, 288, L55

Miller, J. S., & Goodrich, R. W. 1990, ApJ, 355, 456

Mushotzky, R. F. 1982, ApJ, 256, 92

Nesvadba, N. P. H., Lehnert, M. D., De Breuck, C., Gilbert, A. M., & van Breugel, W. ,2008, A&A 491, 407-424

Netzer H., & Peterson B.M., in Astronomical Time Series, ed. D. Maoz, A. Sternberg, & E.M. Leibowitz (Dordrecht: Kluwer), p. 85, 1997.

Neugebauer, G., Morton, D., Oke, J. B., Becklin, E. et al. 1980, ApJ, 238, 502

Osterbrock, D. E. 1977, ApJ, 215, 733

Osterbrock, D.E., 1981, ApJ, 246, 696

Osterbrock, D. E. 1989, Astrophysics of gaseous nebulae and active galactic nuclei, ed. D. E. Osterbrock (University Science Books, Mill Valley, CA)

Osterbrock, D. E., Pogge, R. W. 1985, ApJ, 297, 166

Owen, F. N., O'Dea, C. P., & Keel, W. C. 1990, ApJ, 352, 44

Panessa, F., de Rosa, A., Bassani, L., Bazzano, A., Bird, A., Landi, R., Malizia, A., Miniutti, G., Molina, M., Ubertini, P. 2011, MNRAS, 417, 2426

Peebles, P. J. E. 1993, Principles of Physical Cosmology (Princeton, NJ: Princeton Univ. Press)

Penston, M. V., & Cannon, R. D. 1970, R. Obs. Bull., 159, 85

Penston, M. V., & Perez, E. 1984, MNRAS, 211, 33

Peterson B.M., PASP, 100, 18, 1988.

Peterson, B. M., Ferrarese, L., Gilbert, K. M., Kaspi, S. et al. 2004, ApJ, 613, 682

Pogge, R. 1989, ApJ, 345, 730

Popović, L. Č., Mediavilla, E. G., Bon, E., Stanić, N., & Kubičela, A. 2003, ApJ, 599, 185

Popović, L. Č., Mediavilla, E., Bon, E., & Ilić, D. 2004, A&A, 423, 909

Popović, L. Č., Smirnova, A., Kovačević, J., Moiseev, A., & Afanasiev, V. 2009, AJ, 137, 3548

Popović, L. Č.. & Kovačević, J. 2011, ApJ, 738, 68

Pounds, K. A., Nandra, K., Stewart, G. C., George, I. M., & Fabian, A. C. 1990, Nature, 344, 132

Rowan-Robinson, M. 1977, ApJ, 213, 635

Roy, A.L, Norris, R.P, Kesteven, M.J, Troup, E.R. & Reynolds, J.E, 1994,Astrophys. J,432,496-507

Salpeter, E. E. 1964, ApJ, 140, 796

Sameshima, H., Kawara, K., Matsuoka, Y., Oyabu, S., Asami, N., & Ienaka, N. 2011, MNRAS, 410, 1018

Sanders, D. B., Soifer, B. T., Elias, J., Madore, B., Matthews, K., Neugebauer, G., & Scoville, N. 1988, ApJ, 325, 74

Schmidt, M. 1963, Nature, 197, 1040

Seyfert, C. 1943, ApJ, 97, 28

Shapovalova A.I.P. , L Č. Popović, A.N. Burenkov, V.H. Chavushyan, D. Ilić, A. Kovacević, W. Kollatschny, J. Kovacević, N.G. Bochkarev, J. R. Valdes,J. Torrealba, J. León-Tavares, A. Mercado, E. Bentez, L. Carrasco, D. Dultzin and E. de la Fuente, 2012, sent to ApJs

Shields, G. A. 1978, Nature, 272, 706

Shields, J. C., Rix, H.-W., McIntosh, D. H., Ho, L. C., Rudnick, G., Filippenko, A. V., Sargent, W. L. W., & Sarzi, M. 1999, ApJ, 534, L27

Sigut, T. A. A. & Pradhan, A. K. 2003, ApJS, 145, 15

Singal, A. K. 1993, MNRAS, 262, L27

Storey, P. J., & Hummer, D. G. 1995, MNRAS, 272, 41

Strittmatter, P. A., Serkowski K., Carswell R., Stein W.A., Merill K.M., Burbidge E.M. 1972, ApJ, 175, L7

Sulentic, J. W.; Marziani, P.; Zamfir, S. 2009, New Astronomy Reviews, 53, 198

Szalay A. S., Jain B., Matsubara T., Scranton R. et al., 2003, ApJ, 591, 1

Tadhunter, C., 2008, New Astronomy Reviews 52.6 : 227

Tarchi, A., Castangia, P., Columbano, A., Panessa, F., & Braatz, J. A. 2011, A&A, 532, 125

Tran, H. D. 1995, ApJ, 440, 597

Tsuzuki, Y., Kawara, K., Yoshii, Y., Oyabu, S., Tanabe, T., & Matsuoka, Y. 2006, ApJ,650, 57

Urry, C. M., & Padovani, P. 1995, PASP, 107, 803

Veilleux, S. & Osterbrock, D. E. 1987, ApJS, 63, 295

Verner, E. M., Verner, D. A., Korista, K. T., Ferguson, J. W., Hamann, F., & Ferland, G. J. 1999, ApJS, 120, 101

Veron-Cetty, M., Vron, P., & Goncalves, A. C. 2001, A&A, 372, 730

Veron-Cetty, M.-P., Joly, M.,& Veron, P. 2004, A&A, 417, 515

Vestergaard, M. & Wilkes, B. J. 2001, ApJS, 134, 1

Wills, B. J., Netzer, H., & Wills, D. 1985, ApJ, 288, 94

Wills, B. J. & Browne, I. W. A. 1986, ApJ, 302, 56

Wills, B. J., H. Netzer, M. S. Brotherton, Hingsh H., D. Wills, J. A. Baldwin, G. J Ferland & I. W. A. Browne. 1993, ApJ, 410, 534

Wilson, A. S., Colbert, E. J. M.& Bland-Hawthorne, J. 1994, ApJ, 436, 89

York, D. G.,Adelman, J., Anderson, J. E., et al. 2000, AJ, 120, 1579

Zeldovich, Ya. B. 1964, Dokl. Akad. Nauk. SSSR, 155, 67 (also 158, 811)

Zheng, W., Kriss G. A., Davidsen A. F., & Kruk J. W., 1995, ApJ, 444, 632